De Jaime-Soguero, Chabier; Mujal, Eudald; Oms, Oriol; [et al.]. «Palaeoenvironmental reconstruction of a lower to middle Permian terrestrial composite succession from the Catalan Pyrenees : Implications for the evolution of tetrapod ecosystems in equatorial Pangaea». Palaeogeography, Palaeoclimatology, Palaeoecology, Vol. 632 (December 2023), art. 111837. DOI 10.1016/j.palaeo.2023.111837

Palaeoenvironmental reconstruction of a lower to middle Permian terrestrial composite succession from the Catalan Pyrenees: implications for the evolution of tetrapod ecosystems in equatorial Pangaea

De Jaime-Soguero, C.[1,*], Mujal, E.[2,1], Oms, O.[3], Bolet, A.[4,1,5], Dinarès-Turell, J.[6], Ibáñez-Insa, J.[7], Fortuny, J.[1,*]

[1]*Institut Català de Paleontologia Miquel Crusafont (ICP-CERCA), Universitat Autònoma de Barcelona, Edifici ICTA-ICP, c/ Columnes s/n, Campus de la UAB, 08193 Cerdanyola del Vallès, Barcelona, Spain.*

[2]*Staatliches Museum für Naturkunde Stuttgart, Rosenstein 1, D-70191 Stuttgart, Germany.*

[3]*Departament de Geologia, Universitat Autònoma de Barcelona, E-08193 Bellaterra, Catalonia, Spain.*

[4]*Departamento de Estratigrafía y Paleontología, Universidad de Granada, Avda. Fuente Nueva s/n, 18071 Granada, Spain*

[5]*School of Earth Sciences, University of Bristol, Wills Memorial Building, Queens Road, Bristol BS8 1RJ, United Kingdom*

[6]*Istituto Nazionale di Geofisica e Vulcanologia, Via di Vigna Murata 605, I-00143 Roma, Italy*

[7]*Geosciences Barcelona (GEO3BCN-CSIC), C/ Lluís Solé i Sabarís s/n, 08028 Barcelona, Spain*

*Corresponding authors: chabier.dejaime@icp.cat (C. De Jaime-Soguero) and josep.fortuny@icp.cat (J. Fortuny)

Abstract

Tetrapod diversity in Permian terrestrial ecosystems of southwestern Europe is poorly recorded by bone specimens, but it is better represented by an important tetrapod ichnological record that is relevant to our understanding of vertebrate communities in the equatorial Pangaea. Herein, two tetrapod ichnoassociations from three new ichnosites, within Cisuralian and Guadalupian volcanosedimentary terrestrial successions (the Lower Red Unit and the Upper Red Unit deposits) of the Castellar de n'Hug sub-basin (Catalan Pyrenees, NE Iberian Peninsula) are presented. Tetrapod ichnology in combination with stratigraphic and facies analyses permit a characterisation of these ecosystems. The sedimentary deposits show an evolution from fluvial meandering systems to playa-lake floodplains, denoting increased aridification and seasonality under a monsoonal regime. The ichnofossil record shows how tetrapod assemblages shifted from a prevalence of non-amniotes and eureptiles to a dominance of therapsids, eureptiles and parareptiles. The reported ichnotaxa are distributed in two ichnoassociations. The first preserves *Batrachichnus*, *Dromopus*, *Hyloidichnus*, *Characichnos* and an indeterminate tetrapod morphotype, whereas the second is defined by the presence of *Dromopus*, *Hyloidichnus*, *Brontopus antecursor* and *Pachypes.* The stratigraphically older ichnoassociation, preserved in volcaniclastic and fluvial deposits, presents features of the early *Erpetopus* biochron, whereas the stratigraphically younger one, preserved in playa-lake deposits, is constrained to the *Brontopus* sub-biochron. Biostratigraphic and magnetostratigraphic data suggest a late Cisuralian to middle Guadalupian age for the whole succession. The ichnoassemblage highlights a palaeobiogeographical connection between the Pyrenean Basin and other peri-Tethyan basins, which allows us to expand our knowledge about the palaeoecology and palaeobiodiversity of the Cisuralian to Guadalupian terrestrial ecosystems.

Keywords: Tetrapod ichnology; biostratigraphy; Cisuralian; Guadalupian; Western Tethys.

1. Introduction

The Permian period was marked by profound ecological changes resulting from variations of climatic and environmental conditions. The assembling of all the landmasses in one single continent, Pangaea, together with the reorganisation of cold-water currents (Winguth et al., 2002; LePage et al., 2003; Weldon and Shi, 2003) prompted climate changes and an aridification process, evolving from the Carboniferous ice-house (Saltzman, 2003; Montañez et al., 2007, 2016; Montañez and Poulsen, 2013; Richey et al., 2020) to the Triassic hot-house (MacLeod et al., 2017). During the Cisuralian (early Permian) a change from humid to dry conditions took place, and an intensified monsoonal climate linked to the configuration of landmasses was established (Tabor and Montañez, 2002; Roscher and Schneider, 2006; Roscher et al., 2011; Tabor et al., 2018). This multi-stage warming process was interrupted by different short and relatively humid periods throughout the Permian in low latitudes (Schneider et al., 2006; De la Horra et al., 2012; Michel et al., 2015). These changes were followed by an increase of drought tolerant biota during the Cisuralian that became dominant during the Guadalupian and Lopingian (Marchetti et al., 2022a). Regarding tetrapod faunas, amniotes became widespread throughout Pangaea, diversifying and replacing early tetrapod groups (Sues and Reisz, 1998; Benton et al., 2013). During the early Permian, terrestrial faunas were still dominated by non-amniotes such as temnospondyls and reptiliomorphs, but faunal composition became richer with the diversification of basal amniotes, parareptiles, early diapsids and synapsids (Dunne et al., 2018). The harsh climate-induced environmental conditions caused several ecological crises, such as the end-Guadalupian mass extinction, which profoundly affected terrestrial tetrapod ecosystems (Lucas, 2009a, 2017, 2018; Day et al., 2015; Schneider et al., 2020; Day and Rubidge, 2021). This climate change caused the global extinction of dinocephalian therapsids, while other therapsid families, eureptiles and parareptiles that were better adapted to arid conditions became dominant in terrestrial ecosystems until the end-Permian mass extinction (Lucas, 2009a, 2009b; Hoffman, 2016; Schneider et al., 2020).

The mentioned changes in terrestrial tetrapod ecosystems have been identified in different Permian successions of the western peri-Tethys domain, an equatorial region of Pangaea, which includes present-day Europe and northern Africa (Gand and Durand, 2006; Roscher et al., 2011, De la Horra et al., 2012; Michel et al., 2015; Lucas, 2017, 2018; Mujal et al., 2017, 2018; Schneider et al., 2020; Marchetti et al., 2022a, 2022b; Rmich et al., 2023). The scarce skeletal fossil record of this region restricts our view of how tetrapod faunas were affected through the Permian. Conversely, the tetrapod footprint record is much more diverse, providing a more complete picture of those ecosystems and their evolution (Marchetti et al., 2022a). In this regard, the Cisuralian tetrapod ichnofaunas from the Catalan Pyrenees (NE Iberian Peninsula; Voigt and Haubold, 2015; Mujal et al., 2016a; Marchetti et al., 2021a, preserved in relatively long and continuous stratigraphic successions, are important to understand the evolution of tetrapod communities along with palaeoenvironmental changes (Mujal et al., 2016a, 2018). Regarding post-Cisuralian terrestrial ecosystems in the Pyrenees, tetrapod remains in the form of ichnites and sparse bones have only been described from three localities (Robles and Llompart, 1987; Fortuny et al., 2011; Mujal et al., 2016b, 2017). Outside of the Pyrenees, only a few tetrapod remains have been recovered from Permian successions in the Iberian Peninsula and Balearic Islands to date: Peña Sagra in the Cantabrian Mountains based on tetrapod ichnofauna (Gand et al., 1997; Demathieu et al., 2008; López-Gómez et al., 2019) and tetrapod (both skeletal and ichnological) specimens in the Balearic Islands (Pretus and Obrador, 1987; Liebrecht et al., 2017; Matamales-Andreu et al., 2021a, 2021b, 2021c, 2022, 2023). All in all, Cisuralian–Guadalupian tetrapod ichnofaunas from Iberia remain poorly understood. This is largely because of the lack of a general correlation of stratigraphic successions at Iberian scale allowing identification of changes in the tetrapod communities in conjunction with palaeoenvironmental shifts that can be compared to the global record.

The main goal of this work is to provide a comprehensive study of a continuous Permian terrestrial succession of the Catalan Pyrenees (NE Iberian Peninsula) including both Cisuralian and Guadalupian deposits. Three newly reported tetrapod footprint localities record faunal changes due to a transition from relatively wet to dry environments. Also, they record the coexistence of tetrapod tracks in fluvial deposits interbedded with volcanic pyroclastic intervals, as previously observed in other Cisuralian deposits of the Pyrenean Basin (Mujal et al., 2016a) enlarging our understanding of these complex environments. This multidisciplinary work integrates new lithostratigraphic, sedimentological, magnetostratigraphic and biostratigraphic data, enhancing an accurate geochronological, palaeoenvironmental and faunistic interpretation. The new Permian ichnoassemblage of the Pyrenean Basin shares several ichnotaxa with nearby basins from southwestern Europe and northern Africa, strengthening our view of faunistic changes, environmental evolution, and palaeobiogeography of equatorial Pangaea during the Cisuralian–Guadalupian.

2. Geological setting

The Pyrenees are a WNW-ESE oriented mountain range situated in the NE of the Iberian Peninsula (Fig. 1A–B) that formed during the Alpine orogeny as a result of the collision between the Iberian and European tectonic plates. Their core is composed of igneous and metamorphic rocks related to the Variscan orogeny and includes Cambrian to lower Carboniferous strata (Pereira et al., 2014). The southeastern margin of the Pyrenees is composed of deposits from the late Carboniferous to Oligocene, representing the sedimentary cover deposited between the end of the Variscan and the Alpine cycles (Mey et al., 1968; Nagtegaal, 1969; Gisbert, 1981; Martí, 1996; Pereira et al., 2014; Mujal, 2017).

During the late Palaeozoic, the Iberian area (including the Iberian Peninsula and the Balearic Islands) was located in the western peri-Tethys region, at the eastern part of equatorial Pangaea (Scotese, 2014). The palaeogeographic position of this area was at the East of the inferred suture of the Rheic ocean, between the western end of the subduction zone of the PalaeoTethys sea and the southern margin of the Variscan mountains (Stampfli and Kozur, 2007; Sinisi et al., 2014; Pereira et al., 2014). The western peri-Tethys basins were dominated by fluvial systems, produced by the dismantling of the Variscan orogen (Roscher and Schneider, 2006; Schaltegger and Brack, 2007; Torsvik and Cocks, 2013; Pereira et al., 2014; Michel et al., 2015; Gretter et al., 2015; Mujal et al., 2018). In the Pyrenean region, large amounts of sediments were deposited in intramountain basins limited by directional faults (Gisbert, 1981). In southwestern Europe, including the Iberian area, France, the north of Italy, Sardinia and the Balkan Peninsula, an upper Carboniferouslower Permian magmatism is recorded (Cortesogno et al., 1998, 2004; Lago et al., 2004; Schneider et al., 2006; Gretter et al., 2015; Michel et al., 2015; Pellenard et al., 2017; Majarena et al., 2023). In northeastern Iberia, episodic syn-sedimentary volcanic activity produced calc-alkaline volcanic deposits in these basins (Barrachina and Martí, 1986; Martí, 1996; Pereira et al., 2014). During the Permian, an aridification process and global warming replace the late Carboniferous conditions (Saltzman, 2003; Montañez et al., 2007; Montañez and Poulsen, 2013; Richey et al., 2020). In the southern margin of the Variscan mountain range, where the northeastern of the Iberian area where located, a climatic shift from humid to semi-arid and arid conditions is recorded in rocks of the Permian succession (Gascón and Gisbert, 1987; Gretter et al., 2015; Mujal et al., 2018), which makes this a region of great importance for understanding the environmental evolution of equatorial Pangaea. During the late Palaeozoic, the area corresponding to the present-day Catalan Pyrenees was a rift system developed in the latest phases of the Variscan orogeny. The so-called Pyrenean Basin is a rift system divided into four depocentres or sub-basins: Erillcastell-Estac, Cadí, Castellar de n'Hug, and Campelles-Camprodon (Gisbert 1981, 1986; Speksnijder, 1985;

Saura and Teixell, 2006; Izquierdo-Llavall et al., 2014; Gretter et al., 2015; Mujal, 2017; Fig. 1A). These depocentres have been identified as isolated terrestrial basins limited by strike-slip faults (Gisbert, 1981; Speksnijder, 1985; Saura and Teixell, 2006). Their infilling consists of upper Carboniferous–Middle Triassic volcanic, volcanosedimentary and sedimentary deposits composed of andesitic, dacitic and rhyolitic rocks, pyroclastic successions and rhyodacitic ignimbrites along with sedimentary rocks, dominated by mudstones, sandstones, conglomerates and breccias in alluvial settings and, to a lesser degree, with limestones in palustrine to lacustrine settings (Barrachina and Martí, 1986; Gisbert, 1981; Martí, 1996; Gretter et al., 2015; Lloret et al., 2018; Mujal et al., 2018). The upper Carboniferous–Middle Triassic succession of the Catalan Pyrenees was divided by Gisbert (1981) into five depositional units: Grey Unit (upper Carboniferous), Transition Unit (upper Carboniferous–early Permian), Lower Red Unit (Cisuralian; equivalent to the Peranera Formation in the western Catalan Pyrenees, see Nagtegaal, 1969; Gisbert, 1981; Mujal et al., 2016a, 2016b, 2018), Upper Red Unit (Guadalupian–Lopingian) and Buntsandstein facies unit (Lower–Middle Triassic). These Permian units record highly explosive volcanism that produced great amounts of pyroclastic material, mainly deposited as ignimbrites and cinerites (Barrachina and Martí, 1986; Martí, 1996; Pereira et al., 2014).

The Castellar de n’Hug sub-basin, the focus of this study, is in the eastern part of the Pyrenean rift system (Fig. 1A–B). The stratigraphic sequence encompasses materials from the Carboniferous (Culm facies) to the Triassic, recording four of the five depositional units of Gisbert (1981): the Transition Unit (TU), Lower Red Unit (LRU), the Upper Red Unit (URU) and the Buntsandstein facies units (see also Gisbert et al., 1985; Gretter et al., 2015). Contrary to other upper Palaeozoic sequences of the Pyrenean Basin, the Grey Unit is not recorded in the Castellar de n’Hug sub-basin (Broutin and Gisbert, 1985; Gisbert et al., 1985). The Permian volcanic deposits of this sub-basin have a calc-alkaline composition and appear from the base of the Lower Red Unit to the base of the Upper Red Unit (Pereira et al., 2014). The present study focuses on the Permian red-bed depositional units (LRU, URU).

3. Material and methods

3.1. Stratigraphy and sedimentology

Geological and palaeontological analyses were conducted in three closely located outcrops of the Castellar de n'Hug sub-basin that excellently expose the Permian volcanosedimentary successions: Castellar de n'Hug (CnH, 699.1 m thick), Riera de Monell (RM, 353.0 m thick) and Coll Roig (CR, 268.2 m thick) (Fig. 2). For this study, three stratigraphic sections have been logged, one at each outcrop, by means of a Jacobs staff and a measuring tape with a minimum resolution of 1 cm of bed thickness (see Supplementary Logs). Coordinates are provided in ETRS89 UTM 31T: the stratigraphically lower section of Castellar de n'Hug (699.1 m; base, 419966 E, 4681751 N; top, 419762 E, 4680959 N) and the stratigraphically upper sections of Riera de Monell (353.0 m; base, 416396 E, 4680888 N; top, 416422 E, 4680437 N) and Coll Roig (268.2 m; base, 413306 E, 4681286 N; top, 413133 E, 4680848 N). A correlation of the three sections was also conducted by using synthetic logs of each section (Fig. 2). The lower part of the succession has been studied in the Castellar de n'Hug (CnH) section, the middle part in the three sections and the upper part in the Riera de Monell (RM) and Coll Roig (CR) sections. In the CnH section the upper part is highly tectonised, precluding an appropriate stratigraphic analysis. As will be discussed below, the selected *datum* to correlate the three sections is the change from volcaniclastic deposits to the mudstones with conspicuous mud-cracked surfaces.

A lithofacies analysis was performed through the observation and measurement of the thickness of each stratum, its composition, geometry, sedimentological structures, and fossil content, and follows the nomenclature of Miall (2006) and Gretter et al. (2015). The volcanoclastic materials present in the succession were classified following Martí (1996), Branney and Kokelaar (2002), and Gretter et al. (2015). The architectural interpretation and the facies associations were performed according to the procedures of Miall (2006), Branney and Kokelaar (2002), Gretter et al. (2015) and Matamales-Andreu et al. (2021a). The GPS data of the stratigraphic logs is provided in KMZ format. Additionally, an unnamed aerial vehicle (UAV) was used to create a 3D photogrammetric model of RM and CR sections in high resolution. The great thickness of CnH section precluded obtaining a similar resolution level as in the other two sections and, therefore, it was discarded. 3D models of the sections are freely available in PLY format in Morphosource repository (see Data Availability section below).

3.2. Magnetostratigraphy

For the purpose of retrieving the geomagnetic polarity of the studied Permian succession, 26 samples were taken along the three reported stratigraphic logs (see Fig. 2, Supplementary Logs, Fig. S1, Table S1). The collected samples were named referring to the stratigraphic section from which they were recovered: Castellar de n'Hug (CH1 to CH8 sites), Riera de Monell (RM1 and RM2 sites) and Coll Roig (CR1 to CR16 sites). These were supplemented with an additional 23 samples taken from equivalent outcrops located less than 1 km from the Coll Roig section (sites SG1 and SG2, Solell de la Gallarda from the LRU unit, and CP1 to CP21, la Pardinella de Gavarrós, from the URU unit, respectively, see Supplementary GPS data). As such, the magnetostratigraphic data includes 49 sites spanning most of the studied stratigraphic units. Dip of strata is similar in all the sections, which prevents performing a proper and meaningful fold test. One to three oriented hand-samples were taken from each site and were subsequently cut in standard regular samples (~10 cm^3) for palaeomagnetic measurements. Additionally, powder from representative lithologies were obtained by crushing and pestling samples in an agate mortar for rock-magnetic experiments. Initial natural remanent magnetization (NRM) and remanence during stepwise demagnetization were measured in a 2G Enterprises DC SQUID high-resolution pass-through cryogenic magnetometer (manufacturer noise level of 10^{-12} Am^2) operated in a shielded room at the Istituto Nazionale di Geofisica e Vulcanologia in Rome, Italy. A Pyrox oven in the shielded room was used for thermal demagnetisations and alternating field (AF) demagnetisation was performed with three orthogonal coils installed in line with the cryogenic magnetometer. Progressive stepwise AF demagnetisation was routinely used and applied after a single heating step to 150 °C. AF demagnetisation usually included 14 steps (4, 8, 13, 17, 21, 25, 30, 35, 40, 45, 50, 60, 80, 100 mT). Subsequently, thermal demagnetisation resumed through variable temperature increments (20–100 °C) up to 690 °C. In the context of the studied red-beds, applying a first heating step followed by AF demagnetisation prior to full thermal demagnetisation, makes it possible to both unblock eventual magnetisation carried by goethite (usually unblocking occurs below 120 °C) and also magnetite-like low coercivity ferromagnetic phases. Consequently, magnetic phases even unblocking at relatively low temperatures during the final thermal protocol must be assigned to high coercivity phases (i.e., hematite). Characteristic remanent magnetisations (ChRM) were calculated by Principal Component Analysis (Kirschvink, 1980) from orthogonal vector endpoint demagnetisation diagrams (Zijderveld, 1967) using the online open-source software Paleomagnetism.org (Koymans et al., 2016, 2020). The magnetic stratigraphy is based on virtual geomagnetic pole (VGP) latitudes.

In order to characterise ferromagnetic mineralogy, some rock magnetic experiments were performed in representative samples. Thermomagnetic heating and cooling cycles were measured with an AGICO KLY5 susceptibility bridge with a CS4 furnace attachment with nominal sensitivity (5×10^{-7} SI) and open air into the tube. Hysteresis measurement loops, isothermal remanent magnetization (IRM) acquisition and back-field IRM were measured at room temperature with a Princeton Measurements Corp. Model 3900 MicroMagTM Vibrating Sample Magnetometer (VSM) (noise level 5×10^{-9} Am^2). IRM curve unmixing to identify separated magnetic components was performed with IRM MaxUnmix package (Maxbauer et al., 2016).

3.3. Tetrapod trace fossils

Tetrapod ichnites were analysed following Haubold (1971) and Leonardi (1987) (see Tables S2, S3). Parameters have mainly been measured on footprints with a medium to high degree (2 to 3) of morphological preservation (*sensu* Marchetti et al., 2019a). Three-dimensional (3D) models of selected ichnites were obtained with the photogrammetry technique. Photographs were taken with a digital reflex camera Nikon D3200 with a lens AF-S Nikkon 15-55 mm 1:3.5-5.6 GII Nikon following the procedures of Falkingham (2012), Mallison and Wings (2014) and Mujal et al. (2020). 3D models were processed with three different software: Agisoft Metashape (Professional edition, educational version, v.1.8.3) to generate the mesh and the texture, MeshLab (v.2020.07) to edit the mesh, and ParaView (v.5.5.0) to generate false colour depth maps and contours.

Tetrapod ichnites have been found on the three outcrops, CnH, RM and CR. The material consists of footprints preserved on 19 recovered slabs and 12 unrecovered surfaces that also include trackways. All recovered specimens are stored at the Institut Català de Paleontologia Miquel Crusafont (ICP) and were prepared, when necessary, in its lab. The material was collected during the palaeontological surveillances of 2015, 2019 and 2021, all undertaken with the corresponding legal permits issued by the Servei de Patrimoni Arqueològic i Paleontològic (Departament de Cultura of the Generalitat de Catalunya, Catalan Government). Specimens left in the field have been referenced using the acronyms identifying the locality (CnH, RM or CR), the corresponding position in metres from the base of the stratigraphic section, and an Arabic number to refer to each ichnite in the given surface (as for example RM-176-1).

3.4. Mineralogy

Powder x-ray diffraction (XRD) measurements were performed in order to characterise the mineralogy of the investigated succession (see Text S2 and Table S4). The XRD results were also employed to provide information on the possible origin of samples that were not identified unambiguously in the field or in thin section. Three samples of the LRU were analysed (CH-6, CH-8, CH-9), nine from the lower URU (CH-13, CH-14, RUS-1 to RUS-7) and three of the upper URU (RM-223, RM-254 and CR-246). XRD measurements were acquired at Geosciences Barcelona (GEO3BCN-CSIC) using a Bruker D8-A25 diffractometer (Cu Kα radiation), equipped with a LynxEye position sensitive detector (PSD). The XRD scans were performed between 4° and 60° in 2θ with a 0.035° step size and equivalent counting times of 192 s. Phase identification was carried out by using Bruker's DIFFRAC.EVA software in combination with the Powder Diffraction File (PDF-2) database from the International Center for Diffraction Data (ICDD).

3.5. Institutional abbreviation

IPS, Institut Català de Paleontologia Miquel Crusafont (formerly Institut de Paleontologia de Sabadell), Sabadell, Catalonia, Spain.

4. Results and interpretation

4.1. Stratigraphy and sedimentology

The stratigraphy of the Permian succession in the Catalan Pyrenees has been previously studied by Mey et al. (1968), Nagtegaal (1969), Gisbert (1981), Gisbert et al. (1985), Speksnijder (1985), Martí (1996), Gretter et al. (2015), Mujal et al. (2016a, 2016b, 2017, 2018) and Lloret et al. (2018, 2021a, 2021b). Particularly, Gisbert et al. (1985), Martí (1996), Barrachina and Martí (1986), and Gretter et al. (2015) focused on the origin, composition, and evolution of the Permian red-beds and volcaniclastic deposits of the analysed area of this work. Considering these previous studies, new stratigraphical and sedimentological analyses have been carried out in the outcrops of Castellar de n’Hug (CnH) and, for the first time, also in Riera de Monell (RM) and Coll Roig (CR) (see Supplementary Logs). Also, the palaeontological content of the Permian deposits is analysed in detail for the first time. In this way, a renewed stratigraphic framework is provided, including new data for the Lower Red Unit (LRU) and Upper Red Unit (URU). Based on this, a robust palaeoenvironmental setting and its evolution is provided, allowing for a detailed contextualisation of the palaeontological record. As a whole, a composite section >900 m thick has been obtained (Fig. 2), including volcaniclastic successions interbedded with mudstone, sandstone and conglomerate deposits in the lower portion and mudstone-sandstone deposits in the middle and upper portions.

4.1.1. Facies description and interpretation

This section includes a formal description of the facies observed in the Permian continental deposits of the present study. Eighteen different facies have been identified and classified in two groups: ten sedimentary facies and six volcanic facies (Table 1).

Table 1. Sedimentary lithofacies identified in the study area.

Code (Depositional unit)	**Description**	**Formation process**	**Scheme**
	Sedimentary facies		
Gt (LRU)	Clast-supported breccias with normal grading and trough cross-bedding. Their composition is polymictic, with clasts of lithic fragments. Strata show sigmoidal shape. Between 20 cm to almost 3 m thick.	Stream flow	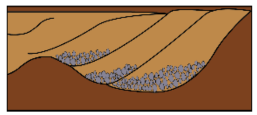
Sr (LRU, URU)	Fine-grained sandstones to mudstones with climbing, unidirectional or wave ripples. Between 10 to 80 cm thick.	Traction plus fallout flows	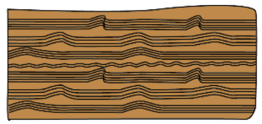
Sh (LRU, URU)	Very fine- to coarse fine-grained sandstones with horizontal parallel lamination. Clasts or pebbles are not common in these facies and may show tabular geometry. Between 10 cm to 1 m thick.	High flow regime	
Sl (LRU, URU)	Fine-grained to very fine sandstones with low angle cross-stratification. They may erode the previous layer and may contain unidirectional ripples. Between 6 cm to 1.4 m thick.	Traction plus fallout flows	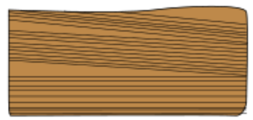

Ss (LRU, URU)	Very fine- to medium-grained sandstones with crude crossbedding (occasionally with presence of pebbles or clasts of quartz, feldspar, andesite, and lithic fragments). Between 20 cm and 1.5 m thick. Lower contact is sometimes erosive into deposits of facies *Fm* or *Fl*.	Scour fills	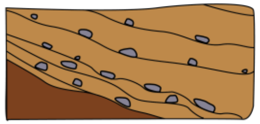
Sm (LRU, URU)	Massive beds composed of very fine- to medium-grained sandstones. They show neither lamination nor arrangement in the grains. Tabular geometry. Most are relatively thin (the average maximum thickness is 20 cm) deposits.	Massive fallout	
Fl (LRU, URU)	Mudstones and very fine-grained (occasionally fine-grained) sandstones with fine lamination, mostly parallel, and occasionally cross lamination (current and wave ripples). Root and vertebrate bioturbation, small edaphic nodules, and plant remains can be present. Tabular geometry. Between15 cm and 4 m thick.	Fallout and occasionally traction flows	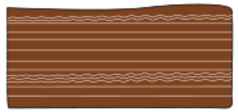
Fm (LRU, URU)	Massive mudstones with mud-cracked surfaces on top. Some mud-cracked surfaces present a decoloured (greyish-greenish colouration) calcareous level on the top of the layer. Vertebrate and invertebrate ichnites, and plant impressions may be present, with raindrop impressions, carbonate and reduction (green) mottles. Centimetric to several metres thick.	Fallout and subaerial exposition	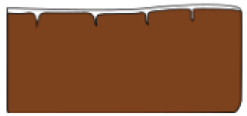
P (LRU, URU)	Massive deposits. They are tabular layers of mudstones and very fine- to fine-grained sandstones with carbonate nodules and root traces that produce a calcareous layer over them. Centimetric to several metres thick.	Pedogenesis	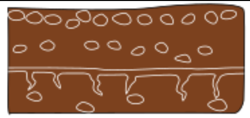
Ps (URU)	Massive mudstones with tabular geometry and with intervals including abundant septariform nodules, floating on the matrix. Up to 15 m thick. The nodules measure between 12 and 45 cm of diameter. Their surface is ornamented with fractures filled with calcite crystal, which are radial or concentric.	Pedogenesis and diagenesis	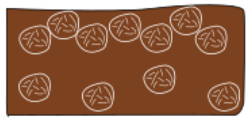
Volcaniclastic facies			
mT (LRU)	Crystal-rich massive tuffs. They are the most common facies. Weathering makes them resemble mudstones. Centimetric to metric layers in thickness. Deposits homogeneous and very well sorted with a vitric matrix composition. Brownish-purple dark colours. Equivalent to facies *MF* of Martí (1996).	Massive fallout	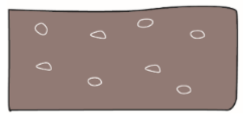

bT (LRU, URU)	Fine-grained deposits that can appear as greenish tabular and solated thin layers (between 2 to 10 cm thick). Thicker deposits can be found at the top of ignimbrites.	Ashfall (cinerites)	
sT (LRU)	Subparallel finely laminated to low-angle bedforms facies that could show antidune structures. Centimetric to subcentimetric laminated deposits containing crystals of quartz and feldspar, and fragments of rhyolite and andesite. They show a tabular shape and display greenish and purples deposits. Equivalent to facies *PLF* of Martí (1996).	Pyroclastic flow	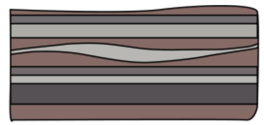
mLT (LRU)	Massive, poorly sorted deposits, usually matrix supported, composed of a chaotic, non-stratified vitric ash matrix deposits, which may contain fragments of pumice and lithic lapilli. The matrix presents purple-dark colour, and the original components have been altered during the diagenesis, as discussed by Martí (1996). Equivalent to facies *PF* of Martí (1996).	Pyroclastic flow	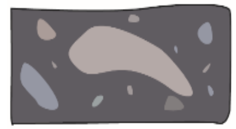
bL (LRU)	Thin-bedded lapilli moderately sorted, with lithic and pumice clasts 1-6 cm wide. The organisation of the clasts may be chaotic, poorly graded.	Rapidly stacked fallout flows	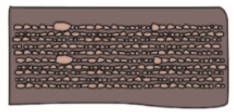
mlBr (LRU)	Massive lithic breccias located at the base of ignimbrites or appearing isolated.. They are chaotically distributed, display angular clasts without lateral accretion composed of angulous fragments and pebbles, included in a matrix of facies *mT* or *mLT*. They are tabular, 2-3 m thick, highly erosive, and very similar to sedimentary breccias.	Dense pyroclastic flow	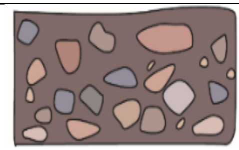

4.1.2. *Facies associations and architectural elements*

Based on the arrangement of the previously described facies, five architectural elements have been recognised (Table 2).

Table 2. Architectural elements recognised in the study area. In brackets, facies that appear only occasionally in the association. The arrows show the vertical succession.

Architectural element	**Facies associations**	**Description and interpretation**	**Unit**	**Scheme**
Lateral accretion (LA)	*Gt* →*Ss* →*Sr/Sm*→*Fl*	Point bars (sigmoidal shape) of meandering channel deposits. Composed of conglomerates at the base and coarse-grained sandstones, grading to medium-/fine-grained sandstone (normal grading).	LRU	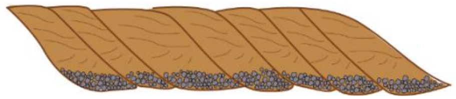
Crevasse splays (*CS*)	*Fl*→*Ss*→*Fm*→*P*	Composed of sandstones (sometimes with intraclasts) with crossbedding and interbedded laminated mudstone, showing a grain-size reduction, with biotic activity recorded in the upper part. They are originating from floodplain systems and are arranged in cyclic events with palaeosols (facies *P*) developed in them.	LRU	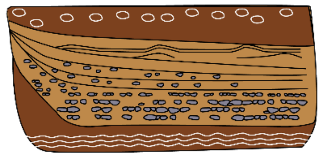
Floodplain fines (*FF*)	*Fl*→*Fm*→*(P)* →*(Sh/Sm)* →*Fm*	Massive deposits of mudstone produced by slow sedimentation, interrupted by sporadic flooding events. Long-term evaporation and desiccation resulted in localised mud-cracked surfaces and palaeosols.	LRU	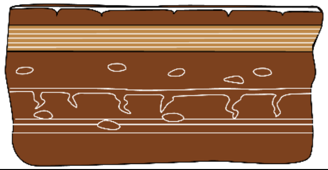
Ephemeral lacustrines (*L*)	*(Fl)Fm*→*(P)* →*Sh/Sm*→Fm	Massive deposits of mudstone produced by seasonal sedimentation, followed by long-time desiccation, producing isolated ponds, massive mud-cracked surfaces and palaeosols. They are interpreted as ephemeral lacustrine facies.	URU	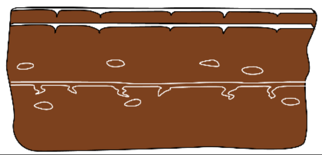
Cinerite (C)	*bT*	Centimetric and isolated layers could eventually be associated to non-observed facies located in distant and different volcanic areas.	LRU	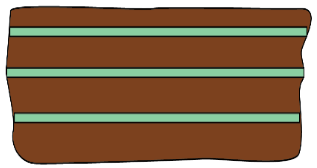

Ignimbrite (*IG*)	*mLA→sT→mL* *mT→ P* *(mL) →mlBr*	Volcanic massive materials produced by different pyroclastic flows of thin bedded tuff deposits, massive lapilli-tuf beccias, cinerites and pedogenetic activity.	LRU	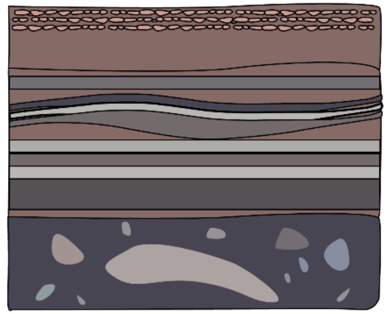

4.1.3. Lower Red Unit (LRU)

The Lower Red Unit (LRU) represents an alternation of different sets of fluvial and volcanic deposits (Fig. 3A–J). The base and the top of this unit contact with the Transition Unit (TU) and Upper Red Unit (URU), respectively. Sedimentary facies include reddish-maroon mudstones (facies *Fl* and *Fm*), sandstones (facies *Sh*, *Sl*, *Sm* and *Ss*) and gravels (facies *Gt*), corresponding to floodplain deposits, meandering fluvial channels and related crevasse splays (architectural elements *LA*, *FF* and *CS*). These fluvial sequences are usually between 10 and 20 m thick, but some are up to 49 m thick (Fig. 2, Supplementary logs). The fluvial sequences are interbedded with red-bed volcaniclastic deposits, occasionally reworked, composed of massive ash-flow deposits (facies *mT*, *bT*, *sT*, architectural element *IG*) and sporadic pyroclastic and lithic breccias (facies *mLT*, *bL*, *mlBT*, architectural element *IG*) produced by calc-alkaline volcanism (Martí, 1996). The thickness of these volcanic sequences is very variable, from deposits a few centimetres thick, such as cinerites (facies *bT*), to long sequences of massive pyroclastic deposits that underwent pedogenesis (12 m thick) and ignimbrite deposits (14 m thick). Calcareous palaeosols (facies *P*) are observed in both fluvial and volcanic deposits, denoting long-time exposure of the sediments. The complete succession of the LRU is only visible at the CnH section, whereas RM and CR sections only include the uppermost volcanoclastic levels (Fig. 2).

At the base of the CnH section, the LRU is dominated by massive ash-flow deposits (facies *mT*, *bT*, *sT*) highly affected by pedogenesis, represented by calcareous nodules and rizholiths (facies *P*), abundant greenish cinerites (facies *bT*), and sporadic deposits of interbedded mudstones (facies *Fm*), sandstones (facies *Ss*) and breccias (facies *Gt*). All these detritic deposits are interpreted as floodplains deposits and isolated channels with lateral accretions (architectural elements *FF* and *LA*). Even though the Transition Unit has been recognised in the studied area (Gisbert et al., 1985; Gretter et al., 2015), the base of the LRU in the CnH section directly but unconformably overlie the marine Carboniferous Culm facies and Devonian carbonates by means of a tectonized unconformity. Some deposits of grey-yellowish sandstones with plant remains (see Text S1) record the presence of the Transition Unit (UT) in the area (Broutin and Gisbert, 1985; Gisbert et al., 1985). However, these levels are not clearly connected to the LRU in the studied succession. Therefore, the Lower Red Unit at CnH starts at 23.5 m of the CnH section and ends at 609 m, coinciding with the disappearance of the volcanic record.

The first part of the CnH section is dominated by volcanic layers, such as massive ignimbrites (facies *bL* and *mlBT*) and ashfall deposits (facies *mT* and *bT*). These deposits are sporadically cut by fluvial deposits, composed of sandstones (facies *Sp*, *Sh*, *Sl*, *Sm* and *Ss*) and gravels (facies *Gt*), as well as reddish-maroon mudstones (facies *Fl* and *Fm*). The detritic deposits appear as massive mudstone layers (architectural element *FF*) and small-sized (sometimes <10 m wide) lateral accretion bars of meandering channels (architectural element *LA*). As a whole, all these deposits correspond to floodplain systems with meandering rivers, represented as small stream channels with low lateral continuity.

At the top of these mainly volcanic stages of the CnH section,other volcanic sequence accounting for 54 m of pyroclastic deposits is found (from 124.6 to 178.8 m in CnH section). This sequence is composed of massive mudstones to fine-grained size ash deposits with microcrystals. They are organised in layers of 2–3 metres, separated by slightly coarser deposits, centimetric ash-beds (facies *bT*) of very fine- to coarse-grain size, or volcanic breccia deposits (facies *mlBr*) containing polymictic clasts of quartz, feldspar, rhyolite, andesite and, occasionally, lithic fragments (Martí, 1996). Calcareous nodules and root traces (facies *P*) are abundant in these ash-flow deposits. Most of the identified ignimbrites show a thickness from 0.5 to 2 m (facies *mT*). However, at 165 m in CnH section, a 13.4 m thick ignimbrite (architectural element *IG*) is present, showing different depositional stages. The base of these deposits comprises a massive purple layer (facies *mLT*) with intraclasts of unvitrified and silicified pumice fall deposits (Martí, 1996; Pereira et al., 2014). The overlying strata show successive levels of subparallel laminated deposits (facies *sT*) with antidune structures (Fig. 3F), representing different volcanic episodes. The thickness of these layers ranges from a subcentimetric level to 60 cm. The complete ignimbritic body is composed of green/white vitreous matrix with small and isolated crystals, including malachite.

Overlying this ignimbrite, at 178.8 m of CnH section, a fluvial-dominated succession is found. . These fluvial deposits are mainly composed of finely laminated and massive mudstones (facies *Fl* and *Fm*; Fig. 3H) sometimes altered to carbonate palaeosols (facies *P*; Fig. 3G), and alternated with sandstone beds (facies *Sh*, *Sl* and *Sm*; Fig. 3I, J). They correspond to overbank and floodplain successions. Despite the presence of massive mudstones (facies *Fm*) in this section, the common mud-cracked surfaces that dominate in the Upper Red Unit (see below) are scarcely represented in the LRU. All these materials are floodplain deposits (architectural element *FF*) with long term exposure, as denoted by the pedogenetic activity and the scarcity of mud-cracks. Occasionally, these deposits exhibit greyish and brownish ignimbrite layers (facies *mT* and *mL*) with long lateral extensions. The thickness of these deposits is very variable, ranging from 0.4 to 3 m, and they also show well-developed palaeosols (facies *P*). At 232.5 m of section CnH, some crevasse splay deposits (architectural element *CS*) appear. They are composed of mudstones and sandstones deposited episodically in a floodplain, arranged in three events with pedogenesis (facies *P*). The whole crevasse splay sequence is 20.2 m thick and integrates three depositional stages of 9.5, 5.2 and 5.4 m. Each event starts with cross-laminated mudstones (facies *Fl*), with wave ripples and bioturbated surfaces: invertebrate traces (especially *Rusophycus*), triopsid and clam shrimp body fossils and plant remains are present (see Text S1). This first interval within each event is the thinner and is interpreted as fluvial deposits. The top of this interval is partially eroded by greyish medium-grained cross-stratified sandstones (facies *Ss*), with greyish mudstones intercalated. Sometimes, these cross-stratified levels contain pebbles, producing local microbreccias (facies *Gt*) without lateral extension. Other sedimentological structures observed in these levels are rip-up clasts and clastic dikes. Finally, the sandstones levels show a decrease of grain size, appearing massive mudstone deposits (facies *Fm* and *Fl*) (Fig. 3H). The uppermost mudstones of each event show pedogenic features, such as calcareous nodules (facies *P*). This part tends to be the thickest within each event, representing sporadic flooding periods where soils developed in nearby areas of a fluvial channel. All these deposits are interpreted as crevasse splay deposits.

These deposits grade vertically into mudstone and sandstone layers, with a progressive increase in grain-size, denoting a higher energy environment. Some metres above (267.5 m of section CnH), we observe a channel composed of cross bedded clast-supported breccias with small (2–3 cm) rounded polymictic pebbles and displaying lateral accretion. The base of these deposits erodes the previous material, and some clastic dikes are preserved. Rip-up clasts show gradation, decreasing in size from the base to the top of the breccias. These structures are interpreted as ribbon point bars of meandering channel deposits (architectural element *LA*).

The meandriform structures are overlaid by polymictic non-graded matrix supported ignimbrite deposits composed of large clasts (up to 10 cm) and without lateral accretion (facies *mlBr*; 287.2 m of section CnH). These ignimbritic breccias give way to a large volcanic sequence dominated by ash fall deposits (facies *mT*) with development of palaeosols (facies *P*). On the top of this volcanic stage (331 m in CnH section) another volcanic event is recorded. Ignimbrites (facies *bT*, *mLT* and *bL*, architectural element *IG*) up to 14.9 m thick and composed of crystal rich layers are recorded. At the base, the ignimbrite shows a massive deposit of purple lapilli-pumice with a chaotic organisation that is progressively cut by successive levels of parallel laminated deposits (facies *sT*), representing different volcanic episodes (Fig. 3C). The thickness of these layers ranges from a subcentimetric level to 80 cm. They show a vitrified matrix and greenish to pinkish colours. In the upper part of the ignimbrite, the vitreous matrix parallel bedded levels change into lapillistone deposits (facies *bL*) with a similar vitreous matrix, showing the last stages of the volcanic event. The following deposits change again to fluvial settings, consisting of crevasse splay deposits (architectural element *CS*) composed of successions of fine-grained sandstones (facies *Ss*, *Sr*, *Sl* and *Sm*), fine laminated and massive mudstones (facies *Fm* and *Fl*), and well developed palaeosols (facies *P*) with presence of reworked fragments of ignimbrites. Some tetrapod ichnites appear in these mudstone deposits (facies *Fm*) at 420 m of the CnH section.

Between 440 and 609 m of the CnH section, deposits comprise ignimbrite breccias (facies *mlBr*) and lapillistones (facies *bL*) (Fig. 3D–E) composed of a vitreous matrix and magmatic crystals. The breccia deposits are clast-supported but matrix-supported breccias containing large-sized angular-shaped clasts (up to 14 cm wide) and without any organisation of grain nor clast size are also present. These layers also do not display any lateral structure, in opposition to point bar deposits, which display a clear lateral accretion. They are interpreted as magmatic material deposited after explosive volcanic activity (Gisbert, 1981; Martí, 1996; Gretter et al., 2015). These volcaniclastic levels tend to become thinner towards the top of the LRU, with a reduction of the clast size between metres 605–627 of the section CnH. These deposits are the uppermost layers of the LRU.

4.1.4. Upper Red Unit (URU)

This unit (Fig. 4A–H) is recorded in the three studied sections (CnH, RM and CR). The entire unit (Fig. 4) is present and has been measured in the sections RM and CR, whereas in the section CnH, the URU is recorded in the upper 73 m of the logged succession. The URU can be divided in two subunits: (1) the lower URU, with its uppermost part characterised by a very fine to medium grain-sized sandstone deposits interlayered with massive or laminated mudstones, and the presence of an interval of septariform nodules at the top, often found in multiple levels; and (2) the upper URU, which consist of a predominantly alternating and cyclic sequence of very fine-grained deposits that continues until the base of the Buntsandstein facies. This division of the URU is the same as documented by Mujal et al. (2017) in a westward, sedimentologically similar area of the Catalan Pyrenees. The lowermost part of the URU is characterised by: (1) a decrease of the grain size with respect to the underlying Lower Red Unit (LRU), starting with reworked conglomerates of the LRU, changing to mudstone and medium grain-sized sandstone in the lower URU and (2) the disappearance of primary volcaniclastic deposits, which are very abundant in the LRU. Progressively, massive mudstones with mud-cracked surfaces (facies *Fm*; Fig. 4B, 4C, 4D, 4E) and sporadic very fine- to fine-grained sandstones (facies *Sh*, *Sl* and *Sm*; Fig 4F) become the dominant lithofacies. Another characteristic element of this unit is the septariform nodules at the top of the lower URU (facies *Ps*), equivalent to the facies 4A2 of Gisbert (1981) (see also Mujal et al., 2017).

At metre 425 of the CnH section, the primary volcanic materials disappear, and the presence of fluvial deposits increases. The clast supported breccias become sporadic, giving way to microconglomerates, sandstones and mudstones. They may still contain volcanic crystals and lithic pebbles resulting from the erosion and reworking of ignimbrites. Nevertheless, the presence of volcanic clasts suddenly stops at the 608.8 m mark of this section and floodplain mudstones (facies *Fm*/*Fl*) become dominant. A similar transitory interval is observed at the base of the RM and CR sections. The lithofacies and architectural elements present in the lower URU are restricted to a few dominant types (Tables 1, 2). Over these breccias, mudstones (facies *Fm*) with mature palaeosols (facies *P*) and thin, sporadic sandstone layers (facies *Sh*, *Sl* and *Sm*) appear. From the base to the top of this subunit a reduction in the grain-size of the sediments is observed, with sandstones being more common closer to the last volcanics of the LRU. Also, the appearance of massive mudstone deposits, sometimes with mud-cracks in the upper parts are recorded. These sedimentary changes reflect a transition between the floodplain deposits of the LRU (architectural element *FF*) and the well-developed playa lake deposits of the upper URU (architectural element *L*). The top of the lower URU is marked by the presence of septariform nodules (facies *Ps*; Fig. 4G, H). They appear in massive mudstones between 2 and 15 m thick. The thickness of these levels is maximum at the

CR section, where the nodules reach up to 40 cm of diameter, while in CnH and RM sections, these nodules rarely exceed 14 cm of diameter.

The top of the lower URU is characterised by a depositional shift. The subsequent deposits are marked by a reduction of the grain-size, being dominated by massive mudstones with mud-cracks (facies *Fm*), defining the upper URU (from the 111.1 to 350 m of RM section and from the 50.3 to 272.8 m of the CR section). Sometimes, these mudstone layers contain carbonate nodules and rhyzoconcretions - products of pedogenetic processes (facies *P*). However, they are less abundant in comparison with the underlying unit. These deposits correspond to shallow ephemeral lacustrine deposits (architectural element *L*), representing massive cyclic mud periodically deposited in wet seasons. After the sedimentation, these environments underwent prolonged desiccation, marked by the development of mud-cracks in cyclic periods of hydration-desiccation. Rarely, these mud-cracked surfaces present lateral changes, showing shallow greyish deposits. Sporadically, the massive mudstone deposits are interbedded by laminated sandy beds of the facies *Fl*, *Sh*, *Sl* and *Sm*. The deposits of the upper URU have a reddish-maroon colour but some of the mud-cracked surfaces display greenish colours because of reduction conditions. The thickness of these deposits generally ranges from 0.5 to 3 m; however, some deposits display successive mud-cracked levels 10–15 cm apart (see the abundant mud-cracked levels between the metres 220-235 of the CR section), sometimes accompanied by fine laminated sandstone (facies *Fl*). Three centimetric deposits are observed that do not display the typical red-bed colour and show an increasing grain-size (at 223 and 254 metres from the RM section and at 246 metres from the CR section) (See Fig. 2). Mineralogical analyses suggest a highly reduced organic-matter-rich fluvial origin for these deposits (see also Text S2 and Table S4). The mud-crack shape is another difference between the lower and upper URU deposits. The lower URU desiccation marks frequently show a shallower gap between mud-cracks, whereas the upper URU deposits display a considerable deeper gap and comparatively rougher surface. These mud-cracked mudstone levels (facies *Fm*) preserve tetrapod footprints, as well as insect and clam shrimp body fossils, invertebrate traces, plant remains, and raindrop impressions in the RM and CR sections.

Although the dominant lithofacies in the uppermost layers of the URU are still mudstone deposits (facies *Fm* and *Fl*), the mudstone levels show changes: (1) the deposits change from the characteristic brown colour of the underlying succession to an orange-reddish colour, (2) the exposed surfaces of facies *Fm* are reduced, becoming pale blue, (3) palaeosols (facies *P*) are almost absent, and (4) grain size gradually increases in the uppermost metres, with some mudstone levels grading to very fined-grained sandstones (facies *Sm*). Fine- to coarse-grained sandstones are not present in this interval. At the top of this unit, the deposits turn into a reddish colour, and the mudstone layers show crystallised veins generated due to tectonic stress. These layers are eroded by the basal conglomerates of the Triassic Buntsandstein facies (facies *Gt*).

4.2. Magnetostratigraphy/magnetic mineralogy

Studied samples present relatively high NRM intensities ranging from 7 mA/m to 20 mA/m and usually produce linear demagnetization trajectories trending toward the demagnetization orthogonal plots after removal of a small viscous secondary overprint at the first demagnetization steps (150 °C and fields below 20 mT) (Fig. 5). Stepwise AF demagnetization after the first heating step does not usually remove much remanence, thus indicating that magnetization is most likely dominated by hematite which unblocks by 680 °C. Reddish sedimentary lithologies exhibit a broad range of unblocking temperatures from about 400 °C up to the maximum applied temperature (Fig. 5A, B, D, E) whereas ignimbrites unblock remanence mostly in the range 610–670 °C (Fig. 5C). Grey sediments unblock remanence below 610 °C (Fig. 5F). All samples have provided negative characteristic remanent magnetization (ChRM) components and taken as primary components indicating reverse polarity throughout the studied succession (Fig. S1 and Table S1). Due to similar bedding attitude in all sections no meaningful fold-test can be performed and statistical parameters both before and after bedding correction are similar (Fig. 6A, B). The mean calculated ChRM component (Dec/Inc = 170.3/-7.1, α_{95} = 7.2) is compatible with data from previous studies (igneous and sedimentary Permian and Triassic rocks) from the Cadí structural unit (Van Dongen 1967) and the Permian reference direction from the Pyrenees (Oliva-Urcia et al., 2012). Although it is recommended a minimum population of 80-100 directions for testing the inclination bias in magnetization, we have attempted the elongation/inclination (E/I) method of Tauxe and Kent (2004), for detection of potential inclination shallowing (Fig. S2C, D). Our limited population of N = 42 suggests only a small shallowing effect of about 2° that would require confirmation with a larger study.

The thermomagnetic curves (magnetic susceptibility vs. temperature curves, Fig. S3) indicate the presence of both magnetite and hematite magnetic phases. The heating curves display a prominent drop of susceptibility between ~500 and 580 °C (Fig. S3A, B) which is consistent with the Curie temperature of magnetite. Susceptibility continues to drop up to 680 °C which denotes the presence of hematite for the red-beds, while its proportion is minor for the greyish beds (Fig. S3C). Thermomagnetic curves are not reversible and new magnetic phases (magnetite, titanomagnetite/maghemite) are created upon heating. Hysteresis measurements for red volcanoclastic lithologies and red sandstones/siltstones usually produce wasp-waisted shaped loops, which is consistent with the presence of both magnetite (low-coercivity) and hematite (high-coercivity) in various proportions (Fig. S2A, B). Grey strata display hysteresis loops dominated by magnetite. IRM acquisition curves and backfield IRM further confirm previous rockmagnetic inferences. For the reddish lithologies IRM do not saturate at the maximum applied field of 1 T and exhibit a "shoulder" at relatively low fields around 0.1 T denoting the magnetite contribution although these samples appear to be dominated by hematite. Conversely, grey lithologies almost saturate at low field (around 01-02 T) (Fig S2C) as is expected for dominance of low-coercivity phases like magnetite. Furthermore, the relatively high coercivity of remanence (Hc) as deduced from the backfield IRM acquisition curves of around 150-300 mT (Fig. S2A, B) singularizes the presence of both magnetite and hematite magnetic carriers. Finally, decomposition of IRM coercivity spectra demonstrate the occurrence of two remanence-bearing components with distinct coercivities (Fig. S2 right panels).

4.3. Systematic ichnology

Batrachichnus Woodworth, 1900

Batrachichnus salamandroides (Geinitz, 1861)

Batrachichnus isp

Fig. 7A–F

Material. Lower Red Unit (LRU): one partial imprint in concave epirelief (IPS126631, at 179 m of CnH section), one footprint with digital scratches not recovered in convex hyporelief (CnH-233-1) and one isolated footprint in convex hyporelief with drag traces (IPS88724, at 236 m of CnH section, Fig. 7E). Lower Upper Red Unit (lower URU): a partial trackway composed of three tracks (one right partial manus-pes sets and one unpaired right manus) in convex hyporelief (Fig. 7A, B), one isolated partial track, and two small-size ichnites (pes and manus, Fig. 7C) with numerous scratches in convex hyporelief in IPS88731 (at 14 m of CR section); three relatively large, rounded digit tips (Fig. 7D) and one smaller imprint associated with swimming traces, in convex hyporelief, in IPS88734 (at 15 m of CR section) (Fig. 7F).

Description. Small to very small digitigrade and semiplantigrade footprints (Table S2). The imprints are slightly wider than long, and the sole and palm impressions are rarely preserved. This morphotype is mostly represented by partial footprints composed of three rounded digit tip imprints, only a few tracks preserve the complete digital and sole/palm impression. Manus tracks (2.31–11.20 mm long, 2.79–12.90 mm wide) are digitigrade to semiplantigrade and tetradactyl. The digit imprints are straight, slender and end in rounded tips, without claw traces. The length of the digit imprints increases from I to III, being digit IV slightly shorter than digit III, and sometimes subequal to digit II in the largest tracks. Imprints of digit IV and digit I show a similar length, being digit I slightly shorter. The deepest digit imprints are those of II and III, which display two phalangeal pads each one. The palm impression is short, has an oval shape and is deeper in the central area, under the imprints of digits II, III and IV, suggesting a median-medial functional prevalence of the autopodia. In some tracks, digit tip imprints are accompanied by narrow, short and sinuous scratches, probably produced by drag movements of the digit tips on the substrate.

All pes impressions are semidigitigrade and incomplete. They are likely longer than the manus imprints, but the absence of complete footprints precludes a confident measuring. Most of the pes imprints are represented by the straight digits I to III, which are in increasing length and rounded digit tips. Pes tracks show slightly longer digit imprints than those of the manus. Pes tracks suggest a medial-median prevalence, because only the first three digits are preserved, with the imprints of digits II and III being the deepest.

The manus-pes set is observable in the partial trackway present in IPS88731. The trackway shows a manus pace angulation of 95º and the manus stride measures 66.21 mm. The pace angulation and stride of pes imprints are impossible to obtain due to the presence only of two consecutive pes tracks. The manus is not overstepped by the pes, being separated by a mean distance of 15.88 mm.

Remarks. The semiplantigrade tetradactyl manus imprints with short and straight digits ending in rounded and clawless digit tips, and the median-medial area more deeply impressed are diagnostic features of the ichnogenus *Batrachichnus* (Gand, 1987; Voigt, 2005; Marchetti et al., 2022b). In upper Palaeozoic–lower Mesozoic terrestrial deposits, tetradactyl imprints with an inferred medial-median functional prevalence of autopodia, relatively short digits and clawless rounded digit tips are diagnostic features of amphibian tracks (Gand, 1987; Voigt, 2005; Voigt et al., 2012; Mujal and Schoch, 2020; Mujal et al., 2020; Marchetti et al., 2022b). These traits are found in two Permian ichnotaxa, *Batrachichnus* and *Limnopus*, sometimes referred as a unique plexus (*Batrachichnus-Limnopus*) when diagnostic features are not recognisable (Tucker and Smith, 2004; Voigt et al., 2011a). Despite the similar morphology between both ichnotaxa, *Batrachichnus* never shows impressions >35 mm long (Haubold, 1970, 1996; Voigt, 2005; Voigt et al., 2011a), and diagnostic features to distinguish them remain in their digit proportions (Voigt, 2005). Imprints assigned to *Batrachichnus* have relatively longer and parallel digit impressions, and the digit IV is markedly longer than digit II in *Limnopus* (Voigt, 2005; Voigt and Haubold, 2015). The described impressions show a digit II markedly larger than IV, and digits II to IV are almost parallelly orientated. Based on these features, the relatively small size, together with the tetradactyl manus with rounded clawless digits allow a referral of these tracks to *Batrachichnus*. The potential trackmakers of *Batrachichnus* have been attributed to small and medium-sized semiaquatic to terrestrial amphibians, including temnospondyls, lepospondyls and “microsaurs” (Haubold and Lucas, 2003; Voigt, 2005; Voigt et al., 2012; Stimson et al., 2012; Petti et al., 2014; Voigt and Haubold, 2015; Cisneros et al., 2020; Allen et al., 2022; Marchetti et al., 2022a).

The herein studied *Batrachichnus* present a low to medium preservation degree (1-2). Also, the *Batrachichnus* specimens show different preservation that results in morphological differences. A major group composed by partial and isolated tracks is observed. Each track is composed of two or three rounded digit tip imprints (IPS126631, CnH-233-1, IPS88724 and IPS88734). Only one complete right manus is observed (IPS88731, 11.20 mm wide and 10.93 mm long, Fig. 7A) related to two semiplantigrade imprints. This imprint preserves part of sole and shows the clear proportions of the digits. It should be remarked that digitigrade imprints seem to be larger than those that are semiplantigrade and they are recovered in the Lower Red Unit and the lower Upper Red Unit. On the other hand, the semiplantigrade imprints seem to be smaller, and they are restricted to the lower Upper Red Unit levels. Those differences probably would be related to different preservation states due to different substrate conditions at the time of impression.

In IPS88731 and IPS88734 a smaller group of ichnites of 2–4 mm manus width and 2–5 mm manus length is preserved. They are related with abundant swimming traces (ichnogenus *Characichnos*, see below). Although most of the swimming scratches and the tracks follow a similar direction, it is difficult to identify complete trackways.

Batrachichnus is one of the most widespread ichnogenus from the upper Palaeozoic that has also been identified in Triassic deposits (Gand, 1987; Voigt, 2012; Schneider et al., 2020; Marchetti et al., 2022a, 2022b). It has been recovered in localities from Europe, northern Africa and North and South America, including northeastern Iberian Peninsula (Voigt and Haubold, 2015; Mujal et al., 2016a), southern France (Gand and Durand, 2006; Marchetti et al., 2022b), northern Italy (Marchetti, 2016; Marchetti et al., 2019b), Poland (Voigt et al., 2012) and Germany (Voigt, 2005), Morocco (Voigt et al., 2011b; Lagnaoui et al., 2014, 2018), in different localities from the USA (Fillmore et al., 2012; Lucas et al., 2014; Voigt and Lucas, 2015; Klein and Lucas, 2021), Canada (Stimson et al., 2012; Allen et al., 2022) and Argentina (Melchor and Sarjeant, 2004). Despite the virtually worldwide distribution of this ichnogenus in terrestrial Permian (and Carboniferous) basins, it is mostly restricted to wet floodplain palaeoenvironments (Voigt, 2005; Voigt et al., 2011a; Mujal et al., 2016a), being absent in other Permian ichnosites of the Iberian area such as Mallorca, suggesting a potential preservational/environmental bias (Matamales-Andreu et al., 2022). The ichnospecies *B. salamandroides* is also recorded in the Artinskian deposits of Lower Red Unit (Peranera Fm.) of the Erillcastell-Estac sub-basin, western Catalan Pyrenees (Voigt and Haubold, 2015; Mujal et al., 2016a, 2018), but there the general morphology differs, being predominantly digitigrade with wider and rounded digits. On the other hand, the studied tracks show several similarities with the upper Guadalupian tracks of Le Luc Basin (Gonfaron, France; Marchetti et al., 2022b), which present a similar length, straight digits with thin rounded and clawless digit tips with a higher pace angulation and a moderate smaller manus stride length. Due to the wide time range of the ichnogenus *Batrachichnus* and the wide taxonomical assignment to small-sized non-amniotes, the morphological variability of this ichnogenus could be explained as similar ichnofossil record produced by different trackmakers. However, the differences may also be related with different locomotion styles of the trackmakers (Leonardi, 1987). Therefore, as *Batrachichnus salamandroides* trackways recovered from the Pyrenean Basin and Le Luc Basin are few and not excellently preserved, more samples are necessary to establish better comparisons between tracks from these basins.

Dromopus Marsh, 1984

***Dromopus* isp.**

Figs. 8A, S4A–E

Material. Lower Red Unit (LRU): A non-recovered partial manus-pes set in concave epirelief (CnH-121-1 and CnH-121-2, Fig. S4E) and one isolated footprint in concave epirelief (Fig. S4A) from Castellar de n'Hug section (IPS126632, at 315 m). Lower Upper Red Unit (lower URU): a manus-pes set (Fig. S4C) and an isolated track in concave epirelief recovered from IPS88733 (at 14 m in CR section); two recovered ichnites in convex hyporelief (Fig. S4B, IPS88734, 15 m in CR section) and three non-related and unrecovered ichnites CR-15-1 (Fig. 8A), CR-15-2 and CR-15-3. Upper Upper Red Unit (upper URU): two slabs from RM section (Fig. S4D, IPS88735 recovered at 129 m and IPS126630 recovered at 205 m) with partial imprints in concave epirelief, one isolated footprint in convex hyporelief (IPS126634) and one unrecovered ichnite (CR-69-1) preserved in concave epirelief on the same surface as the unrecovered *Brontopus antecursor* ichnites from CR section (see below).

Description. Lacertoid-like, pentadactyl asymmetric tracks with long, slender and slightly inward curved digit imprints. Impressions are relatively small, ectaxonic, digitigrade to semiplantigrade and mostly incomplete. Manus and pes footprints are longer (8.31–21.28 mm) than wide (5.90–15.22 mm). The digit imprints usually end with acute triangular claw impressions. The digit I-IV imprints are arranged in a prominent group. On the other hand, the short digit V imprint is directed outwards, straight and more proximally (posteriorly) positioned than the other digit imprints. The relative length of the digits increases from I to IV, digit IV being longer than digit III. Digit V imprint is slightly shorter than digit II. The depth of each digit impression increases towards the tip.

Some well-preserved tracks (Figs. 8A, S4A–C) display phalangeal pad impressions in digits II, III, IV and V. The digit II imprint shows two phalangeal pads, being the distalmost the deepest. Digit III imprint presents three phalangeal pads of which the intermediate one is the deepest. Digit IV imprint presents four phalangeal pads, being the distalmost three the deepest. Digit V imprint has two phalangeal pads. The sole/palm impression is mainly absent or very shallow; when present, it shows a short and convex proximal margin (Fig. S4A, B).

Only two manus-pes sets have been observed. They are composed of partial imprints that preserve digits II-IV (CnH-121-1, 2 and IPS88733). The imprints of the sets show similar orientation without overlapping, and the manus occupy an inner position in comparison with the pes. Footprints of each set display the same morphology, only differentiated by a slightly larger size of the pes than the manus. The manus-pes distance (17.1–73.4 mm) is two times the size of the manus. All these imprints are partial (preserve digital imprints of digits II to IV) and no trackways have been identified. Regarding preservation, some surfaces yield mostly complete ichnites (Figs. 8A, S4A, B), whereas in others only the imprints of digits II, III and IV are preserved (Fig. S4C, D). The isolated nature of the majority of the tracks of this morphotype precludes a clear distinction between manus and pes imprints.

Remarks. The digitigrade to semiplantigrade imprints, the slender digits, their proportions (being digit IV markedly longer than digit III) and arrangement (digits I to IV grouped and inwardly curved and digit V more proximal, laterally-oriented and straight), and the deeper impression of the distal parts of digits II, III and IV, are all diagnostic features of *Dromopus* (Haubold and Lucas, 2003; Voigt et al., 2011b, 2012; Voigt and Lucas, 2015; Marchetti et al., 2021b). Morphological preservation degree of 1.5-2 in most of study tracks.- This ichnogenus shares many features with *Rhynchosauroides* (Marchetti et al., 2017). Usually, in the Permian record, *Dromopus* has been recognised in Cisuralian to Lopingian outcrops, whereas *Rhynchosauroides* is identified in Lopingian and younger strata. Therefore, the ichnological record of both ichnotaxa overlaps at the late Permian. Therewith, *Rhynchosauroides* show a heteropodial manus-pes set with a markedly shorter digits impressions and more semiplantigrade tracks in manus impression. On the other hand, *Dromopus* shows a high degree of homopody resulting from an only slightly smaller size of the manus (Voigt et al., 2012, Marchetti et al., 2021b, 2022b) and a pes with lesser curved digit imprints than in

Rhynchosauroides (Marchetti et al., 2019c). Another difference to the latter is that Digit V in *Dromopus* is relatively long (as digit II) and is outward oriented, in comparison with *Rhynchosauroides*, which presents a short digit V (similar to digit I) with a backward orientation(Marchetti et al., 2022b). Finally, the manus-pes set of the herein study presents a manus positioned in front of the pes imprint, with slightly more deeply impressed pes track, which is a feature more related to *Dromopus* imprints (Valentini et al., 2007; Marchetti et al., 2017). Therefore, in spite of the similarity between the ichnogenus *Dromopus* and *Rhynchosauroides*, the observed features in the herein studied ichnites best match the description of *Dromopus*.

This ichnotaxon is the most common and widespread one, together with *Batrachichnus*, in Pennsylvanian (upper Carboniferous) to Cisuralian (lower Permian) strata (Schneider et al., 2020; Marchetti et al., 2021b, 2022a). *Dromopus* shows an extremely wide extramorphological variation. Tridactyl and didactyl footprints, mostly complete footprints, lacking digit I imprint, or showing digit IV as an isolated tip imprint have been recovered in localities from Mallorca (Matamales-Andreu et al., 2022), France (Gand and Durand, 2006), Italy (Marchetti et al., 2015a, 2015b, 2017, 2019b, 2019c 2020a), United Kingdom (Haubold and Sarjeant, 1973), Germany (Voigt, 2005, 2012), Poland (Voigt et al., 2012), USA (Lucas and Hunt, 2005; Lucas et al., 2014; Voigt et al., 2015) and Morocco (Voigt et al., 2011a, 2011b). Focusing on the Pyrenean Basin, *Dromopus* is recorded in the Peranera Formation (Voigt and Haubold, 2015; Mujal et al., 2016a). Also, westwards from the study area a similar morphotype assigned to a *Dromopus-Rhynchosauroides* plexus from the uppermost Permian facies has been reported (Mujal et al., 2017). *Dromopus* has been related to small- to medium-sized araeoscelid diapsids and non-varanodontine varanopids (Gand, 1988; Haubold and Lucas, 2003; Voigt, 2005; Gand and Durand, 2006; Spindler et al., 2019, Marchetti et al., 2021a, 2022a).

b

Hyloidichnus Gilmore, 1927

Hyloidichnus isp.

Figs. 8B–C, S5A–C

Material. Lower Red Unit (LRU): a right manus-pes set in convex hyporelief (IPS135414, at 232m in the CnH section) and one isolated footprint in concave epirelief (Fig. S5C) from CnH section (IPS126632, at 315 m in the CnH section). Lower Upper Red Unit (lower URU): one isolated unrecovered footprint (CR-15-5) and one ichnite related to scratches (IPS126633) in concave epirelief from CR section (at 15 m). Upper Upper Red Unit (upper URU): a manus-pes set and two partial imprints unrecovered (Figs. 8C, S5A) in concave epirelief (RM-177-14 to RM-177-17) accompanied by few scratches, two partial imprints in recovered concave epirelief in IPS88735 from RM section (at 129 m) (Fig. S5B).

Description. Footprints of a quadrupedal tetrapod with plantigrade to digitigrade and pentadactyl imprints. The manus and pes imprints show a marked heteropody in shape, but presenting wide digit tips in both, which may show curved and inwardly rotated claw traces (Fig. 8C). In some samples, digits are only represented by isolated tip imprints, separated from the basal part of the digit (Figs. 8C, S5B).

Manus are semiplantigrade and pentadactyl imprints, wider (26.82 mm) than long (18.00 mm). The digit imprints are slender and slightly hourglass-shaped, showing a slight inward rotation and rounded digit tip imprints. Digit imprints show an increase in length from I to IV, being digit III subequal to digit IV. Digits I and II are the deepest. Digit V is outward rotated, its length is like that of digit I and it is only preserved by the tip. Only the distal part of the palm imprint is preserved, being deeper under digits II, III and IV. The divarication between digits I and V is >100º. The manus is rotated inwards and anteriorly positioned with respect to the pes.

Pes tracks are larger than manus tracks and they show a similar length and width proportions (19.68–26.83 mm long, 22.68–27.74 mm wide). Digits are straight and relatively thinner and longer in comparison with those of the manus tracks. Imprints of digits I-IV are in increasing length, being digit IV slightly longer than digit III, and digits II and I markedly shorter. Imprints of digits I and II are deeper, indicative of a medial functional prevalence of the autopodium, like in the manus. Digit V imprint is rotated outwards, being as long as digit I. The sole imprint is deeper under the imprints of digits I and II, reducing progressively in digit III and being absent in digit IV and V. The sole has a rounded shape with a shallow proximal convex margin, being more complete and better preserved than the palm imprint. The mean divarication angle of the digits also varies in manus and pes tracks being higher in the manus (Table S2).

In the manus-pes sets of the studied material, two main arrangements have been observed. In most cases the pes is not overstepping the manus imprints, but in one specimen (IPS135414, Fig. 8C) the pes digit imprints are overprinting the palm impression.

Remarks. Pentadactyl semiplantigrade footprints with straight, hourglass-shaped long and elongated digits terminate in pointed tips, heteropody with an inward rotated manus smaller than pes, digit proportions and digit I as long as digit V are all diagnostic features of *Hyloidichnus* (Haubold, 1971; Gand, 1987; Gand and Durand, 2006; Marchetti et al., 2013, 2020b; Marchetti, 2016; Mujal et al., 2016a; Voigt and Lucas, 2018; Marchetti et al., 2013, 2020b; Logghe et al., 2021; Matamales-Andreu et al., 2021b, 2022, 2023). Although not very common, overstepping of the manus tracks by the corresponding pes imprints has been observed elsewhere, which might be related to different locomotion styles (walking vs. running; see Logghe et al., 2021; Matamales-Andreu et al., 2023).This ichnogenus shares many features, like the shape of the digits, the short palm/sole and the rotated digit tips with *Varanopus, Notalacerta* and *Merifontichnus* (Gand and Durand, 2006; Voigt et al., 2010; Voigt and Haubold, 2015; Marchetti et al., 2020b).In comparison with *Varanopus*, the relatively short digit V is a diagnostic character of *Hyloidichnus*, against the markedly longer digit V (similar to digit III) (Voigt et al., 2010). Additionally, the marked inward rotation of the manus impressions and the straight digit impressions are also diagnostic features of *Hyloidichnus* that differ from *Varanopus* (Voigt et al., 2005, 2010). Moreover, the ichnogenus *Notalacerta* is characterised by inwardly curved slender digits imprints and a relatively longer pedal digit V imprint, close to the length of digits II and III (Lucas et al., 2004; Marchetti et al., 2020b). Finally, the assignment to *Merifontichnus* is also discarded, because this ichnogenus is characterised by homopody with tracks wider than long, and slender and radiating digit imprints (Gand et al., 2000; Gand and Durand, 2006; Marchetti, 2016).

This ichnotaxon has been recovered in different Cisuralian outcrops of the Iberian area, in the Pyrenean Peranera Formation (Voigt and Haubold, 2015; Mujal et al., 2016a), in the Cantabrian Mountains (Gand et al., 1997) and in the Balearic Islands (Matamales-Andreu et al., 2021b, 2022, 2023). Similarly, *Hyloidichnus* is a well-known ichnotaxon from France (Gand, 1987; Gand and Durand, 2006; Logghe et al., 2021; Marchetti et al., 2022b), Italy (Marchetti et al., 2013, 2015a, 2015b; Marchetti, 2016), Morocco (Voigt et al., 2010; Hminna et al., 2012; Zouicha et al., 2021; Rmich et al., 2023), USA (Lucas et al., 2014) and Argentina (Melchor and Sarjeant, 2004).

The herein described specimens present a morphological degree of 1.5-2. The studied footprints are markedly smaller than other *Hyloidichnus* described in the Permian of the Pyrenean Basin. The samples described by Voigt and Haubold (2015) and Mujal et al. (2016a) measure between 41 and 75 mm of length, a similar size observed in other peri-Tethyan Permian tracks: in Mallorca (Matamales-Andreu et al., 2022) or in the Ikakern Formation in Morocco (Voigt et al., 2010; Rmich et al., 2023). However, they are similar in size with those from Menorca (Matamales-Andreu et al. 2021b), some of them measuring between 22.8–26.4 mm of length. Also, the small size of these samples is similar to some *Hyloidichnus* imprints from other peri-Tethyan basins, such as the Guadalupian locality of Gonfaron (France) (Logghe et al., 2021; Marchetti et al., 2022b).

Hyloidichnus has been referred to captorhinid producers (Haubold, 1971, 2000; Voigt et al., 2010; Marchetti, 2016, Logghe et al., 2021, Matamales-Andreu et al., 2021b). Voigt et al. (2010) considered that *Hyloidichnus* could be referred to more derived captorhinomorphs, the moradisaurines, a correlation supported by the recent study of Matamales-Andreu et al. (2023). The presence of *Hyloidichnus* in the Pyrenean Basin and the recent discoveries of moradisaurines in Mallorca and Menorca islands, as well as captorhinomorph tracks (Liebrecht et al. 2017, Matamales-Andreu et al., 2021b, 2022, 2023), reinforce the common presence of these herbivorous reptiles in the Permian equatorial latitudes of Pangaea (Logghe et al., 2021; Matamales-Andreu et al., 2021b, 2022).

Brontopus **Heyler and Lessertisseur, 1963**

Brontopus antecursor **(Ellenberger, 1983)**

Figs. 9A–D

Material. Upper Upper Red Unit (upper URU): A mud-cracked surface including two isolated footprints and a trackway composed of six complete manus-pes sets in concave epirelief (RM-177-1 to RM-177-14; Fig. 9A–C) and two isolated manus footprints in concave epirelief (RM-207-1, 2) of RM section. One isolated pes (CR-69-1), a muddy surface with 12 imprints in concave epirelief (CR-69-2 to CR-69-13) (Fig. 9D) and one isolated footprint (CR-69-14) from the same stratigraphic level of CR section. All material remains in situ (uncollected).

Description. The trackway (RM-177-1 to RM-177-12) is composed of six manus-pes sets, both manus and pes being pentadactyl and plantigrade imprints. The ichnites are relatively large and show high expulsion rims. The impressions show a general rounded, smoothed shape except those affected by mud-cracks, which may present more angular areas. The median-lateral area of the tracks is the deeper area, denoting a median-lateral prevalence of the autopodia. A clear heteropody is distinguished between manus-pes impressions, with manus tracks smaller than pes tracks. Manus imprints are larger than wide, being 82.32–148.87 mm long and 82.21–117.26 mm wide, and sometimes they are preserved as round digit tip imprints separated from the palm imprint. Digit imprints are nearly equidistantly distributed around the palm impression, showing a length increase from digit I to III, a subequal length in digits III and IV, and a shorter digit V, subequal to digit II. Digits II-IV imprints are subparallel and compose a compact group anteriorly oriented. Digits I, II and III imprints may show a slightly inward rotation. The digit I imprint is sometimes not preserved. The palm impression is oval with a deep extension of the outer (lateral) part of the heel, which produces a narrowing in the proximal part of the imprint. The metacarpal-phalangeal portion is the most impressed area of the manus imprints, occupying the inner and central part of the palm, suggesting a median functional prevalence of the autopodium.

Pes imprints are 113.32–268.45 mm long and 95.70–132.65 mm wide, being notably larger than manus tracks. Pes tracks are divided in three areas, from distal to proximal: digit imprints (with rounded tips and sometimes separated from the sole), the distal part of the sole imprint (which is the deepest area) and the proximal part of the sole (the heel impression) (as extensive as the sole but markedly shallower). Pes digit imprints are slightly larger and slenderer than those of the manus, though their relative lengths are similar, as is the divarication between all of them (20–25º between each digit). Sometimes, digits are preserved as rounded impressions separated from the sole imprint by an expulsion rim, similar to what is observed in some manus tracks. The distal sole impression is very compact and anteroposteriorly elongated. The distal sole imprint also presents a markedly narrowing process in the inner part of the impression, developing into the narrow connection between the distal sole and the heel in the lateral (outer) side, and gives an asymmetric hourglass shape to the imprint. The heel impression is usually of similar size to the distal sole; however, this area varies markedly in the pes tracks from different specimens. In the pes tracks of RM section, the heel impression is of similar size to the distal sole impression, and they show a marked inward elongation regarding the rest of the footprint. Conversely, the heel impressions preserved in the CR section do not show any inner elongation, and their proportions change, being the heel impression area of the CR tracks smaller than the distal sole depression. As in manus tracks, the metatarsal-phalangeal portion is the deepest part of the pes imprints.

In the trackway of RM (external width: 420–450 mm), manus and pes are alternately arranged, with the manus impressions located at the height of the heel impression of the pes track of the subsequent set. Both pes and manus tracks are subparallel to the trackway midline, being pes impressions slightly inward rotated. The mean distance between manus and pes tracks in a set is of 290 mm. The stride length of the tracks has a mean value of 960 mm, and the pace angulation comprises values between 115º and 125º (see Table S3).

Remarks. The presence of short digit imprints with a relatively wide sole and palm imprints with a paw-like shape are distinctive features of *Dimetropus*, *Brontopus*, *Dolomitipes* and *Dicynodontipus* (Marchetti et al., 2019c; Matamales-Andreu et al., 2021c). The relatively large size, the paw-like shape of the tracks, the parallel tracks to the trackway midline, the mesaxonic and the short digital impressions (sometimes point-shaped) located equally around the distal area of the imprint are diagnostic features of *Brontopus* (Gand et al., 2000; Marchetti et al., 2019c). The high pace angulation (higher than 90º), the pes proportions (notably longer than wide) with hourglass shape, as well as the relatively small manus in comparison with the pes (marked heteropody), allow a referral of the ichnites from RM and CR to *Brontopus antecursor* (Ellenberger, 1983; Gand et al., 2000; Marchetti et al., 2019c).

The quadrupedal trackway, with pentadactyl, plantigrade with a general median-lateral functional prevalence inferred for the autopodia footprints is characteristic of synapsid tracks (Mujal et al., 2020). The *B. antecursor* footprints herein studied are similar to other ichnotaxa with heteropodal impressions presenting elongated/hourglass-shape and attributed to synapsid trackmakers: *Brontopus giganteus* (Gand et al., 2000; Valentini et al., 2009; Marchetti et al., 2019c), *Dolomitipes* (De Klerk, 2002; Marchetti et al., 2017), *Dimetropus osageorum* (Sacchi et al., 2014; Romano et al., 2020), and *Dicynodontipus* (Rühle von Lilienstern, 1944; De Klerk, 2002; Da Silva et al., 2012; Francischini et al., 2018). The main difference between *B. antecursor* and *B. giganteus* is the oval shape (instead of hourglass shape) of the sole, the lower pes/manus proportions, the similar length and width of the pes (instead longer than wider) and the lower pace angulation of *B. giganteus* (Marchetti et al., 2019c). On the other hand, *Dolomitipes* is characterised by manus impressions markedly wider than long with a similar size or even larger than pes impressions, differing from *B. antecursor* and the herein studied specimens, thus precluding their assignation to *Dolomitipes*. In *Dimetropus osageorum* the manus-pes set show a primary overlapping, with the manus placed closely in contact or at a very short distance to the pes, and a slightly lesser pace angulation (110º in manus and 112º in pes). Their digits are short and robust. Digit IV is the longest, followed by digit III and II. Digit I shows inward rotation and extremely short length and digit V present a similar length to digit I (Sacchi et al., 2014; Romano et al., 2020). Instead, the ichnites of RM section show longer and thinner digits, located equally around the sole and palm impressions, and the digit V imprint is located closer to digits II, III and IV (i.e., more distally located); therefore, these tracks cannot be attributed to *D. osageorum*. Other Permian synapsid tracks reported from the Catalan Pyrenees and Mallorca have been assigned to *Dimetropus leisnerianus* (Mujal et al., 2016a; Matamales-Andreu et al., 2022), as well as to cf. *Dimetropus* isp. (Matamales-Andreu et al., 2021c). However, the relatively short digits, marked mesaxony, strong heteropody with hourglass-shaped pes, slender and relatively long of the studied ichnites differ from the Iberian record of *Dimetropus*. Other potential synapsid tracks in the Pyrenean Basin are the Morphotype I, from the uppermost Permian site of Coll de Terrers (Mujal et al., 2017), which may be similar to *Dolomitipes* (Mujal et al., 2020; Marchetti et al., 2022b). The quadrupedal ichnites of this morphotype display manus markedly wider than long with thin phalangeal impressions and rounded digit tip imprints, pes tracks overstep manus tracks, and the pace angulation (90º) is lower than in *B. antecursor* and the herein studied trackway. Also, the herein described footprints differ in some diagnostic features of *Dicynodontipus*, such as the strong mesaxony, the wider than long manus imprint, which is larger and deeper than the pes impression, and the low pace angulation (Marchetti et al., 2019c). According to all these observations, all ichnites from RM and CR sections can be confidently assigned to *B. antecursor*. The morphological preservation degree is 2-2.5.

B. antecursor has been identified from the French Guadalupian red-beds of La Lieude Formation and Pradineaux Formation (Ellenberger, 1983; Gand et al., 1995, 2000; Gand and Durand, 2006; Marchetti et al., 2019c). It was firstly described by Ellenberger (1983), who originally named these tracks as *Eodicynodontipus antecursor*. Recently, Marchetti et al. (2019c) synonymised *Eodicynodontipus* with *Brontopus*, but maintaining the material as a distinct ichnospecies, proposing the combination *B. antecursor*. Marchetti et al. (2019c) also synonymised the ichnotaxa *Pseudopithecus recurvidigitus*, *Eocynodontipus sibleyrasi*, *Planipes caudatus* and *Planipes brachydactylus* to *Brontopus antecursor*. *Brontopus* has been related to dinocephalian trackmakers, a therapsid group dominant in the Guadalupian (Day et al., 2015; Lucas, 2017, 2018). Due to the high pace angulation and the manus-pes proportions, *Brontopus antecursor* has been related to anteosaurid dinocephalian therapsids (Marchetti et al., 2019c).

Pachypes Leonardi et al. 1975

Pachypes isp.

Figs. 9E, S6A–B

Material. Upper Upper Red Unit (upper URU): a right footprint not recovered (RM-209-1; Fig. 9E) and a partial and eroded unrecovered imprint (RM-209-2; Fig. S6A) in concave epirelief, both from RM section. A left partial manus not recovered in concave epirelief (CR-69-15) from CR section (Fig. S6B).

Description. Pentadactyl, semiplantigrade footprints wider (78.28–95.70 mm) than long (60.40–93.30 mm). The impression shows quadrangular shape and is mesaxonic, being the palm area under digits II, III and IV the deepest. Digit imprints are sturdy, relatively short, and with rounded tips. The digit length increases from II to IV, which are rotated inwards, and these imprints compose a tight group, showing superposition at their base. Digit IV imprint is the longest and deepest. Digit I imprint is subequal in size to digit II, but the former shows a clear proximal orientation. Digit V imprint is the shortest and the thinnest, markedly proximally positioned. All digits are relatively short and are located closely to the palm/sole imprint, which is elliptical, wider than long and deeply impressed. The distal margin of the palm/sole imprint shows a semicircular embayment.

Remarks. Relatively large-sized, pentadactyl, mesaxonic and semiplantigrade tracks with sturdy superimposed digits with rounded terminations that increase from II to IV, the small size of the digit V and deep sole/palm impression are diagnostic features of *Pachypes* (Leonardi et al., 1975; Valentini et al., 2008; 2009; Marchetti et al., 2021a). Currently, three ichnospecies are considered valid for this ichnogenus: *P. dolomiticus*, *P.*

ollieri and *P. loxodactylus* (Marchetti et al., 2021a). They are distinguished by the thickness of the digit imprints, their organisation in the track and the level of superimposition, being *P. dolomiticus* the most compact morphotype, *P. loxodactylus* the larger and more spaced one, and *P. ollieri* presenting an intermediate configuration (Marchetti et al., 2021a). The morphological preservation degree of the studied samples is 1-1.5, hindering ichnospecific identification. The ichnite RM-209-2 shows tightly close, markedly thick and superimposed digits, and the digit V is proximally positioned and relatively small and thin in comparison with the rest. All these features are found in *P. dolomiticus* and *P. ollieri*. Due to the poor preservation, the absence of a complete manus-pes set and a trackway impression, and the absence of clear diagnostic features, an open ichnospecific identification is favoured.

Pachypes has already been documented in the Lower Red Unit (Cisuralian) of the Pyrenean Basin, attributed to *P. ollieri* (Marchetti et al., 2021a). On the other hand, morphotype II described in the uppermost Permian of Coll de Terrers (Mujal et al., 2017) shares features with this ichnotaxon, such as the slightly wider than long and relatively large tracks with robust digits, but with a bit more superimposed and thicker digits in the manus track. The ichnogenus *Pachypes* as a whole shows a wide chronological and geographical range, found from the Cisuralian to the Lopingian of different countries such as Spain (Mujal et al., 2017, Marchetti et al., 2021a; Matamales-Andreu et al., 2022), France (Gand and Durand, 2006), Italy (Valentini et al., 2009; Dalla Vecchia et al., 2012; Marchetti et al., 2017, 2019b, 2020a, 2021a), Germany (Buchwitz et al., 2017; Marchetti et al., 2019d), Russia (Gubin et al., 2003; Surkov et al., 2007; Valentini et al., 2009), Morocco (Voigt et al., 2010), Niger (Smith et al., 2015) and the USA (Lucas and Hunt, 2005; Marchetti et al., 2021a). *Pachypes* has been related with medium-large size pareiasauromorph parareptiles as probable trackmakers (Valentini et al., 2009; Marchetti et al., 2021a).

Characichnos **Whyte and Romano 2001**

Characichnos **isp.**

Figs. 7A, 7F

Material. Lower Upper Red Unit (lower URU): Associated with *Batrachichnus* (see above). Two recovered slabs (IPS88731, at 14 m from the base of CR section, and IPS88734 at 15 m of CR section) with numerous scratches in convex hyporelief (Fig. 7B).

Description. The slabs IPS88731 and IPS88734 contain relatively small, narrow, straight and clawless digit scratches. Their size is relatively small, each scratch showing a mean width of 3-5 mm and variable length. Each track is composed of three elongated and parallel traces (scratches) produced by the drag of digits II, III and IV. Each scratch shows a deeper area in the same limit. Slab IPS88734 has six scratches, however, no clear groups of tracks nor trackways can be identified.

Remarks. Elongated and parallel scratches are interpreted as drag traces of digits during swimming locomotion (Whyte and Romano, 2001). These scratches are the most representative ichnological remains of slab IPS88734. Due to the dimension of these swimming traces, the rounded and clawless ending of the scratches, and the presence of a complete footprint with similar proportions in the same slabs, traces can be assigned to *Characichnos* (Whyte and Romano, 2001). Previous swimming traces recovered from the Peranera Formation (Pyrenean Basin) were related to *Batrachichnus salamandroides* (Mujal et al., 2016a), and similar occurrences were recorded in Italy (Petti et al., 2014), Morocco (Voigt et al., 2011b), Germany (Voigt, 2005) and the USA (Lucas et al., 2011b). Some samples of the Italian Orobic Basin (Petti et al., 2014) show a clear transition from swimming to walking tracks in submerged environments. Considering previous interpretations, *Characichnos* tracks herein studied are assigned to natation tracks. Due to the similar size between *Characichnos* and *Batrachichnus* in the slabs IPS88731 and IPS88734, and the previous association between both ichnotaxa in other Permian basins, they were probably impressed by a similar trackmaker.

5. Discussion

5.1. Palaeoenvironmental and climatic interpretation

Sedimentation of the Lower Red Unit in the Catalan Pyrenees has been interpreted to be undertaken in mass flows, stream floods and meandering channels (Nagtegaal, 1969; Gisbert, 1981; Speksnijder, 1985; Gretter et al., 2015; Mujal et al., 2016a, 2018; Lloret et al., 2018) (Fig. 10). In the same way, sedimentary rocks of the Castellar de n'Hug sub-basin correspond to fluvial settings, represented by floodplain massive deposits, meandering channel and crevasse splay deposits, the latter containing all the tetrapod ichnites recovered from the LRU (Figs. 2, 10; Text S2 and Table S4). This fluvial system is similar to other LRU successions of the Catalan Pyrenees (Mujal et al., 2016a, 2018). However, this landscape changes in surrounding contemporaneous basins. The Artinskian–lower Kungurian succession of La Sagra Formation, in the Cantabrian Mountains, is interpreted as floodplain deposits exposed to drier intervals (Gand et al., 1997; Juncal et al., 2016; López-Gómez et al., 2019). In the Balearic Islands, the Cisuralian successions of the Bec de s'Àguila Formation (Mallorca) and P1 unit in Menorca are composed of alluvial fan deposits (Matamales-Andreu et al., 2021b; 2022). Finally, the Lodève Basin shows fluvial systems with sheetflood and braided rivers in strata of the Rabejac Formation (Sakmarian) (Schneider et al., 2006) that evolve into playa systems with calcareous desiccated surfaces in upper Cisuralian sections corresponding to the Salagou Formation (Artinskian–Kungurian) (Schneider et al., 2006; Michel et al., 2015). Furthermore, the fluvial deposits of the LRU herein studied are interlayered with volcaniclastic deposits. In fact, the volcaniclastic materials characterise this unit, being the most abundant of the CnH section of the LRU succession. These volcanic deposits are common in the Carboniferous–Permian basins of SW Europe (Lago et al., 2004; Dallagiovanna et al., 2009; Maino et al., 2012; Gretter et al., 2015). In the Catalan Pyrenees, volcanism was product of an extensive tectonic dynamics in intramountain basins (Martí, 1996). Its chronology ranges from the Pennsylvanian to the Guadalupian, and resulted in a wide range of igneous rocks, from calc-alkaline pyroclastic rhyolitic-andesitic rocks to alkaline basalts (Martí, 1996, 2022; Pereira et al., 2014).

Mujal et al. (2018) suggested a semi-arid to arid climatic conditions with strong seasonal precipitations for the Lower Red Unit red-beds of the Erillcastell-Estac sub-basin. The LRU in the Castellar de n'Hug sub-basin records similar climatic conditions, highlighted by the presence of reddish colour, calcic pedotypes, the presence of calcified roots (rhizoliths) and green mottles, which reinforce the palaeoclimatic interpretation for the climatic tendency described by Mujal et al. (2018) (see also Lloret et al., 2021a). Also, Nagtegaal (1969) proposed a relatively flat and laterally extended landscape and Martí (1996) proposed a possible local modification of the weather due to the injection of water vapour during the explosive eruptions in the Lower Red Unit of the Pyrenees, as supported also by Mujal et al. (2018).

Regarding the Upper Red Unit (Fig. 11), it documents the described transition to arid conditions in central and southern European Permian deposits (Roscher and Schneider, 2006; Durand, 2008; Tabor and Poulsen, 2008; De la Horra et al., 2012; Mujal et al., 2017). In the study area, the palaeoenvironments of the first deposits after the disappearance of volcaniclastic material from the LRU correspond to playa lakes with ephemeral lacustrine water bodies (lowermost deposits of the lower URU). Desiccation marks are present in this sub-unit, becoming more common in the uppermost deposits, and are only interrupted locally by small channels (Figs. 2, 4, 11). However, the desiccation marks in the mudstone surfaces do not reach their maximum maturity until the upper URU deposits. This is indicated by the mud-crack patterns, with Y-junctions that give an hexagonal shape characteristic of repeated dry-wet cycles (Bohn et al., 2005; Goehring et al., 2010; Goehring, 2013). Some mudstone surfaces preserve a shallow depression in their limits with a smooth surface, whereas other mud-crack surfaces show considerable deeper gap space and a rougher surface. These differences suggest a major desiccation exposition in the deeper gap spaced mud-cracks. Despite both structures are observed along the URU succession, the first one is less common in the upper URU deposits, suggesting the aridification process and the increased seasonality of this sub-unit in comparison with the lower URU.

In other Permian localities of the Catalan Pyrenees, the limit between the lower and upper URU is recorded as a paraconformity or sedimentary hiatus between both units (Gisbert, 1981; Mujal et al., 2017). In the present study, this hiatus is recorded between the coarser sedimentary systems in the lower URU, immediately followed by mature ephemeral lake deposits of mudstone in the upper URU. This depositional shift reflects a transition to finer-grained sediments, an increasing seasonality and the dominance of mud-cracked surfaces. This boundary is also accompanied by the appearance of septariform nodules in mudstones. These septariform nodules have been also described as indicators of the limit between the lower and upper URU in the Cadí sub-basin (Coll de Terrers locality) considered as middle–late Permian (Mujal et al., 2017). Also, Gisbert (1981) described mudstones with septarian nodules (facies 4A2) as typical facies from the Upper Red Unit of the Catalan Pyrenees. According to this author, these facies would represent peripherical areas of the playa system with ephemeral lacustrine water bodies with an intense formation of pedogenetic nodules, which develop into septariform nodules with nucleus composed of volcanic tuffs. The presence of septariform nodules in the lower/upper URU boundary (facies *Ps*), could be explained by a progressive environmental change from peripherical floodplain deposits with ephemeral shallow lakes with a higher humidity, to a central area of a playa system, with more developed mud-cracks.

Finally, the upper URU is composed of cyclic alternations, from massive mud-cracked surfaces of mudstones or very fine-grained sandstones (usually at the top of the mud-cracked level; see also Text S2 and Table S4). These facies coincide with the description of the facies 4A1 (Gisbert, 1981), typical from the URU deposits of the central areas of the Pyrenean Basin (Gisbert, 1981; Speksnijder, 1985; Gretter et al., 2015; Mujal et al., 2016b, 2017). They correspond to playa deposits in distal alluvial systems distinguished by wide mud-cracks produced by recurrent desiccation events, with temporal lacustrine environments (Gisbert, 1981). The environmental interpretation of these deposits in the western European Permian basins is that they are correlated to floodplain events under a monsoonal regime (Roscher et al., 2011). The wet season would be represented by the accumulation of massive levels of mudstones, whereas the dry season would result in the formation of shallow ephemeral lacustrine ponds and mud-cracks that denote prolonged subaerial exposition and desiccation (Gisbert, 1981; Gisbert et al., 1985; Mujal et al., 2016b, 2017). Another Permian succession of the peri-Tethyan region with a similar depositional system is the Salagou Formation (Lòdeve Basin, France), showing cyclic deposits of massive clayish siltstones with abundant desiccation cracks (Schneider et al., 2006). These deposits were firstly interpreted as Wuchiapingian (late Permian). However, recent studies suggest an age of topmost Artinskian–basal Roadian (Michel et al., 2015). Also, the sediments of La Lieude Formation (overlying the Salagou Formation) dated as Roadian–Wordian, were deposited in fluvio-alluvial environments. Similar depositional conditions are observed in the Permian basins of Provence (France). While the Le Motte Formation (late Capitanian) includes playa deposits with desiccation cracks and interlayered green coloured levels, the Pradineaux Formation (Roadian–Wordian) preserve streamflow and ignimbrite deposits (Durand, 2008; Marchetti et al., 2022b). In the Iberian Ranges, even though they present slightly younger deposits, similar climatic conditions are observed (De la Horra et al., 2012). These sedimentary materials, more related to alluvial fan, braided river and floodplain systems of the Alcotas Formation (Capitanian–Wuchiapingian), denote a climatic alternation of wet to arid/semiarid long-term phases (De la Horra et al., 2012). Similar Guadalupian and Lopingian successions recording marked seasonality have been reported from the central Pangaean Moradi Formation of Niger (Tabor et al., 2011; Smith et al., 2015; Looy et al., 2016) and the southern Pangaean Karoo Basin of southern Africa (Gastaldo et al., 2005, 2015; Belica et al., 2017; Marchetti et al., 2019c).

5.2. Vertebrate fauna of the Pyrenean Basin

In agreement with the sedimentological record, the vertebrate ichnological assemblage herein reported shows changes along the stratigraphic succession, revealing two different tetrapod ichnoassociations: a first one in the Lower Red Unit (LRU) and lower Upper Red Unit (lower URU), and a second one in the upper Upper Red Unit (upper URU).

The tetrapod ichnoassociation observed in the LRU and the lower URU is characterised by the presence of non-amniote tracks, and the absence of medium- to large-sized tracks (Figs. 10, 11). In the LRU, it includes *Batrachichnus* (IPS126631), *Dromopus* (CnH-112-1, CnH-112-2 and IPS126632) and *Hyloidichnus* (IPS126632). Tracks are scarce and are mostly restricted to floodplain fine-laminated mudstones (facies *Fl*) corresponding to crevasse splay deposits. On the other hand, these layers contain sometimes bioturbated surfaces, with invertebrate traces (especially *Rusophycus*), triopsid and clam shrimps body fossils and plant remains (see Text S1). However, the presence of ichnofossils is scarce in the studied LRU unit, including several laminated deposits barren of fossils, which are usually replaced by deposits of higher-energetic fluvial events (with presence of facies *Sl*, *Ss* and *Sm*). The fine-laminated mudstone beds with biotic activity represent rhythmical fluvial deposits of seasonal water bodies with suitable conditions for the establishment of relatively complex ecosystems, including small- to medium-sized tetrapods.

Tetrapod tracks of this first ichnoassociation are more abundant in the lower URU (14–18 m from the CR section), including *Batrachichnus*, *Dromopus* isp., *Hyloidichnus* isp. and *Characichnos* isp. This ichnofauna appears related to shallow subaquatic conditions (fine-laminated mudstones with presence of unidirectional ripples, related with playa-lakes, facies *Fl*) and to dry subaerial conditions (massive mud-cracked mudstones, facies *Fm*). Firstly, some surfaces with poorly developed mud-cracks preserving *Dromopus* isp. and *Hyloidichnus* in concave epirelief appear at the 14 m of the CR section. While *Hyloidichnus* is only represented by partial impressions, *Dromopus* is represented by numerous specimens, though always isolated. In a fine-laminated mudstone layer (just one metre above, at 15 m of the CR section), some samples (IPS88731 and IPS88734) preserve ichnites in convex hyporelief in surfaces without mud-cracks. These samples are rich in small-sized and medium-sized *Batrachichnus* and preserve partial imprints of large-sized *Batrachichnus* and *Dromopus*. Also, numerous relatively small *Characichnos* isp. traces appear in both samples, being related with the small-sized *Batrachichnus*, as also identified elsewhere (Lucas et al., 2011b; Petti et al., 2014; Mujal et al., 2016a). Despite the environmental transition from a floodplain into a playa-lake recorded in the lower URU, these shallow aquatic bodies share the ichnodiversity with the layers with tetrapod imprints observed in the LRU, showing that small-sized temnospondyls were the dominant tetrapods, together with small-sized reptiles. Instead, the drier levels were dominated by small- to medium-sized reptiles. This is somewhat similar to the palaeoenvironmental distribution identified by Mujal et al. (2016a) on the LRU of the western Catalan Pyrenees (see further discussion below). The ichnofauna and facies in the lower URU suggest a change: despite the presence of temnospondyl tracks (*Batrachichnus* and *Characichnos*) in the shallow water bodies, the dry land ichnofaunas start to be dominated by tracks of non-diapsid eureptiles (*Hyloidichnus*) and araeoscelid diapsids and non-varanodontine varanopids (*Dromopus*), but with the absence of “pelycosaur”-grade synapsids (Schneider et al., 2020; Marchetti et al., 2022a).

The palaeodiversity and palaeoenvironmental settings of this first tetrapod ichnoassociation are similar to the ones discussed by Mujal et al. (2016a, 2018) in fluvial deposits interbedded with volcaniclastic material westwards. These authors described an ichnoassemblage divided in two environmentally constrained ichnoassociations. In comparison with these ichnoassociations, the ichnites of the first ichnoassociation described in this work are related to floodplain deposits, represented by *Batrachichnus*, *Dromopus* and deformed impressions of *Hyloidichnus*. The ichnoassociation 1 described by Mujal et al. (2016a) and the LRU ichnites of the present work remark the presence of fauna dependent of water bodies, dominated by amphibians and small amniote tracks. Although reduced, the composition of the first ichnoassociation herein described generally fits with the ichnofauna related with the *Erpetopus* biochron (Lucas, 2007; Fillmore et al., 2012; Voigt and Lucas, 2013, 2018; Schneider et al., 2020; Marchetti et al., 2022b).

The absence of large-sized animal might be as a result of an environmental bias. Large-sized ichnotaxa (e.g., *Limnopus*, *Ichniotherium*, *Amphisauropus*, *Hylodichnus*, *Tambachichnium* and *Dimetropus*) are common in Cisuralian ichnoassemblages from European, northern African, and North American strata (Gand and Durand, 2006; Voigt and Lucas, 2018; Schneider et al., 2020; Marchetti et al., 2021b). In fact, *Limnopus* and *Dimetropus* have been recorded in the Artinskian deposits of the Erillcastell-Estac sub-basin (Mujal et al. 2016a). In the same way, it is striking the lack of non-amniote tracks in similar palaeoenvironments from the Cisuralian of Mallorca (Matamales-Andreu et al., 2022). As discussed by these authors, this could be related to a palaeoenvironmental/taphonomic bias of non-amniote tracks linked to their low preservation potential due to the settings where the trackmakers inhabited (see also Mujal and Schoch, 2020). In the same way, these ecosystems were likely under wet conditions, allowing for the establishment of large non-amniotes. The absence of these ichnogenera in the studied area could be related to an environmental bias, maybe due to more localised drought areas that would preclude the presence of these faunas. The increasing arid conditions during the Cisuralian probably affected the diversity of the Iberian tetrapod faunas, particularly non-amniotes such as temnospondyls, with a life cycle related to water bodies (Schoch, 2014). However, the presence of large-sized non-amniotes has been described in strongly seasonal dry environments, such as the Nigerian temnospondyls from the Moradi Formation (central Pangaea) (Sidor et al., 2005; Steyer et al., 2006; Smith et al., 2015).

Therefore, even though the composition of the first tetrapod ichnoassociation described in this work matches with the general tendencies of the earliest *Erpetopus* biochron in the northern hemisphere, the present results might be biased due to the scarce fossil material available and the possible presence of environmental and taphonomical biases. Regarding the presence of non-diapsid reptiles, the absence of "pelycosaurs", but still a dominant presence of small- to medium-sized temnospondyls in the lower URU, tentatively points this first tetrapod ichnoassociation to the late *Dromopus*–early *Erpetopus* biochrons (Artinskian–Kungurian; Voigt and Lucas, 2018; Schneider et al. 2020).

Regarding the second tetrapod ichnoassociation in the study area, the fluvial settings present in the LRU and lower URU disappear in the upper URU, giving path to ephemeral playa-lake conditions. This ichnoassociation contains footprints correlated to large-sized amniotes (*Brontopus antecursor* and *Pachypes*), but sporadic small- to medium-sized amniotes (represented by *Dromopus* and *Hyloidichnus*) are also present in extensively exposed surfaces with mud-cracks (Figs. 11, 12). These deposits correspond to shallow water playa-lakes (architectural element *L*). As the previous ichnoassociation, this second one also contains bioturbated surfaces, with invertebrate trace fossils identified as *Acripes* and *Rusophycus*, triopsid and clam shrimps body fossils, an insect wing and plant remains. This ichnoassociation is also characterised by the absence of non-amniote tracks. As abovementioned, the *Erpetopus* biochron starts with the decrease of non-amniote taxa (Schneider, 2020; Marchetti et al., 2022a). Also, in the late Cisuralian–early Guadalupian, a replacement took place among tetrapod communities, affecting non-amniotes as well as to-date "pelycosaur" dominated assemblages due to the radiation of great number of parareptiles and therapsid taxa (Lucas, 2017, 2018; Marchetti et al., 2022a). This event could be recorded in the upper URU by the presence of *Brontopus* and *Pachypes*.

The main distinctive feature of this second ichnoassociation is the presence of large therapsid and parareptile tracks. Based on osteological record, a global faunal transition in the Guadalupian is related to basal synapsid extinction and the worldwide radiation of therapsids, especially dinocephalians, as also supported by the footprint record (Lucas, 2006, 2009a, 2018; Day et al., 2015; Voigt and Lucas, 2018; Marchetti et al., 2019c; Schneider et al., 2020). The *Brontopus* tracks herein reported are an early record of this transition in the Iberian Peninsula. This ichnogenus is correlated to dinocephalian anteosaurids as most probable trackmakers (Marchetti et al., 2019c). These therapsids were the most widespread and abundant tetrapods during the Guadalupian, and their presence ceased at the end this epoch, in the dinocephalian extinction event (Lucas, 2009a; Day et al., 2015; Voigt and Lucas, 2018; Schneider et al., 2020). *Brontopus antecursor* was first recovered in French Guadalupian deposits (Gand et al., 1995; Gand and Durand, 2006), where it is accompanied by other relatively large tapinocephalid-titanosuchid dinocephalian therapsid and parareptile tracks, like *Brontopus giganteus* and *Pachypes ollieri*, respectively (Marchetti et al., 2019c, 2021a).

The presence of *Hyloidichnus* and *Dromopus* seems to be a constant along the Permian succession of the study area. It has been suggested that sauropsids (including *Hylodichnus* trackmakers) underwent an expansion during the late Artinskian in fluvio-lacustrine, aeolian and near-marine environments of North America and Europe, replacing non-amniote faunas, due to their better adaption to dry environments (Modesto et al., 2016, Marchetti et al., 2019e, 2022a; Matamales-Andreu et al., 2021b). Following the aridification and increasing seasonality trend observed in Permian deposits of the Pyrenean Basin, the environmental conditions likely favoured the establishment of these reptiles in the floodplains. This could explain the increasing presence of captorhinomorph tracks (especially *Hyloidichnus*) in the URU. Fern fossil remains have been recovered in the upper URU (see Text S1), being a possible food source for these animals. In view of the *Hyloidichnus* tracks previously described in the Cisuralian deposits of the Erillcastell-Estac sub-basin (western Catalan Pyrenees), the studied tracks show a similar size to those described by Voigt and Haubold (2015) and Mujal et al. (2016a), the latter ichnites being slightly larger. On the other hand, in comparison with other *Hyloidichnus* tracks recovered in nearby Permian basins, the herein studied tracks are similar in shape and size to those from Menorca, southern France and Morocco (Voigt et al., 2010; Logghe et al., 2021, Marchetti et al., 2022b; Matamales-Andreu et al., 2021b).

On the other hand, *Dromopus* is the most wide-spread ichnogenus along the succession, appearing in dry and subaquatic palaeoenvironments. This suggests an adaptative capability of the trackmakers to proliferate in different environments, or that this ichnogenus includes a wide variability of trackmakers, possibly explaining the wide distribution of this ichnotaxon (Schneider et al., 2020; Marchetti et al., 2022a, 2022b). In the same way as in the first ichnoassociation, the presence of *Dromopus* and *Hyloidichnus* in the upper URU tends to be more related to moist and soft substrates, sometimes accompanied by digit drags. This fact could be due to a taphonomic bias. After the track impression, these soft surfaces would have undergone a process of dehydration, manifested by desiccation marks and raindrop impressions. In hard substrates, the small sized trackmakers would not be heavy enough to produce imprints or these would disappear in the desiccation process, and only large-sized tetrapods would be recorded. Thus, the lesser abundance of *Dromopus* between the first ichnoassociation (the most abundant ichnogenus) in comparison with the second one (only three partial specimens) is most probably related to preservation/taphonomy biases.

On a wider perspective, the reduction of non-amniote ichnotaxa, the appearance of therapsids and parareptiles and the constant presence of eureptile tracks in the stratigraphically youngest deposits seem to follow the ichnodiversity trend of Permian basins of the peri-Tethys (Voigt et al., 2010; Mujal et al., 2017; Schneider et al., 2020; Marchetti et al., 2017, 2019b, 2022b). These widespread ichnoassemblages in equatorial areas of Pangaea would result from faunistic corridors (areas with more humid conditions than the general arid settings) that allowed tetrapods to spread. In the same way, the previous (ichno-) faunas to the Guadalupian extinction event observed in intramountain basins of the peri-Tethyan region, tend to show similar compositions (Schneider et al., 2020), highlighting the continuous communication in continental basins of eastern equatorial Pangaea.

5.3. Age constraints of the Permian succession

The analysed Permian succession is >900 metres long. Magnetostratigraphic samples from the Lower Red Unit (LRU) and the Upper Red Unit (URU) indicate that this succession falls within the Kiaman Reverse Superchron, which lasted from the late Carboniferous to the late Guadalupian (~318–267 Ma; Hounslow and Balabanov, 2018; Brandt et al., 2021). This wide age range is further constrained by previous radiometric dating (Pereira et al., 2014) and biostratigraphic data.

Pereira et al. (2014) proposed an age of 290–286 Ma (Artinskian) for a Castellar de n'Hug ignimbrite of the LRU (Fig. 2), corresponding to the Artinskian. Most of the analysed crystals of the ignimbrite located in the LRU at 350 m of the base of CnH section yield a mean age of 290 ± 1.2 Ma, with the youngest population of crystals providing an age of 283.4 ± 1.9 Ma (late Artinskian–early Kungurian), as the best estimation of depositional age (Pereira et al., 2014; Fig. 2), suggesting a late Cisuralian age (late *Dromopus*–early *Erpetopus* biochron; Figs. 2, 10, 13).

The presence of *Brontopus* in the upper URU suggests a Guadalupian age for this succession in the study area, because this ichnotaxon is considered a biomarker of this epoch, defining the *Brontopus* sub-biochron (Marchetti et al., 2019d; Schneider et al., 2020). A Guadalupian age for the upper URU in the Castellar de n'Hug sub-basin contrasts with the age inferred westwards in the Pyrenean Basin (Mujal et al., 2017).Therefore, the URU might have different ages in different regions (likely, sub-basins) of the Pyrenean Basin, even if the stratigraphic stacking and palaeoenvironmental succession in general is similar (e.g., Gisbert, 1981; Speksnijder, 1985; Mujal et al., 2017). This might be supported by the fact that other palaeogeographically close Permian basins such as the French Lodève and Provence basins are built up by very similar sedimentological successions but of clearly different Permian ages (e.g., Schneider et al., 2006; Durand, 2008; Michel et al., 2015; Logghe et al., 2021; Marchetti et al., 2022b).

Based on previous considerations, together with the absence of characteristic ichnotaxa from the late Guadalupian–Lopingian, such as *Dolomitipes, Karoopes, Capitosauroides, Dicynodontipus*, *Rhynchosauroides* or archosauromorph ichnogenera (Schneider et al., 2020; Marchetti et al., 2022b), we propose a Roadian–early Wordian age (early–middle Guadalupian) for the upper URU tetrapod ichnoassociation in the studied succession. These chronologies fit with the nearest recorded dinocephalian ichnoassemblages in La Lieude Formation (Lodève Basin, France) and Pradineaux Formation (Provence, France) (Zheng et al., 1992; Durand, 2008). Finally, the upper URU deposits stratigraphically above the last occurrence of *Brontopus*, which are >100 m thick, still show reverse polarity and are therefore likely still within the Kiaman Superchron, thus suggesting a middle Wordian age at most.

6. Conclusions

A detailed stratigraphical and sedimentological study of the Permian succession from the central-eastern Catalan Pyrenees (NE Iberian Peninsula) has allowed to characterise the two depositional units. Firstly, the Lower Red Unit (LRU, Artinskian–Kungurian) is composed of volcaniclastic material interbedded with alluvial deposits. Secondly, the Upper Red Unit (URU, Kungurian–Guadalupian) can be divided in two depositional stages, a coarser sub-unit more related to peripheral floodplain deposits (lower URU) and a second sub-unit deposited under monsoonal conditions consisting of a repetition of flooding events exposed to drier conditions in a playa-lake system (upper URU). It is possible to identify an aridification process from the fluvial setting at the base of the succession to seasonal water bodies gradually becoming more common and exposed during prolonged periods of desiccation at the top.

The tetrapod fossil record of the Pyrenean Basin shows the evolution of the faunas during the Cisuralian and the Guadalupian, as observed elsewhere. Two different tetrapod ichnoassociations have been identified: (1) an older ichnoassociation composed of tracks and trackways of small-medium size related to amphibian-eureptile trackmakers inhabiting shallow water bodies of fluvial environments of the LRU and lower URU; this ichnoassociation corresponds to the early *Erpetopus* biochron (Artinskian–Kungurian ages); (2) a second tetrapod ichnoassociation, recorded in shallow lacustrine deposits in the upper URU, dominated by tracks of medium-large size animals related to dinocephalian therapsids, but also with the presence of eureptile and parareptile tracks. The presence of *Brontopus antecursor* allows to assign the second ichnoassociation to the *Brontopus* sub-biochron, suggesting an early–middle Guadalupian age. In comparison to other Permian red-beds of the Iberian Peninsula, and despite the similar lithologies and palaeoenvironmental settings observed, the ichnoassociations denote different faunistic compositions. The whole ichnoassemblage shows a similar composition to that of other Permian peri-Tethyan basins, suggesting a close contact and interchange of the tetrapod faunas within this palaeoregion.

Acknowledgements

We acknowledge support from the CERCA programme (ICP) from the Generalitat de Catalunya and the research projects "Evolució dels ecosistemes amb faunes de vertebrats del Permià i el Triàsic de Catalunya" (ref. 2014/100606), "Evolució dels ecosistemes durant la transició Paleozoic–Mesozoic a Catalunya" (ref. CLT009/18/00066) and "El final d'una Era i el sorgiment dels ecosistemes moderns: les faunes de vertebrats del Carbonífer al Triàsic de Catalunya (ref. ARQ001SOL-167-2022 - CLT0009_22_000020) based at the ICP and financially supported by the Departament de Cultura (Generalitat de Catalunya). Our special thanks to Dr. Jean-Sébastien Steyer (MNHN, Paris), Dr. Romain Garrouste (MNHN, Paris), Dr. Mireia Plà and Daniel Falk (University College Cork) for fieldwork support. We thank Dr. Josep Gisbert (University of Zaragoza, Zaragoza) for sharing stratigraphic logs for comparison. We thank Dr. Lorenzo Marchetti (MfN, Berlin) for sharing a 3D model of *Brontopus antecursor* for comparison. Thanks to Terradron (Jaume Balagué) for UAV drone aerial images. Joan Casòliva and the Natural Park of Cadí-Moixeró are acknowledged for logistic support and permission for field actions. We thank Dr. David P. Groenewald (ICP) for a proofread of the manuscript. We thank Roc Olivé for the artwork, supported by a project of the Fundación Española para la Ciencia y la Tecnología (Ministerio de Ciencia e Innovación, Spanish Government). C.J.S. is granted by a FI AGAUR fellowship (ref. 2020 FI_B 00472) funded by the Secretaria d'Universitats i Recerca del Departament d'Economia i Coneixement de la Generalitat de Catalunya and the European Social Fund. The present manuscript is part of the PhD thesis of C.J.S. within the Geology PhD program of the Universitat Autònoma de Barcelona. This work is part of the Ramon y Cajal grant to J.F. [RYC2021-032857-I] financed by

MCIN/AEI/10.13039/501100011033 and the European Union «NextGenerationEU» / PRTR. C.J.S. and J.F. are members of the consolidated research group (GRC) 2021 SGR 01184. J.F. acknowledges support of the grant PID2020-117118GB-I00 funded by Agencia Estatal de Investigación (MCIN/AEI/10.13039/501100011033). A.B. is supported by a María Zambrano Fellowship (funded by Ministerio de Universidades of the Spanish Government, the Plan de Recuperación, Transformación y Resiliencia and the European Union «Next Generation». A.B. acknowledges the support of the RNM 190 (Basin Analysis) group of the Universidad the Granada. We acknowledge the reviewers Dr. Lorenzo Marchetti and Dr. Abdelouahed Lagnaoui for comments and suggestions, and Prof. Howard Falcon-Lang for editorial work.

Data Availability

Datasets (raw data and 3D models) related to this article can be found at MorphoSource (ark:/87602/m4/517940, ark:/87602/m4/517937, ark:/87602/m4/517933, ark:/87602/m4/517930), an open-source online 3D data repository hosted by Duke University Research Computing.

For review purposes the following link provide access to the raw data and 3D models: https://www.morphosource.org/projects/000515081/temporary_link/xSQfZBS8Ygz9XTwB3YfHMxhp?locale=en

References

Allen, L.F., Stimson, M. R., King, O.A., Norrad, R.E., Lucas, S.G., Mann, A., Hinds, S.J., Park, A.F., Calder, J.H., Maddin, H., Montplaisir, M., 2022. A *Batrachichnus salamandroides* trackway from the Minto Formation of central New Brunswick, Canada: implications for alternative trackmaker interpretations. Atl. Geol. 58, 239–260. https://doi.org/10.4138/atlgeo.2022.010

Barrachina, A., Martí, J., 1986. Las ignimbritas de Castellar N'Hug (Pirineo Catalán). Acta Geol Hisp. 21, 561–568.

Belica, M.E., Tohver, E., Pisarevsky, S.A., Jourdan, F., Denyszyn, S., George, A.D., 2017. Middle Permian paleomagnetism of the Sydney Basin, Eastern Gondwana: testing Pangea models and the timing of the end of the Kiaman Reverse Superchron. Tectonophysics 699, 178–198. https://doi.org/10.1016/j.tecto.2016.12.029

Benton, M.J., Ruta, M., Dunhill, A.M., Sakamoto, M., 2013. The first half of tetrapod evolution, sampling proxies, and fossil record quality. Palaeogeogr. Palaeoclimatol. Palaeoecol. 372, 18–41. https://doi.org/10.1016/j.palaeo.2012.09.005

Bohn, S., Pauchard, L., Couder, Y., 2005. Hierarchical crack pattern as formed by successive domain divisions. Phys. Rev. E. 71, 046214

Brandt, D., Ernesto, M., Constable, C., 2021. Consistent and contrasting aspects of the geomagnetic field across epochs with distinct reversal frequencies revealed by modeling the Kiaman superchron. Geochem. Geophys. 22, e2021GC009866. https://doi.org/10.1029/2021GC009866

Branney, M.J., Kokelaar, P., 2002. Pyroclastic density currents and the sedimentation of ignimbrites. Geol. Soc. Lond. Mem. 27, London. 192 pp.

Broutin, J., Gisbert, J., 1985. Entorno paleoclimático y ambiental de la flora stephano-autuniense del Pirineo catalán. In: Compte rendus Dixième International de Stratigraphie et de Géologie du Carbonifère, pp. 53–66.

Buchwitz, M., Luthardt, L., Marchetti, L., Trostheide, F., Voigt, S., Schneider, J.W., 2017. A Middle to Late Permian tetrapod tracksite from northern Germany. In Bordy, E. (ed.) 2nd conference of continental ichnology, Nuy Valley, Western Cape, South Africa, Abstract Book, 15 pp.

Cisneros, J.C., Day, O.M., Groenenwald, J., Rubidge, B., 2020. Small footprints expand Middle Permian amphibian diversity in the South African Karoo. Palaios 35 (1), 1–11. https://doi.org/10.2110/palo.2018.098

Cortesogno, L., Cassinis, G., Dallagiovanna, G., Gaggero, L., Oggiano, G., Ronchi, A., Seno,S., Vanossi, M., 1998. The post-Variscan volcanismin the Late Carboniferous–Permian sequences of Ligurian Alps, Southern Alps and Sardinia. Lithos 45, 305–328.

Cortesogno, L., Gaggero, L., Ronchi, A., Yanev, S., 2004. Late orogenic magmatism andsedimentation within Late Carboniferous to Early Permian basins in the Balkan terrane (Bulgaria): geodynamic implications. Int. J. Earth. Sci. 93, 500–520.

Da Silva, R.C., Sedor, F.A., Fernandes, A.C.S., 2012. Fossil footprints from the Late Permian of Brazil: an example of hidden biodiversity. J. South Am. Earth Sci. 38, 31–43.

Dalla Vecchia, F.M., Ponton, M., Muscio, G., 2012. Two new ichnosites from the Permo-Triassic of Carnic Alps (Friuli Venezia Giulia, NE Italy). Gortania 34, 41–50.

Dallagiovanna, G., Gaggero, L., Maino, M., Seno, S., Tiepolo, M., 2009. U-Pb zircon ages for post-Variscanvolcanism in the Ligurian Alps (northern Italy). J. Geol. Soc. London 166, 101–114. https://doi.org.10.1144/001676492008-027

Day, M.O., Rubidge, B.S., 2021. The Late Capitanian Mass Extinction of terrestrial vertebrates in the Karoo Basin of South Africa. Front. Earth Sci. 9:631198. https://doi.org/10.3389/feart.2021.631198Day, M.O., Ramezani, J., Bowring, S.A., Sadler, P.M., Erwin, D.H., Abdala, F., Rubidge, B.S., 2015. When and how did the terrestrial mid-Permian mass extinction occur? Evidence from the tetrapod record of the Karoo Basin, South Africa. Proc. Royal Soc. B. 282 (1811), 1–8. https://doi.org/10.1098/rspb.2015.0834

De Klerk, W.J., 2002. A dicynodont trackway from the Cistecephalus assemblage zone in the Karoo, east of Graaff-Reinet, South Africa. Palaeont. Afr. 38, 73–91.

De la Horra, R., Galán-Abellán, A.B., López-Gómez, J., Sheldon, N.D., Barrenechea, J.F., Luque, F.J., Arche, A., Benito, M.I., 2012. Paleoecological and paleoenvironmental changes during the continental Middle-Late Per-mian transition at the SE Iberian Ranges, Spain. Glob. Planet. Change 94–95, 46–61. https://dx.doi.org/10.1016/j.gloplacha.2012.06.008

Demathieu, G.R.S., Torcida Fernández-Baldor, F., Urién Montero, P., Pérez-Lorente, F., 2008. Icnitas de grandes vertebrados terrestres en el Pérmico de Peña Sagra (Cantabria, España). Libro de resúmenes. XXIV Jornadas de la Sociedad Española de Paleontología, 28–29.

Dunne, E.M., Close, R.A., Button, D.J., Brocklehurst, N., Cashmore, D.D., Lloyd, G.T., Butler, R.J., 2018. Diversity change during the rise of tetrapods and the impact of the ‘carboniferous rainforest collapse'. Proc. Royal Soc. B. 285(1872), 20172730. https://doi.org/10.1098/rspb.2017.2730

Durand, M., 2008. Permian to Triassic continental successions in southern Provence (France): an overview. Boll. Soc. Geol. Ital. 127, 697–716.

Ellenberger, P., 1983. Sur l'intérêt paléontologique de la dalle à pistes de la Lieude (commune de Mérifons, Hérault, France). Société de la Protection de la Nature du Languedoc Roussillon Bulletin 1, 1–10.

Falkingham, P.L., 2012. Acquisition of high resolution 3D models using free, open-source, photogrammetric software. Paleontol. Electron. 15, 1–15. https://doi.org/ 10.26879/264

Fillmore, D.L., Lucas, S.G., Simpson, E.L., 2012. Ichnology of the MississippianMauch Chunk Formation, eastern Pennsylvania. Bull. N. M. Mus. Nat. Hist Sci. 54, 136.

Fortuny, J., Bolet, A., Sellés, A.G., Cartanyà, J., Galobart, À., 2011. New insights on the Permian and Triassic vertebrates from the Iberian Peninsula with emphasis on the Pyrenean and Catalonian basins. J. Iber. Geol. 37(1), 65–86. https://doi.org/10.5209/rev_JIGE.2011.v37.n1.5

Francischini, H., Dentzien-Dias, P., Lucas, S.G., Schultz, C.L., 2018. Tetrapod tracks in Permo–Triassic eolian beds of southern Brazil (Paraná Basin). PeerJ 6, e4764. https://doi.org/10.7717/peerj.4764

Gand, G., 1987. Les traces de Vertébrés tétrapodes du Permien français (paléontologie, stratigraphie, paléoenvironnements). Dissertation thesis, Université de Bourgogne, Dijon.

Gand, G., 1988. Les traces de vertébrés tétrapodes du Permien francais. PhD Thesis Université de Bourgogne Edition Centre des Sciences de la Terre, Dijon.

Gand, G., Durand, M., 2006. Tetrapod footprint ichno-associations from French Permian basins. Comparisons with other Euramerican ichnofaunas. Geol. Soc. Spec. Publ. 265(1), 157–177. https://doi.org/10.1144/GSL.SP.2006.265.01.07

Gand, G., Demathieu, G., Ballestra, F., 1995. La palichnofaune de vertébrés tétrapodes du Permien supérieur de l'Estérel (Provence, France). Palaeontogr. Abt. 235, 97–139.

Gand, G., Kerp, H., Parsons, C., Martínez-García, E., 1997. Palaeoenvironmental and stratigraphic aspects of the animal traces and plant remains in Spanish Permian red beds (Peña Sagra, Canta-brian Mountains, Spain). Geobios 30(2), 295–318.

Gand, G., Garric, J., Demathieu, G., Ellemberger, P., 2000. La palichnofaune de vertébrés térapodes du Permien Supérieur du bassin de Lodève (Languedoc-France). Palaeovertebrata 29,1–82.

Gascón, F., Gisbert, J., 1987. La evolución climática del Stephaniense, Pérmico y Buntsandstein del Pirineo catalán en base al estudio de paleosuelos. Cuadernos de Geología Ibérica 11, 97–114.

Gastaldo, R.A., Adendorff, R., Bamford, M., Labandeira, C.C., Neveling, J., Sims, H., 2005. Taphonomic Trends of Macrofloral Assemblages Across the Permian–Triassic Boundary, Karoo Basin, South Africa. Palaios 20 (5), 479–497. https://doi.org/10.2110/palo.2004.P04-62

Gastaldo, R.A., Kamo, S.L., Neveling, J., Geissman, J.W., Bamford, M., Looy, C.V., 2015. Is the vertebrate-defined Permian-Triassic boundary in the Karoo Basin, South Africa, the terrestrial expression of the end-Permian marine event? Geology 43, 939–942.

Geinitz, H.B., 1861. Dyas oder die Zechsteinformation und das Rothliegend: Die animalischen Ueberreste der Dyas (Vol. 1). Engelmann.

Gilmore, G.W., 1927. Fossil footprints from the Grand Canyon II. Smithson. Misc. Collect. 80, 1–78.

Gisbert, J., 1981. Estudio geológicopetrológico del Estefaniense-Pérmico de la sierra del Cadí (Pirineo de Lérida): Diagénesis y Sedimentología. PhD Thesis, Universidad de Zaragoza, Spain.

Gisbert, J., 1986. Els temps tardihercinians. A: Santa-nach, P. (Ed.), Història Natural dels Països Cata-lans, Geologia I. Editorial Enciclopèdia Catalana, Barcelona, 197–242.

Gisbert, J., Martí, J., Gascón, F., 1985. Guía de la excursión al Stephaniense, Pérmico y Triásico inferior del Pirineo catalán. II Coloquio de estratigrafía y paleogeografía del Pérmico y Triásico de España, La Seu d'Urgell, 1–78.

Goehring, L., 2013. Evolving fracture patterns: columnar joints, mud cracks and polygonal terrain. Philos. Trans. Royal Soc. 371, 202120353, http://dx.doi.org/10.1098/rsta.2012.0353

Goehring, L., Conroy, R., Akther, A., Clegg, W.J., Routh, A.F., 2010. Evolution of mud-crack patterns during repeated drying cycles. Soft Matter 6, 3562–3567. https://doi.org/10.1016/j.palaeo.2022.111181

Gretter, N., Ronchi, A., López-Gómez, J., Arche, A., De la Horra, R., Barrenechea, J.F., Lago, M., 2015. The Late Palaeozoic-Early Mesozoic from the Catalan Pyrenees (Spain): 60 Myr of environmental evolution in the frame of the western peri-Tethyan palaeogeography. Earth Sci. Rev. 150, 679−708.

Gubin, Y.M., Golubev, V.K., Bulanov, V.V., Petuchov, S.V., 2003. Pareiasaurian tracks from the Upper Permian of Eastern Europe. Paleontol. J. 37, 514–523.

Haubold, H., 1970. Versuch der Revision der Amphibien-Fährten des Karbon und Perm. Freiberger Forschungshefte C 260, 83–11.

Haubold, H., 1971. Ichnia Amphibiorum et Reptiliorum fossilium. In: Wellnhofer, P. (Ed.). Encyclopedia of Paleoher-petology 18. Fischer Verlag, Stuttgart and Portland, 124 pp.

Haubold, H., 1996. Ichnotaxonomie und Klassifikation von Tetrapodenfährten aus dem Perm. Hallesches Jahrbuch für Geowissenschaften B 18, 23–88.

Haubold, H. 2000. Tetrapodenfährten aus dem Perm‑Kenntnisstand und Progress 2000. Hallesches Jahrbuch für Geowissenschaften B 22, 1–16.

Haubold, H., Lucas, S.G., 2001. Die Tetrapodenfährten der Choza Formation (Texas) unddas Artinsk-Alter der Redbed-Ichnofaunen des Unteren Perm. Hallesches Jahrbuch für Geowissenschaften. B 23, 79–108.

Haubold, H., Lucas, S.G., 2003. Tetrapod footprints of the lower permian choza formation at Castle Peak, Texas. PalZ. 77, 247–261. https://doi.org/10.1007/bf03006940

Haubold, H., Sarjeant, W., 1973. Tetrapodenfährten aus dem Keele und Enville Groups (Permokarbon; Stefan und Autun) von Shropshire und South Staffordshire, Großbrittannien. Zeitschrift der Dtsch. Gesellschaft., Berlin 1, 895–933.

Haubold, H., Stapf, H., 1998. The Early Permian tetrapod track assemblage of Nierstein, Standenbühl Beds, Rotliegend, Saar-Nahe Basin, SW-Germany. Hallesches Jahrbuch für Geowissenschaften B 20, 17–32.

Heyler, D., Lessertisseur, J., 1963. Pistes de Tetrapodes permiens dans la region de Lodève (Herault). Mem. Mus. Natl. Hist. Nat. 11, 125–221.

Hminna, A., Voigt, S., Saber, H., Schneider, J.W., Hmich, D., 2012. On a moderately diverse continental ichnofauna from the Permian Ikakern Formation (Argana Basin, Western High Atlas, Morocco). J. African Earth Sci. 68, 15–23. https://doi.org/10.1016/j.jafrearsci.2012.03.011

Hoffman, R., 2016. The end-Permian mass extinction. In: Mángano, M.G., Buatois, L.A. (Eds.), The Trace-Fossil Record of Major Evolutionary Events. Precambrian and Paleozoic Vol. 1. Springer, Dordrecht, pp. 325–349.

Hounslow, M.W., Balabanov, Y.P., 2018. A geomagnetic polarity timescale for the Permian, calibrated to stage boundaries. Geol. Soc. Spec. Publ. 450 (1), 61. https://doi.org/10.1144/SP450.8

Izquierdo-Llavall, E., Casas-Sainz, A., Oliva-Urcia, B., Scholger, R., 2014. Palaeomagnetism and magnetic fabrics of the Late Palaeozoic volcanism in the Castejón-Laspaúles basin (Central Pyrenees). Implications for palaeoflow directions and basin configuration. Geol. Mag. 151, 777−797.

Juncal, M., Diez., J.B., Broutin, J., Martínez-García, E., 2016. Palynoflora from the Permian Sotres Formation (Picos de Europa, Asturias, Northern Spain). Span. J. Palaeontol. 31 (1), 85−94.

Kirschvink, J.L., 1980. The least-squares line and plane and the analysis of palaeomagnetic data. Geophys. J. Int. 62(3), 699–718.

Klein, H., Lucas, S.G., 2021. The Triassic tetrapod footprint record. Bul.. N. M. Mus. Nat. Hist. Sci. Bul. 83,1–194.

Koymans, M.R., Langereis, C.G., Pastor-Galán, D., van Hinsbergen, D.J.J., 2016.

Paleomagnetism.org: An online multi-platform open source environment for paleomagnetic data analysis. Comput. and Geosci. 93, 127–137. https://doi.org/10.1016/j.cageo.2016.05.007

Koymans, M.R., van Hinsbergen, D.J.J., Pastor-Galán, D., Vaes, B., Langereis, C.G., 2020. Towards FAIR Paleomagnetic Data Management Through Paleomagnetism.org 2.0. Geochem. Geophys. 21(2), e2019GC008838. https://doi.org/10.1029/2019GC008838

Lagnaoui, A., Voigt, S., Saber, H., Schneider, J.W., 2014. First occurrence of tetrapod footprints from Westphalian strata of the Sidi Kassem Basin, Central Morocco. Ichnos 21:4, 223–233. https://doi.org/10.1080/10420940.2014.955096

Lagnaoui, A., Voigt, S., Belahmira, A., Saber, H., Klein, H., Hminna, A., Schneider, J.W., 2018. Late carboniferous tetrapod footprints from the Souss basin, western High Atlas mountains. Morocco. Ichnos 25 (2–3), 81–93. https://doi.org/10.1080/10420940.2017.1320284

Lago, M., Arranz, E., Pocovi, A., Gale, C., Gil-Imaz, A., 2004. Permian magmatism and basin dynamics in the southern Pyrenees: a record of the transition from late Variscan transtension to early Alpine extension. In: Wilson, M., Neumann, E.-R., Davies, G.R., Timmerman, M.J., Heeremans,M., Larsen, B.T. (Eds.), Permo-Carboniferous Magmatism and Rifting in Europe. Geol. Soc. Spec. Publ., 223, 439–464.

Leonardi, G., 1987. Glossary and Manual of Tetrapod Footprint Palaeoichnology. Departamento Nacional de Produção Mineral, Brasilia, 117 pp.

Leonardi , P., Conti , M.A., Leonardi , G., Mari-Otti , N., Nicosia, U., 1975. *Pachypes* dolomiticus n. gen. n.sp.; Pareiasaur footprint from the 'Val Gardena Sandstone'(Middle Permian) in the western Dolomites (N. Italy). Atti Accad. Naz. dei Lincei 57, 221–232.

LePage, B.A., Beauchamp, B., Pfefferkorn, H.W., Utting, J., 2003. Late Early Permian plant fossils from the Canadian High Arctic: a rare palaeoenvironmental/climatic window in northwest Pangea. Palaeogeogr. Palaeoclimatol. Palaeoecol. 191, 345–372.

Liebrecht, T., Fortuny, J., Galobart, A., Müller, J., Sander, P.M., 2017. A large, multiple-tooth-rowed captorhinid reptile (Amniota: Eureptilia) from the Upper Permian of Mallorca (Balearic Islands, Western Mediterranean). J. Vertebr. Paleontol. 37 (1),e1251936. https://doi.org/10.1080/02724634.2017.1251936

Logghe, A., Mujal, E., Marchetti, L., Nel, A., Pouillon, J-M., Giner, S., Garrouste, R., Steyer, J.-S., 2021. *Hyloidichnus* trackways with digit and tail drag traces from the Permian of Gonfaron (Var, France): New insights on the locomotion of captorhinomorph eureptiles. Palaeogeogr. Palaeoclimatol. Palaeoecol., 573, 110436. https://doi.org/10.1016/j.palaeo.2021.110436

Lloret, J., Ronchi, A., López-Gómez, J., Gretter, N., De la Horra, R., Barrenechea, J.F., Arche, A., 2018. Syn-tectonic sedimentary evolution of the continental late Palaeozoic-early Mesozoic Erill Castell-Estac Basin and its significance in the development of the central Pyrenees Basin. Sediment. Geol. 374, 134–157. https://doi.org/10.1016/j.sedgeo.2018.07.014

Lloret, J., De la Horra, R., López-Gómez, J., Barrenechea, J.F., Gretter, N., Ronchi, A., 2021a. Permian and Triassic paleosols in the fluvial-lacustrine record of the central Pyrenees Basin, Spain: A stratigraphic tool for interpreting syn-tectonic sedimentary evolution and paleoclimate. Newsl. Stratigr. 54 (3), 377–404. https://doi.org/ 10.1127/nos/2021/0625

Lloret, J., López-Gómez, J., Heredia, N., Martín-González, F., De la Horra, R., Borruel-Abadía, V., Ronchi, A., Barrenechea, J.F., García-Sansegundo, J., Galé, C., Ubide, T., Gretter, N., Diez, J.B., Juncal, M., Lago, M., 2021b.Transition between Variscan and Alpine cycles in the Pyrenean-Cantabrian Mountains (N Spain): Geodynamic evolution of near-equator European Permian basins, Glob. Planet. Change 207, 103677. https://doi.org/10.1016/j.gloplacha.2021.103677

Looy, C.V., Ranks, S.L., Chaney, D.S., Sanchez, S., Steyer, J.S., Smith, R.M.H., Sidor, C.A., Myers, T.S., Ide, O., Tabor, N.J., 2016. Biological and physical evidence for extreme seasonality in centran Permian Pangea. Palaeogeogr. Palaeoclimatol. Palaeoecol. 451, 210–226.

López-Gómez, J., Martín-González, F., Heredia, N., De la Horra, R., Barrenechea, J.F., Cadenas, P., Juncal, M., Diez, J.B., Borruel-Abadía, V., Pedreira, D., García-Sansegundo, J., Farias, P., Galé, C., Lago, M., Ubide, T., Fernández-Viejo, G., Gand, G., 2019. New lithostratigraphy for the Cantabrian Mountains: a common tectonostratigraphic evolution for the onset of the Alpine cycle in the W Pyrenean realm, N Spain. Earth Sci. Rev. 188, 249–271.

Lucas, S.G., 2006. Global Permian tetrapod biostratigraphy and biochronology. In: Lucas, S.G., Cassinis, G., Schneider, J.W. (Eds.), Non-Marine Permian Biostratigraphy and Biochronology. Geol. Soc. London, Special Publications 265 (1), 65–93.

Lucas, S.G., 2007. Tetrapod footprint biostratigraphy and biochronology. Ichnos 14 (1–2), 5–38. https://doi.org/10.1080/10420940601006792

Lucas, S.G., 2009a. Global middle Permian reptile mass extinction: the dinocephalian extinction event. Geol. Soc. Am. Abstr. Programs 41 (7), 360.

Lucas, S.G., 2009b. Timing and magnitude of tetrapod extinctions across thePermo-Triassic boundary. J. Asian Earth Sci. 36 (6), 491–502.

Lucas, S.G., 2017. Permian tetrapod extinction events. Earth Sci. Rev. 170, 31–60. https://doi.org/10.1016/j.earscirev.2017.04.008

Lucas, S.G., 2018. Permian tetrapod biochronology, correlation and evolutionary events. Geol. Soc. Spec. Publ. 450, 405–444. https://doi.org/10.1144/SP450.12

Lucas, S.G., Hunt, A.P., 2005. Permian tetrapod tracks from Texas. Bull. N. M. Mus. Nat. Hist Sci. 30, 202–206.

Lucas, S.G., Spielmann, J.A., 2009. Tetrapod footprints from the Lower Permian YesoGroup, Mockingbird Gap, Socorro County, New Mexico. New Mexico Geological Society Guidebook, 60th Field Conference, Geology of the Chupadera Mesa Region, 305–310.

Lucas, S.G., Lerner, A.J., Bruner, M., Shipman, P., 2004. Middle Pennsylvanian ichnofauna from eastern Oklahoma, USA. Ichnos 11, 45–55. https://doi.org/10.1080/10420940490442322

Lucas, S.G., Voigt, S., Lerner, A.J., Nelson, W.J., 2011. Late Early Permian continental ichnofauna from Lake Kemp, north-central Texas, USA. Palaeogeogr. Palaeoclimatol. Palaeoecol. 308, 39–404. https://doi.org/10.1016/j.palaeo.2011.05.047

Lucas, S.G., Krainer, K., Voigt, S., Berman, D.S., Henrici, A., 2014. The Lower Permian Abo Formation in the northern Sacramento Mountains, southern New Mexico. New Mexico Geological Society, 65th Fall Field Conference Guidebook, Geology of the Sacramento Mountains Region 65, 287–302.

MacLeod, K.G., Quinton, P.C., Bassett, D.J., 2017. Warming and increased aridity during the earliest Triassic in the Karoo Basin, South Africa. Geology 45(6), 483–486. https://doi.org/10.1130/G38957.1

Maino, M., Dallagiovanna, G., Gaggero, L., Seno, S., Tiepolo, M., 2012. U–Pb zircon geochronological and petrographic constraints on late to post-collisional Variscan magmatism and metamorphism in the Ligurian Alps, Italy. Geol. J. 47, 632-652. https://doi.org/10.1002/gj.2421

Majarena, U., Galé, C., Esteban, J.J., Lago, M., Gil-Imaz, A., 2023. The magmatism of Atienza (NW Iberian Chain, Spain): age, origin and architecture of the magmatic plumbing system. J. Iber. Geol. 49, 47–69. https://doi.org/10.1007/s41513-023-00206-w

Mallison, H., Wings, O., 2014. Photogrammetry in Paleontology, a practical guide. Journal of Paleontological Techniques 12, 1–31.

Marchetti, L., 2016. New occurrences of tetrapod ichnotaxa from the Permian Orobic Basin (Northern Italy) and critical discussion of the age of the ichnoassociation. Pap. Palaeontol. 2(3), 1–24. https://doi.org/10.1002/spp2.1045

Marchetti, L., Avanzini, M., Conti, M.A., 2013. *Hyloidichnus bifurcatus* Gilmore,1927 and *Limnopus heterodactylus* (King, 1845) from the Early Permian of Southern Alps (N Italy): A new equilibrium in the ichnofauna. Ichnos 20(4), 202–217. http://dx.doi.org/10.1080/10420940.2013.846261

Marchetti L., Ronchi, A., Santi, G., Schirolli, P., Conti, M.A., 2015a. Revision of a classic site for Permian tetrapod ichnology (Collio Formation, Trompia and Caffaro valleys, N. Italy), new evidences for the radiation of captorhinomorph footprints. Palaeogeogr. Palaeoclimatol. Palaeoecol. 433, 140–155. https://doi.org/10.1016/j.palaeo.2015.04.005

Marchetti L., Ronchi, A., Santi, G., Voigt, S., 2015b. The Gerola Valley site (Orobic Basin, Northern Italy): A key for understanding late Early Permian tetrapod ichnofaunas. Palaeogeogr. Palaeoclimatol. Palaeoecol. 439, 97–116. https://doi.org/10.1016/j.palaeo.2015.02.032

Marchetti, L., Belvedere, M., Mietto, P., 2017. Lopingian tetrapod footprints in the Venetian Prealps (Italy): new discoveries in a largely incomplete panorama. Acta Palaeontol. Pol. 62, 801–817. https://doi.org/ 10.4202/app.00392.2017

Marchetti, L., Belvedere, M., Voigt, S., Klein, H., Castanera, D., Díaz-Martínez, I., Marty, D., Xing, L., Feola, S., Melchor, R.N., Farlow, J.O., 2019a. Defining the morphological quality of fossil footprints. Problems and principles of preservation in tetrapod ichnology with examples from the Palaeozoic to the present. Earth Sci. Rev. 193, 109–145. https://doi.org/10.1016/j.earscirev.2019.04.008

Marchetti, L., Voigt, S., Klein, H., 2019b. Revision of the Late Permian tetrapod tracks from the Dolomites (Trentino-Alto Adige, Italy). Hist. Biol. 31, 748–783. https://doi.org/10.1080/08912963.2017.1391806

Marchetti, L., Klein, H., Buchwitz, M., Ronchi, A., Smith, R.M.H., Klerk, W.J. De, Sciscio, L., Groenewald, G.H., 2019c. Permian-Triassic vertebrate footprints from South Africa: Ichnotaxonomy, producers and biostratigraphy through two major faunal crises. Gondwana Res. 72, 139–168. https://doi.org/10.1016/j.gr.2019.03.009

Marchetti, L., Voigt, S., Lucas, S.G., 2019d. An anatomy-based study of the Lopingian eolian tracks of Germany and Scotland reveals the first evidence of the end-Guadalupian mass extinction at low paleolatitudes of Pangea. Gondwana Res. 73, 32–53. https://doi.org/10.1016/j.gr.2019.03.013

Marchetti, L., Voigt, S., Lucas, S.G., Francischini, H., Dentzien-Dias, P., Sacchi, R., Mangiacotti, M., Scali, S., Gazzola, A., Ronchi, S., Millhouse, A., 2019e. Tetrapod ichnotaxonomy in eolian paleoenvironments (Coconino and De Chelly formations, Arizona) and late Cisuralian (Permian) sauropsid radiation. Earth Sci. Rev. 190, 148–170. https://doi.org/10.1016/j.earscirev.2018.12.0

Marchetti, L., Ceoloni, P., Leonardi, G., Massari, F., Mietto, P., Sacchi, E., Valentini, M., 2020a. The Lopingian tetrapod ichnoassociation from Italy, a key for the understanding of low-latitude faunas before the end-Permian crisis. J. Mediterr. Earth Sci. 12, 61–81. https://doi.org/10.3304/jmes.2020.17065

Marchetti, L., Voigt, S., Lucas, S.G., Stimson, M.R., King, O.A., Calder, J.H., 2020b. Footprints of the earliest reptiles: *Notalacerta missouriensis*–Ichnotaxonomy, potential trackmakers, biostratigraphy, palaeobiogeography and palaeoecology. Ann. Soc. Geol. Pol. 90, 271–290. https://doi.org/10.14241/asgp.2020.13

Marchetti, L., Voigt, S., Mujal, E., Lucas, S.G., Francischini, H., Fortuny, J., Santucci, V.L., 2021a. Extending the footprint record of Pareiasauromorpha to the Cisuralian: earlier appearance and wider palaeobiogeography of the group. Pap. Palaeontol. 7, 1297–1319. https://doi.org/10.1002/spp2.1342

Marchetti, L., Voigt, S., Buchwitz, M., MacDougall, M.J., Lucas, S.G., Fillmore, D.L., Stimson, M.R., King, O.A., Calder, J.H., Fröbisch, J., 2021b. Tracking the origin and early evolution of reptiles. Front. Ecol. Evol., 9:696511. https://doi.org/10.3389/fevo.2021.696511

Marchetti, L., Forte, G., Kustatscher, E., DiMichele, W.A., Lucas, S.G., Roghi, G., Juncal, M.A., Hartkopf-Fröder, C., Krainer, K., Morelli, C., Ronchi, A., 2022a. The Artinskian Warming Event: an Euramerican change in climate and the terrestrial biota during the early Permian. Earth Sci. Rev. 226, 103922. https://doi.org/10.1016/j.earscirev.2022.103922

Marchetti, L., Logghe A., Mujal, E., Barrier, P., Montenat, C., Nel, A., Pouillon, J.M., Garrouste, R., Steyer, S., 2022b. Vertebrate tracks from the Permian of Gonfaron (Provence, Southern France) and their implications for the late Capitanian terrestrial extinction event. Palaeogeogr. Palaeoclimatol. Palaeoecol. 599, 111043. https://doi.org/10.1016/j.palaeo.2022.111043

Marsh, O.C., 1894. Footprints of vertebrates in the Coal Measures of Kansas. Am. J. Sci. 48, 81–84.

Martí, J., 1996. Genesis of crystal-rich volcaniclastic facies in the Permian red beds of the Central Pyrenees (NE Spain). Sediment. Geol. 106, 1–19. https://doi.org/10.1016/0037-0738(95)00143-3

Martí, J. 2022. Volcano Geology Applications to Ancient Volcanism-Influenced Terrains: Paleovolcanism. In Updates in Volcanology - Linking Active Volcanism and the Geological Record. IntechOpen. https://doi.org/10.5772/intechopen.108770

Matamales-Andreu, R., Peñalver, E., Mujal, E., Oms, O., Scholze, F., Juárez, J., Galobart, À., Fortuny, J., 2021a. Early–Middle Triassic fluvial ecosystems of Mallorca (Balearic Islands): biotic communities and environmental evolution in the equatorial western peri-Tethys. Earth Sci. Rev. 222, 103783. https://doi.org/10.1016/j.earscirev.2021.103783

Matamales-Andreu, R., Roig-Munar, F.X., Oms, O., Galobart, À., Fortuny, J., 2021b. A captorhinid-dominated assemblage from the palaeoequatorial Permian of Menorca (Balearic Islands, western Mediterranean). Earth Environ. Sci. Trans. R. Soc. Edinb. 112, 125–145. https://doi.org/10.1017/S1755691021000268

Matamales-Andreu, R., Mujal, E., Galobart, À., Fortuny, J., 2021c. Insights on the evolution of synapsid locomotion based on tetrapod tracks from the lower Permian of Mallorca (Balearic Islands, western Mediterranean). Palaeogeogr. Palaeoclimatol. Palaeoecol. 579. https://doi.org/10.1016/j.palaeo.2021.110589

Matamales-Andreu, R., Mujal, E., Dinarès-Turell, J., Kustatscher, E., Roghi, G., Oms, O., Galobart, À., Fortuny, J., 2022. Early–middle Permian ecosystems of equatorial Pangaea:Integrated multi-stratigraphic and palaeontological review of thePermian of Mallorca (Balearic Islands, western Mediterranean). Earth Sci. Rev. 228, 103948. https://doi.org/10.1016/j.earscirev.2022.103948

Matamales-Andreu, R., Mujal, E., Galobart, À., Fortuny, J., 2023. A new medium-sized moradisaurine captorhinid eureptile from the Permian of Mallorca (Balearic Islands, western Mediterranean) and correlation with the co-occurring ichnogenus Hyloidichnus. Papers in Palaeontology, e1498. https://doi.org/10.1002/spp2.1498

Maxbauer, D.P., Feinberg, J.M., Fox, D.L., 2016. MAX UnMix: A web application for unmixing magnetic coercivity distributions. Comput. and Geosci. 95, 140–145. https://doi.org/10.1016/j.cageo.2016.07.009

Melchor, R.N., Sarjeant, W.A.S., 2004. Small amphibian and reptile footprints from the Permian Carapacha basin, Argentina. Ichnos 11, 57–78. https://doi.org/10.1080/10420940490428814

Mey, P.H.W., Nagtegaal, P.J.C., Roberti, K.J., Hartevelt, J.J.A., 1968. Lithostratigraphic subdivision of post-Hercy-nian deposits in the south-central Pyrenees, Spain. Leidse Geologische Mededelingen 44, 221–228.

Miall, A.D., 2006. The geology of fluvial deposits: Sedimentary facies, basin analysis, and petroleum geology. 4th ed. Springer, Berlin, Heidelberg, New York. 582 pp.

Michel. L.A., Tabor, N.J., Montañez, I.P., Schmitz, M.D., Davydov, V.I., 2015. Chronostratigraphy and paleoclimatology of the Lodève Basin, France: Evidence for a pan-tropical aridification event across the Carboniferous-Permian boundary. Palaeogeogr. Palaeoclimatol. Palaeoecol. 430, 118–131. https://doi.org/10.1016/j.palaeo.2015.03.020

Modesto, S.P., Flear, V.J., Dilney, M.M., Reisz, R.R., 2016. A large moradisaurine tooth plate from the Lower Permian of Texas and its biostratigraphic implications. J. Vertebr. Paleontol. 36 (6), e1221832 https://doi.org/10.1080/02724634.2016.1221832

Montañez, I.P., Poulsen, J., 2013. The Late Paleozoic Ice Age: an evolving paradigm. Annu. Rev. Earth Planet. Sci. 41, 629–656. https://doi.org/10.1146/annurev.earth.031208.100118

Montañez, I.P., Tabor, N.J., Niemeier, D., DiMichele, W.A., Frank, T.D., Fielding, C.R., Isbell, J.L., Birgenheier, L.P., Rygel, M.C., 2007. CO2-forced climate and vegetation instability during late Paleozoic deglaciation. Science 315, 87–91. https://doi.org/10.1126/science.1134207

Montañez, I.P., McElwain, J.C., Poulsen, C.J., White, J.D., DiMichele, W.A., Wilson, J.P., Griggs, G., Hren M.T., 2016. Climate, pCO2 and terrestrial carbon cycle linkages during late Palaeozoic glacial–interglacial cycles. Nat. Geosci. 9, 824–828. https://doi.org/10.1038/ngeo2822

Mujal, E., Schoch, R.R., 2020. Middle Triassic (Ladinian) amphibian tracks from the Lower Keuper succession of southern Germany: Implications for temnospondyl locomotion and track preservation. Palaeogeogr. Palaeoclimatol. Palaeoecol. 543, 109625. https://doi.org/10.1016/j.palaeo.2020.109625

Mujal, E., Fortuny, J., Oms, O., Bolet, A., Galobart, À., Anadón, P., 2016a. Palaeoenvironmental reconstruction and early Permian ichnoassemblage from the NE Iberian Peninsula (Pyrenean Basin). Geol. Mag. 153, 578–600. https://doi.org/10.1017/S0016756815000576

Mujal, E., Gretter, N., Ronchi, A., López-Gómez, J., Falconnet, J., Diez, J.B., De la Horra, R., Bolet, A., Oms, O., Arche, A., Barrenechea, J.F., Steyer, J.B., Fortuny, J., 2016b. Constraining the Permian/Triassic transition in continental environments: Stratigraphic and paleontological record from the Catalan Pyrenees (NE Iberian Peninsula).Palaeogeogr. Palaeoclimatol. Palaeoecol. 445, 18–37. https://doi.org/10.1016/j.palaeo.2015.12.008.

Mujal, E., Fortuny, J., Pérez-Cano, J., Dinarès-Turell, J., Ibáñez-Insa, J., Oms, O., Vila, I., Bolet, A., Anadón, P., 2017. Integrated multi-stratigraphic study of the Coll de Terrers late Permian–Early Triassic continental succession from the Catalan Pyrenees (NE Iberian Peninsula): A geologic reference record for equatorial Pangaea. Glob. Planet. Change 159, 46–60. https://doi.org/10.1016/j.gloplacha.2017.10.004

Mujal, E., Fortuny, J., Marmi, J., Dinarès-Turell, J., Bolet, A., Oms, O., 2018. Aridification across the Carboniferous–Permian transition in central equatorial Pangea: The Catalan Pyrenean succession (NE Iberian Peninsula). Sediment. Geol.

363, 48–68. https://doi.org/10.1016/j.sedgeo.2017.11.005

Mujal, E., Marchetti, L., Schoch, R.R., Fortuny, J., 2020. Upper Paleozoic to Lower Mesozoic tetrapod ichnology revisited: photogrammetry and relative depth pattern inferences on functional prevalence of autopodia. Front. Earth Sci. 8, 248. https://doi.org/10.3389/feart.2020.00248

Müller, A.H., 1954, Zur ichnologie und stratonomie des Oberrotliegenden von Tambach (Thüringen): PalZ 28, 189–203.

Nagtegaal, P.J.C., 1969. Sedimentology, paleoclimatology, and diagenesis of post-Hercynian continental deposits in the south-central Pyrenees, Spain. Leidse Geologische Mededelingen 42, 143–238

Nicosia, U., Ronchi, A., Santi, G., 2000. Permian tetrapod footprints from W Orobic basin (Northern Italy). Biochronological and evolutionary remarks. Geobios 33(6), 753–768.

Oliva-Urcia, B., Pueyo, E.L., Larrasoaña, J.C., Casas, A.M., Román-Berdiel, T., Van der Voo, R., Scholger, R., 2012. New and revisited paleomagnetic data from Permian–Triassic red beds: Two kinematic domains in the west-central Pyrenees. Tectonophysics 522, 158–175.

Pellenard, P., Gand, G., Schmitz, M., Galtier, J., Broutin, J., Steyer, J.S., 2017. High precision U-Pb zircon ages for explosive volcanism calibrating the NW European continental Autunian stratotype. Gondwana Res. 51, 118–136. 10.1016/j.gr.2017.07.014

Pereira, M.F., Castro, A., Chichorro, M., Fernández, C., Díaz-alvarado, J., Martí, J., Rodríguez, C., 2014. Chronological link between deep-seated processes in magma chambers and eruptions : Permo-Carboniferous magmatism in the core of Pangaea (Southern Pyrenees). Gondwana Res. 25, 290–308. https://doi.org/10.1016/j.gr.2013.03.009

Petti, F.M., Bernardi, M,, Ashley-Ross, M.A., Berra, F., Tessarollo, A., Avanzini, M., 2014. Transition between terrestrial-submerged walking and swimming revealed by Early Permian amphibian trackways and a new proposal for the nomenclature of compound trace fossils. Palaeogeogr. Palaeoclimatol. Palaeoecol. 410, 278–289. https://doi.org/10.1016/j.palaeo.2014.05.032

Pretus, J.LL., Obrador, A., 1987. Presencia de restos óseos en el Pérmico de Menorca (nota previa). Bolletí de la Societat d'Història Natural de les Balears 31, 149–152.

Rmich, A., Lagnaoui, A., Hminna, A., Saber, H., Zouheir, T., Lallensack, J.N., 2023. Captorhinid trackways from mid- to late Permian red beds in Morocco: Implications for locomotion and the palaeobiogeography of northwest Gondwana. Palaeogeogr. Palaeoclimatol. Palaeoecol. 625, 111700. https://doi.org/10.1016/j.palaeo.2023.111700

Richey, J.D., Montañez, I.P., Goddéris, Y., Looy, C. V., Griffis, N.P., Dimichele, W.A., 2020. Influence of temporally varying weatherability on CO2-climate coupling and ecosystem change in the late Paleozoic. Clim. Past. 16, 1759–1775. https://doi.org/10.5194/cp-16-1759-2020

Robles, S., Llompart, C., 1987. Análisis paleogeográfico y consideraciones paleoicnológicas del Pérmico superior y Triásico inferior en la transversal del río Segre (Alt Urgell, Pirineo de Lérido). Cuadernos de Geología Ibérica 11, 115–130.

Romano, M., Citton, P., Avanzini, M., 2020. A review of the concepts of ‘axony’ and their bearing on tetrapod ichnology. Hist. Biol. 32, 611–619. https://doi.org/10.1080/08912963.2018.1516766

Roscher, M., Schneider, J. W., 2006. Permo-Carboniferous climate: Early Pennsylvanian to Late Permian climate development of central Europe in a regional and global context. Geol. Soc. Spec. Publ. 265(1), 95–136. https://doi.org/10.1144/gsl.sp.2006.265.01.05

Roscher, M., Stordal, F., Svensen, H., 2011. The effect of global warming and global cooling on the distribution of the latest Permian climate zones. Palaeogeogr. Palaeoclimatol. Palaeoecol. 309(3-4), 186–200. https://doi.org/10.1016/j.palaeo.2011.05.042

Sacchi, E., Cifelli, R., Citton, P., Nicosia, U., Romano, M., 2014. *Dimetropus osageorum* n. isp. from the early Permian of Oklahoma (USA): A trace and its trackmaker. Ichnos 21, 175–192. https://doi.org/10.1080/10420940.2014.933070

Rühle von Lilienstern, H., 1939. Fährten und Spuren im *Chirotherium*-Sandstein von Südthüringen. Fortschritte der Geologie und Palaontologie 12, 293–387.

Saltzman, M.R., 2003. Late Paleozoic ice age: oceanic gateway or pCO2. Geology 31, 151–154.

Saura, E., Teixell, A., 2006. Inversion of small basins: effects on structural variations at the leading edge of the Axial Zone antiformal stack (Southern Py-renees, Spain). J. Strct. Geol. 28(11), 1909–1920.

Schaltegger, U., Brack, P., 2007. Crustal-scale magmatic systems during intracontinental strike-slip tectonics: U, Pb and Hf isotopic constraints from Permian magmatic rocks of the Southern Alps. Int. J. Earth. Sci. 96(6), 1131–1151. https://doi.org/10.1007/s00531-006-0165-8

Schneider, J.W., Körner, F., Roscher, M., Kroner, U., 2006. Permian climate development in the northern peri-Tethys area – The Lodève basin, French Massif Central, compared in a European and global context. Palaeogeogr. Palaeoclimatol. Palaeoecol. 240, 161–183. https://doi.org/10.1016/j.palaeo.2006.03.057

Schneider, J.W., Lucas, S.G., Scholze, F., Voigt, S., Marchetti, L., Klein, H., Opluštil, S., Werneburg, R., Golubev, V.K., Barrick, J.E., Nemyrovska, T., Ronchi, A., Day, M.O., Silantiev, V.V., Rößler, R., Saber, H., Linnemann, U., Zharinova, V., Shen, S., 2020. Late Paleozoic-early Mesozoic continental biostratigraphy-Links to the Standard Global Chronostratigraphic Scale. Paleoworld 29 (2), 186–238. https://doi.org/10.1016/j.palwor.2019.09.001

Schoch, R.R. 2014. Life cycles, plasticity, and palaeoecology in temnospondyl amphibians. Palaeontology, 57, 517–529.

Scotese, C.R., 2014. Atlas of Middle & Late Permian and Triassic Paleogeographic Maps, maps 43 - 48 from Volume 3 of the PALEOMAP Atlas for ArcGIS (Jurassic and Triassic) and maps 49 – 52 from Volume 4 of the PALEOMAP PaleoAtlas for ArcGIS (Late Paleozoic), Mollweide Projec-tion, PALEOMAP Project, Evanston, IL.

Sidor, C.A., O'Keefe, F.R., Damiani, R., Steyer, J.-S., Smith, R.M.H., Larsson, H.C.E., Sereno, P.C., Ide, O., Maga, A., 2005. Permian tetrapods from the Sahara show climate controlled endemism in Pangaea. Nature 434, 886–889.

Sinisi, R., Mongelli, G., Mameli, P., Oggiano, G., 2014. Did the Variscan relief influence the Permian climate of Mesoeuropeα Insights from geochemical and mineralogical proxies from Sardinia (Italy). Palaeogeogr. Palaeoclimatol. Palaeoecol. 396, 132–154. https://doi.org/10.1016/j.palaeo.2013.12.030

Smith, R.M.H., Sidor, C.A., Tabor, N.J., Steyer, J.S., 2015. Sedimentology and vertebrate taphonomy of the Moradi Formation of northern Niger: A Permian wet desert in the tropics of Pangaea. Palaeogeogr. Palaeoclimatol. Palaeoecol. 440, 128–141. https://doi.org/10.1016/j.palaeo.2015.08.032

Speksnijder, A., 1985. Anatomy of a strike-slip fault controlled sedimentary basin, Permian of the Southern Pyrenees, Spain. Sediment. Geol. 44, 179–223.

Spindler, F., Werneburg, R., Schneider, J.W., 2019. A new mesenosaurine from the lower Permian of Germany and the postcrania of *Mesenosaurus* : implications for early amniote comparative osteology. PalZ 93, 303–344. https://doi.org/10.1007/s12542-018-0439-z

Stampfli, G.M., Kozur, H.W., 2007. Europe from the Variscan to the Alpine cycles. Geol. Soc. Lond. Mem. 32 (1), 57–82. https://doi.org/10.1144/GSL.MEM.2006.032.01.04

Steyer, J.-S., Damiani, R., Sidor, C.A., O'Keefe, F.R., Larsson, H.C.E., Magal, A., Ide, O., 2006. The vertebrate fauna of the Upper Permian of Niger. IV. *Nigerpeton ricqlesi* (Temnospondyli: Cochleosauridae), and the edopoid colonization of Gondwana. J. Vertebr. Paleontol. 26(1), 18–28.

Stimson, M., Lucas, S.G., Melanson, G., 2012. The smallest known tetrapod footprints: *Batrachichnus salamandroides* from the Carboniferous of Joggins, Nova Scotia, Canada. Ichnos 19, 127–140. https://doi.org/10.1080 /10420940.2012.685206

Sues, H.D., Reisz, R.R., 1998. Origins and early evolution of herbivory in tetrapods. Trends Ecol. Evol. 13, 141–145. https://doi.org/10.1016/S0169-5347(97)01257-3

Surkov, M.V., Benton, M.J., Twitchett, R.J., Tverdokhlebov, V.P., Newell, A.J., 2007. First occurrence of footprints of large therapsids from the Upper Permian of European Russia. Palaeontology, 50, 641–652.

Tabor, N.J., Montañez, I.P., 2002. Shifts in late Paleozoic atmospheric circulation over western equatorial Pangean: Insights from pedogenic d18O compositions. Geology 30(12), 1127–1130.

Tabor, N.J., Poulsen, C.J., 2008. Palaeoclimate across the Late Pennsylvanian–Early Permian tropical palaeolatitudes: a review of climate indicators, their distribution, and relation to palaeophysiographic climate factors. Palaeogeogr. Palaeoclimatol. Palaeoecol. 268, 293–310. https://doi.or/10.1016/j.palaeo.2008.03.052

Tabor, N.J., Smith, R.M.H., Steyer,S., Sidor, C.A., Poulsen, J., 2011. The Permian Moradi Formation of northern Niger: Paleosol morphology, petrography and mineralogy. Palaeogeogr. Palaeoclimatol. Palaeoecol. 299, 200–213. https://doi.org/10.1016/j.palaeo.2010.11.002

Tabor, N.J., Sidor, C.A., Smith, R.M.H., Nesbitt S.J., Angielczyk, K.D., 2018. Paleosols of the Permian-Triassic: proxies for rainfall, climate change and major changes in terrestrial tetrapod diversity, J. Vertebr. Paleontol 37, 240–253. https://doi.org/10.1080/02724634.2017.1415211

Taner, L., 2013. A Pennsylvanian tetrapod trackway from Joggins, Nova Scotia: the size continuum of *Batrachichnus salamandroides*. Bull. N. M. Mus. Nat. Hist Sci. 60, 427–431.

Tauxe, L., Kent, D.V., 2004. A simplified statistical model for the geomagnetic field and the detection of shallow bias in paleomagnetic inclinations: was the ancient magnetic field dipolar? In: J.E.T. Channell, D.V. Kent, W. Lowrie and J.G. Meert (Eds.), Timescales of the paleomagnetic field. https://doi.org/10.1029/145GM08

Torsvik, T.H., Cocks, L.R.M., 2013. Gondwana from top to base in space and time. Gondwana Res. 24, 999–1030. http://dx.doi.org/10.1016/j.gr.2013.06.012

Tucker, L., Smith, M.P., 2004. A multivariate taxonomic analysis of the Late Carboniferous vertebrate ichnofauna of Alveley, Southern Shropshire, England. Palaeontology 47, 679–710.

Valentini, M., Conti, M.A., Mariotti, N., 2007. Lacertoid footprints of the Upper Permian Arenaria di Val Gardena Formation (Northern Italy). Ichnos. 14, 193–218.

Valentini, M., Conti, M.A., Nicosia, U., 2008. Linking tetrapod tracks to the biodynamics, paleobiogeography, and paleobiology of their trackmakers: *Pachypes dolomiticus* Leonardi et al., 1975, a case study. Acta Geologica 83, 237–246.

Valentini, M., Nicosia, U., Conti , M.A., 2009. A re-evaluation of *Pachypes*, a pareiasaurian track from the Late Permian. Neues Jahrb. fur Geol. Palaontol. - Abh. 251, 71–94.

Van Allen, H.E.K., Calder, J.H., Hunt, A.P., 2005. The trackway record of a tetrapod commu-nity in a walchian conifer forest from the Permo-Carboniferous of Nova Scotia. Bull. N. M. Mus. Nat. Hist. Sci. 30, 322–332.

Van Dongen, P.G., 1967. The rotation of Spain: palaeomagnetic evidence from the eastern Pyrenees. Palaeogeogr. Palaeoclimatol. Palaeoecol. 3, 417–432.

Vergés, J., 1993. Estudi geològic del vessant sud del Pirineu oriental i central. Evolució cinemàtica en 3D. PhD Thesis Universitat de Barcelona, Barcelona.

Voigt, S., 2005. Die Tetrapodenichnofauna des kontinentalen Oberkarbon und Perm im Thüringer Wald – Ichnotaxonomie, Paläoökologie und Biostratigraphie. Cuvillier Verlag, Göttingen, 305.

Voigt, S., 2012. Tetrapodenfährten im Rotliegend. Schriftenreihe der Deutschen Gesellschaft für Geowissenschaften 61, 161–175.

Voigt, S., Haubold, H., 2015. Permian tetrapod footprints from the Spanish Pyrenees. Palaeogeogr. Palaeoclimatol. Palaeoecol. 417, 112–120. https://doi.org/10.1016/j.palaeo.2014.10.038

Voigt, S., Lucas, S.G., 2013. Carboniferous–Permian tetrapod footprint biochronozonation. In: Lucas, S.G., DiMichele, W.A., Barrick, J.E., Schnei-der, J.W., Spielmann, J.A. (Eds.), The Carboniferous–Permian Transition.Bull. N. M.

Mus. Nat. Hist Sci. 60, 444.

Voigt, S., Lucas, S.G., 2015. On a diverse tetrapod ichnofauna from Early Permian red beds in San Miguel County, north-central New Mexico. New Mexico Geological Society Guidebook 66th Field Conference, 241–252.

Voigt, S., Lucas, S.G., 2018. Outline of a Permian tetrapod footprint ichnos-tratigraphy. In: Lucas, S.G., Shen, S.Z. (Eds.), The Permian Timescale. Geol. Soc. London, Special Publications 450, 387–404. https://doi.org/10.1144/SP450.10

Voigt, S., Small, B.J., Sanders, F., 2005. A diverse terrestrial ichnofauna from the Maroon Formation (Pennsylvanian-Permian), Colorado : Biostratigraphic and paleoecological significance. Bull. N. M. Mus. Nat. Hist Sci. 30, 342–51.

Voigt, S., Hminna, A., Saber, H., Schneider, J.W., Klein, H., 2010. Tetrapod footprints from the uppermost level of the Permian Ikakern Formation (Argana Basin , Western High Atlas, Morocco). J. African Earth Sci. 57, 470–478. https://doi.org/10.1016/j.jafrearsci.2009.12.003

Voigt, S., Saber, H., Schneider, J.W., Hmich, D., Hminna, A., 2011a. Late Carboniferous-Early Permian Tetrapod ichnofauna from the Khenifra Basin, Central Morocco. Geobios 44, 399–407. https://doi.org/10.1016/j.geobios.2010.11.008

Voigt, S., Lagnaoui, A., Hminna, A., Saber, H., Schneider, J.W., 2011b. Revisional notes on the Permian tetrapod ichnofauna from the Tiddas Basin, central Morocco. Palaeogeogr. Palaeoclimatol. Palaeoecol. 302, 474–483. https://doi.org/10.1016/j.palaeo.2011.02.010

Voigt, S., Niedzwiedzki, G., Raczynski, P., Mastalerz, K., Ptaszynski, T., 2012. Early Permian tetrapod ichnofauna from the Intra-Sudetic Basin, SW Poland. Palaeogeogr. Palaeoclimatol. Palaeoecol. 314, 173–180. https://doi.org/10.1016/j.palaeo.2011.10.018

Voigt, S., Lucas, S.G., Buchwitz, M., Celeskey, M., 2013. *Robledopus macdonaldi*, a new kind of basal eureptile footprint from the Early Permian of New Mexico. Bull. N. M. Mus. Nat. Hist Sci. 60, 445–459.

Weldon, E.A., Shi, G.R., 2003. Global distribution of Terrakea Booker, 1930 (Productidina, Brachiopoda): implications for Permian marine biogeography and Eurasia-Gondwana correlations. XVth International Congress on Carboniferous and Permian Stratigraphy. Utrecht, 2003, Abstracts 583.

Woodworth, J.B., 1900. Vertebrate footprints on Carboniferous shales of Plainville, Massachusetts. Geol. Soc. Am. Bull. 11, 449–454.

Whyte, M.A., Romano, M., 2001. A dinosaur ichnocoenosis from the Middle Jurassic of Yorkshire, UK. Ichnos 8, 223–234. https://doi.org/10.1080/10420940109380189

Winguth, A.M.E., Heinze, C., Kutzbach, J.E., Maier-Reimer, E., Mikolajewicz, U., Rowley, D., Rees, A., Ziegler, A.M., 2002. Simulated warm polar currents during the middle Permian. Paleoceanography 17(4), 1057. https://doi.org/10.1029/2001pa000646

Zheng, J.S., Mermet, J.-F., Toutin-Momn, N., Hanes, J., Gondolo, A., Morin, R., Féraud, G., 1992. Datation 40Ar-39Ar du magmatisme et de filons minéralisés permiens en Provence orientale (France). Geodin. 5 (1991/1992), 203–215.

Zijderveld, J.D.A., 1967. A.C. Demagnetization of Rocks: Analysis of Results. Dev. in Solid Earth Geophys. 3, 254–286.

Zouicha, A., Voigt, S., Saber, H., Marchetti, L., Hminna, A., El Attari, A., Ronchi, A., Schneider, J. W., 2021. First record of permian continental trace fossils in the jebilet massif, Morocco. J. African Earth Sci. 173, 104015. https://doi.org/10.1016/j.jafrearsci.2020.104015

FIGURE CAPTIONS

Figure 1. Geographical and geological setting. A. Location in Europe and regional geology of the Pyrenees; modified from Vergés (1993). B. Detailed map of Castellar de n'Hug area with the location of the three studied sections and outcrops; modified from IGME, MAGNA 255, 36-11, la Pobla de Lillet.

Figure 2. Stratigraphic framework of Castellar de n'Hug sub-basin with the three studied sections (CnH, RM and CR) correlated. The main features (characteristic sedimentary structures and occurrence of tetrapod footprints) are indicated. The chronological data is discussed throughout the text. The correlation datum corresponds to the last volcaniclastic level of the LRU. The detailed stratigraphic sections are provided in the Supplementary Logs.

Figure 3. Lower Red Unit (LRU) in the Castellar de n'Hug sub-basin. A. General aspect of the unit in the CnH section, showing fluvial red-beds alternated with coarse volcaniclastic deposits. The white arrow points the section direction. B. Point bars with lateral accretion from meandering channel deposits in the CnH section. The white arrow points the section direction C. Ignimbrite composed of parallel stratified pyroclastic beds with a vitrified matrix from the CnH section. D. Matrix supported massive breccias with tabular shape, corresponding to massive pyroclastic deposits (facies *mlBr*). E. Volcaniclastic breccia with large pyroclasts from the last volcaniclastic levels of the CnH section. F. Laminated pyroclastic facies with antidunes structures (facies *sT*) in the CnH section. G. Well-developed palaeosols with carbonate nodules and root marks. H. Laminated mudstone with ripples (facies *Fl*) in the CnH section. I. Fine-grained sandstone with climbing ripples (facies *Sr*) in the CnH section. J. Parallelly laminated medium- to coarse-grained sandstones (facies *Sh*) in the CnH section.

Figure 4. Upper Red Unit (URU) in the Castellar de n'Hug sub-basin. A. Landscape overview of the Coll Roig section (CR). The white arrow points the section direction B.

Upper URU deposits of massive mudstones with cyclic occurrence of mud-cracked surfaces, from the Riera de Monell (RM) section. The white arrow points the section direction C. Massive mudstones with a mud-cracked surface on top (to the right of the photograph) from the CR section. D. Overbank mudstone deposit with a carbonate mud-cracked layer on top from the RM section. E. Mud-cracked surface including moulds of plant trunks with radial fractures from the CR section. F. Thin cross-laminated fine-grained sandstone layer interbedded in a massive mudstone. G. Level of septarian nodules distributed within a massive mudstone representing the transition between the lower URU and the upper URU from the CR section. H. Large septarian nodule, characteristic of the transition between the lower URU and the upper URU from the CR section.

Figure 5. Representative orthogonal demagnetisation diagrams with bedding corrected coordinates (tectonic). The natural remanent magnetisation (NRM) intensity, the lithology type and some demagnetisation steps are indicated. Closed (open) symbols represent the projection of the vector end-points on the horizontal (vertical) plane and denote declination (inclination). A thick grey line shows the linear fitted reverse ChRM direction.

Figure 6. A. ChRM directional and VGP results in geographic (in situ). B. Bedding-corrected (tectonic) coordinates. Both A and B are for all studied samples, and both depict the confidence envelope (A95) and parachute are depicted; red dots are those that fall outside of the 45° cut-off. For full directional data see Table S1. C. Elongation (E) vs. inclination (I) as a function of increasing unflattening factor (f). Dashed thick line is E vs. I trend from the TK03.GDA model. Also shown results from bootstrapped datasets (E/I correction method from Tauxe and Kent, 2004 as implemented in open-source software https://www.paleomagnetism.org, Koymans et al., 2016, 2020). D. Cumulative distribution of 1000 bootstrapped TK03.GAD intersections. Blue shaded area delimits the confidence bounds containing the central 95% of the “corrected inclinations”.

Figure 7. Tetrapod footprints I: *Batrachichnus* isp. A. IPS88731 with three related ichnites in convex hyporelief composed of two right manus, one partial right pes and small-size pes and manus. B. False-colour depth map with contours and interpretation of a right manus and corresponding interpretation (B’). C. Detailed picture of the small-sized pes and manus and corresponding interpretation (C’). D. Detailed picture of IPS88734 with partial large-sized imprint in convex hyporelief and (D’) interpretation of the impression. E. Detailed picture of IPS88724 with partial large-sized imprint with drag

traces in convex hyporelief and (E’) interpretation of the impression. F. IPS88734 with partial trackway and numerous small-sized scratches identified as *Characichnos* isp. in convex hyporelief and (F’) interpretation.

Figure 8. Tetrapod footprints II. A. Right footprint of *Dromopus* isp. in concave epirelief from Coll Roig section (CR-15-1). B. Left manus-pes set of *Hyloidichnus* isp. in concave epirelief from Riera de Monell section (RM-177-14, RM-177-15). C. Left manus-pes set of *Hyloidichnus* isp. in convex hyporelief from Castellar de n’Hug section (IPS135414). All footprints include false-colour depth maps with contours (A’–C’) and interpretive outlines (A’’–C’’).

Figure 9. Tetrapod footprints III. *Brontopus antecursor* (A–D) and *Pachypes* isp. (E). A. Trackway from Riera de Monell section (RM-177-1 to 12). B. Left manus-pes set within the trackway (RM-177-7; RM-177-8). C. Right manus-pes set within the trackway (RM-177-5; RM-177-6). D. Tracks from Coll Roig section (from CR-69-2 to CR-69-4). E. Right footprint of *Pachypes* isp. from Riera de Monell section (RM-209-1). All footprints are in concave epirelief and include false-colour depth maps with contours (A’–E’) and interpretive outlines (A’’–E’’).

Figure 10. Palaeoenvironmental reconstruction of the LRU based on the stratigraphic section in CnH. On the right, the fossil assemblage (tetrapod ichnoassociation 1) and the palaeoenvironment is represented, showing a floodplain with meandering fluvial systems interbedded with volcanic material. Symbols of the stratigraphic log described in Figure 2.

Figure 11. Palaeoenvironmental evolution of the URU based on the stratigraphic sections in RM (left) and CR. (right) The fossil ichnoassemblage shows an evolution from floodplain environments (tetrapod ichnoassociation 1) to seasonal playa-lake systems (tetrapod ichnoassociation 2). Symbols of the stratigraphic log described in Figure 2.

Figure 12. Reconstruction of the ichnoassociation 2 of the upper URU in the study area representing the playa-lake palaeoenvironment with mud-cracked surfaces and its related fauna: on the left, *Brontopus antecursor* trackmaker, on the centre *Hyloidichnus* tracks, on the right, partially hidden, *Dromopus* trackmaker. Far right, *Hyloidichnus* trackmakers. Note the presence of notostracan arthropods in the shallow water body and insect in the trunk. Credit of the artwork: Roc Olivé / Institut Català de Paleontologia Miquel Crusafont.

Figure 13. Tetrapod footprint chronostratigraphy in the study area. The dark bars represent the chronological record of ichnotaxa worldwide and the grey bars represent uncertain occurrences (data from Schneider et al., 2020; Marchetti et al., 2021a, 2022b). Black dashed lines mark the ichnoassociation distribution, and the red dashed lines represent the temporal range of the sub-biochrons of the *Erpetopus* biochron.

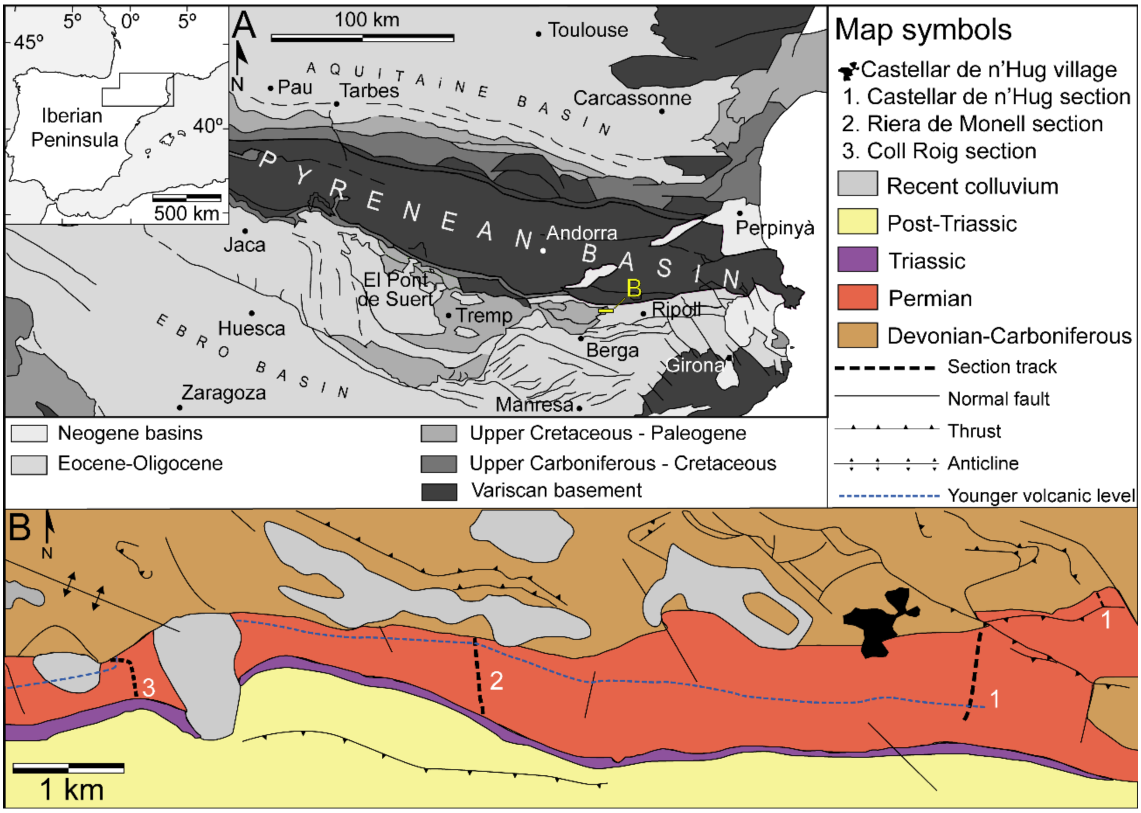

A
100 km
Toulouse
Pau
Tarbes
AQUITAINE BASIN
Carcassonne
PYRENEAN BASIN
Andorra
Perpinyà
Jaca
El Pont de Suert
Tremp
B
Ripoll
Berga
Girona
Huesca
EBRO BASIN
Zaragoza
Manresa
5º
0º
5º
45º
40º
Iberian Peninsula
500 km
Map symbols
Castellar de n'Hug village
1. Castellar de n'Hug section
2. Riera de Monell section
3. Coll Roig section
Recent colluvium
Post-Triassic
Triassic
Permian
Devonian-Carboniferous
Section track
Normal fault
Thrust
Anticline
Younger volcanic level
Neogene basins
Eocene-Oligocene
Upper Cretaceous - Paleogene
Upper Carboniferous - Cretaceous
Variscan basement
B
N
1
2
3
1 km

Figure 1.

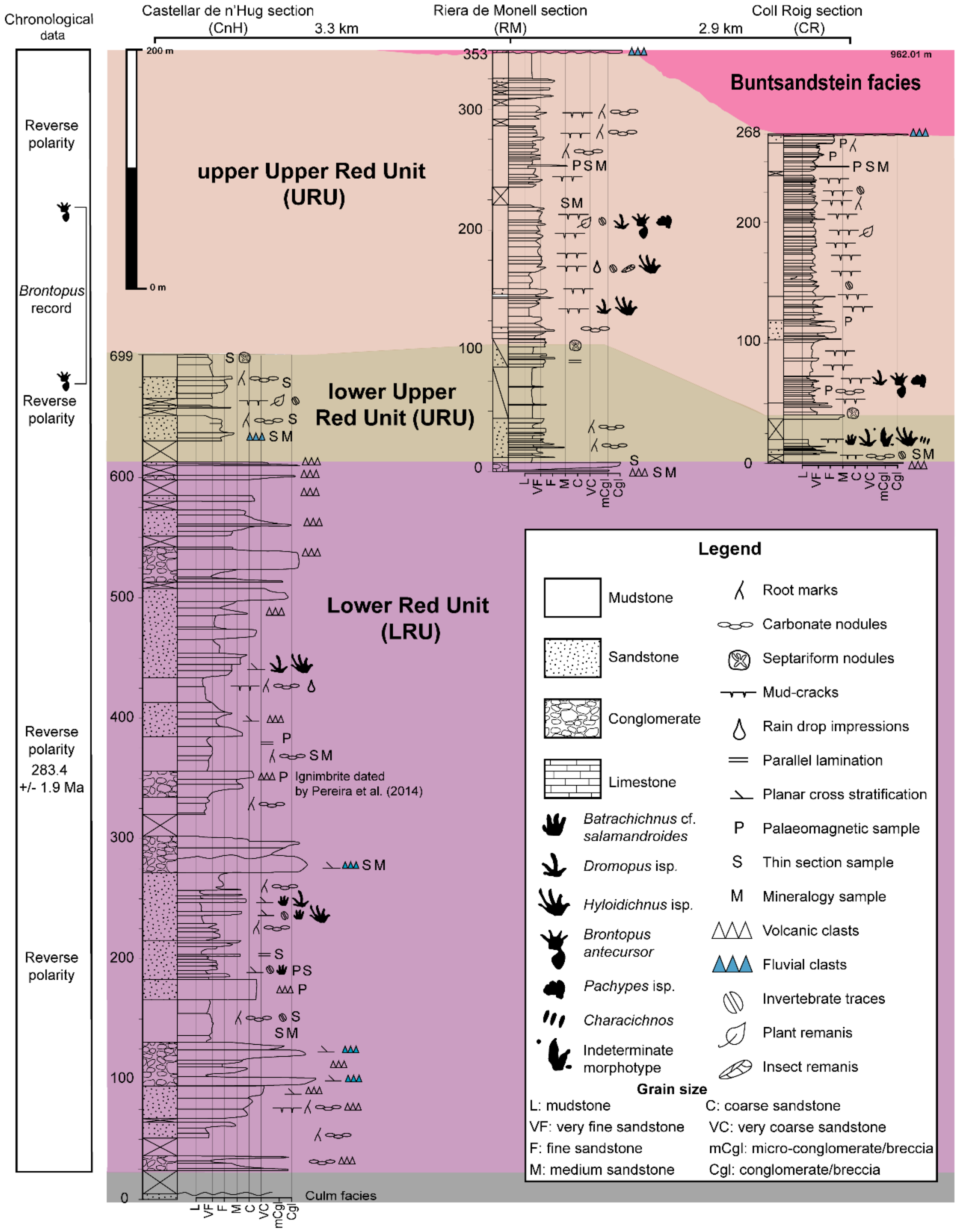

Chronological data
Castellar de n'Hug section (CnH)
3.3 km
Riera de Monell section (RM)
2.9 km
Coll Roig section (CR)
Reverse polarity
Brontopus record
Reverse polarity
Reverse polarity
283.4 +/- 1.9 Ma
Reverse polarity
200 m
0 m
962.01 m
Buntsandstein facies
upper Upper Red Unit (URU)
lower Upper Red Unit (URU)
Lower Red Unit (LRU)
Ignimbrite dated by Pereira et al. (2014)
Culm facies
L VF F M C VC mCgl Cgl
Legend
Mudstone
Sandstone
Conglomerate
Limestone
Batrachichnus cf. salamandroides
Dromopus isp.
Hyloidichnus isp.
Brontopus antecursor
Pachypes isp.
Characichnos
Indeterminate morphotype
Root marks
Carbonate nodules
Septariform nodules
Mud-cracks
Rain drop impressions
Parallel lamination
Planar cross stratification
P Palaeomagnetic sample
S Thin section sample
M Mineralogy sample
Volcanic clasts
Fluvial clasts
Invertebrate traces
Plant remanis
Insect remanis
Grain size
L: mudstone
VF: very fine sandstone
F: fine sandstone
M: medium sandstone
C: coarse sandstone
VC: very coarse sandstone
mCgl: micro-conglomerate/breccia
Cgl: conglomerate/breccia

Figure 2.

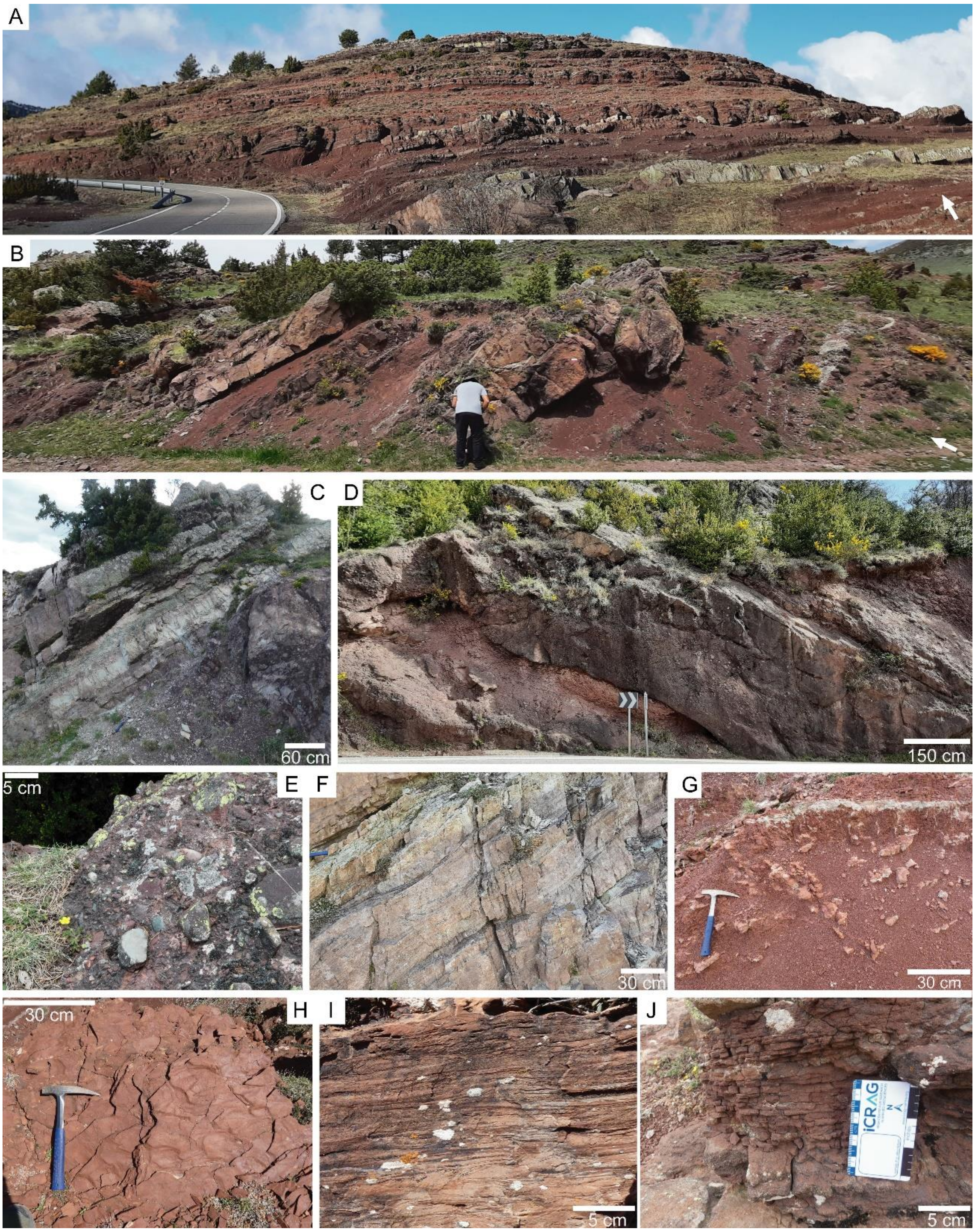

Figure 3.

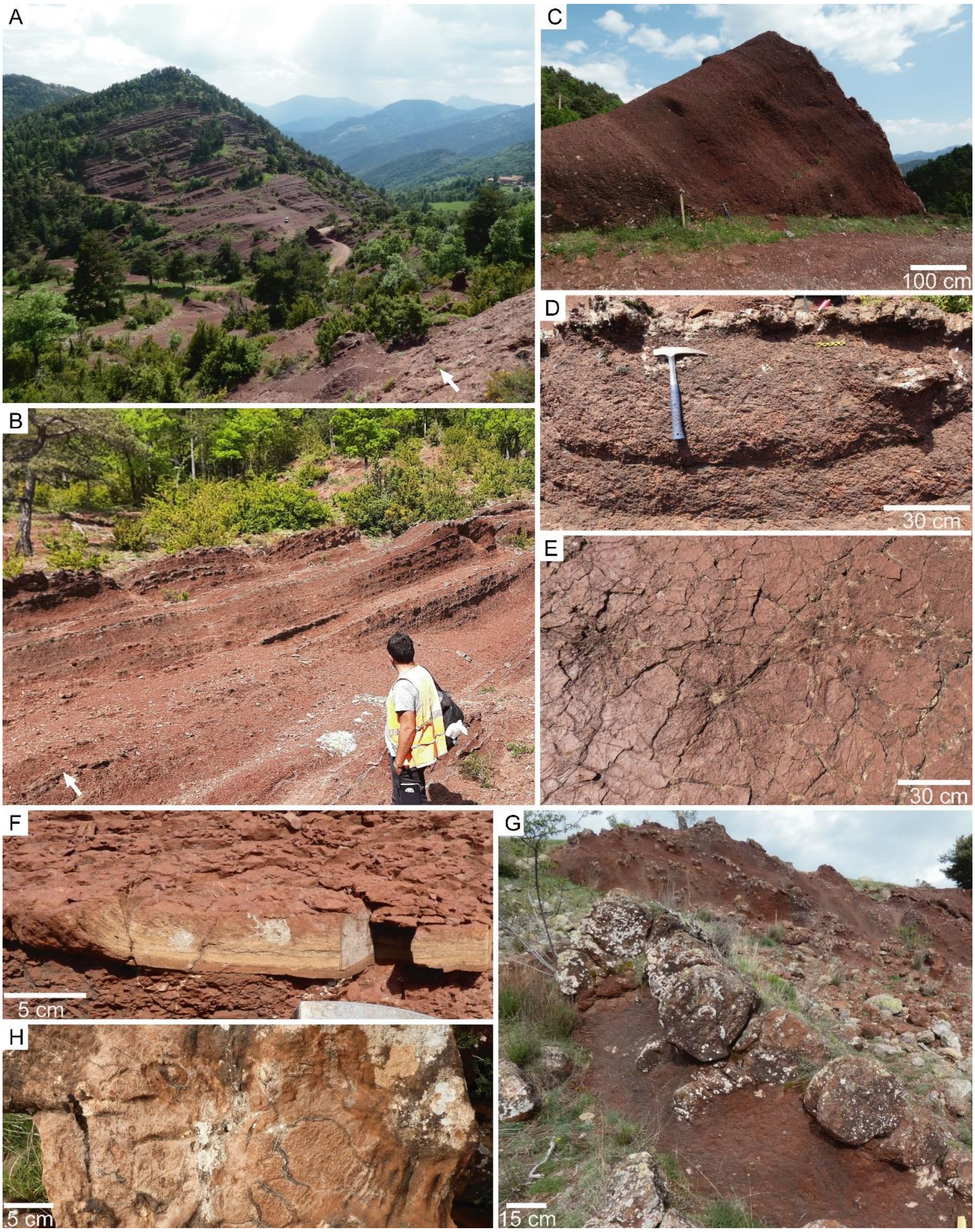

Figure 4.

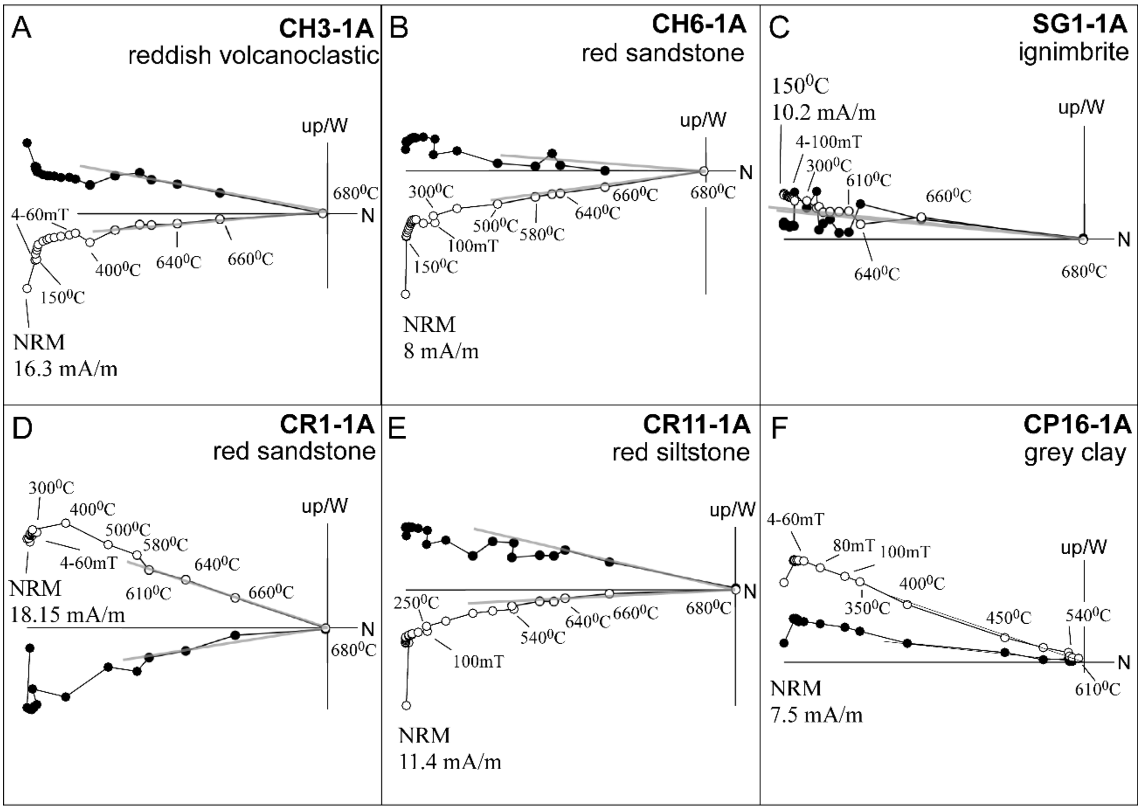
A
CH3-1A
reddish volcanoclastic
up/W
N
680⁰C
4-60mT
400⁰C
640⁰C
660⁰C
150⁰C
NRM
16.3 mA/m
B
CH6-1A
red sandstone
up/W
N
680⁰C
300⁰C
100mT
150⁰C
500⁰C
580⁰C
640⁰C
660⁰C
NRM
8 mA/m
C
SG1-1A
ignimbrite
150⁰C
10.2 mA/m
4-100mT
300⁰C
610⁰C
660⁰C
up/W
N
640⁰C
680⁰C
D
CR1-1A
red sandstone
300⁰C
400⁰C
500⁰C
580⁰C
4-60mT
640⁰C
610⁰C
660⁰C
NRM
18.15 mA/m
up/W
N
680⁰C
E
CR11-1A
red siltstone
up/W
N
250⁰C
100mT
540⁰C
640⁰C
660⁰C
680⁰C
NRM
11.4 mA/m
F
CP16-1A
grey clay
4-60mT
80mT
100mT
400⁰C
350⁰C
450⁰C
540⁰C
up/W
N
610⁰C
NRM
7.5 mA/m

Figure 5.

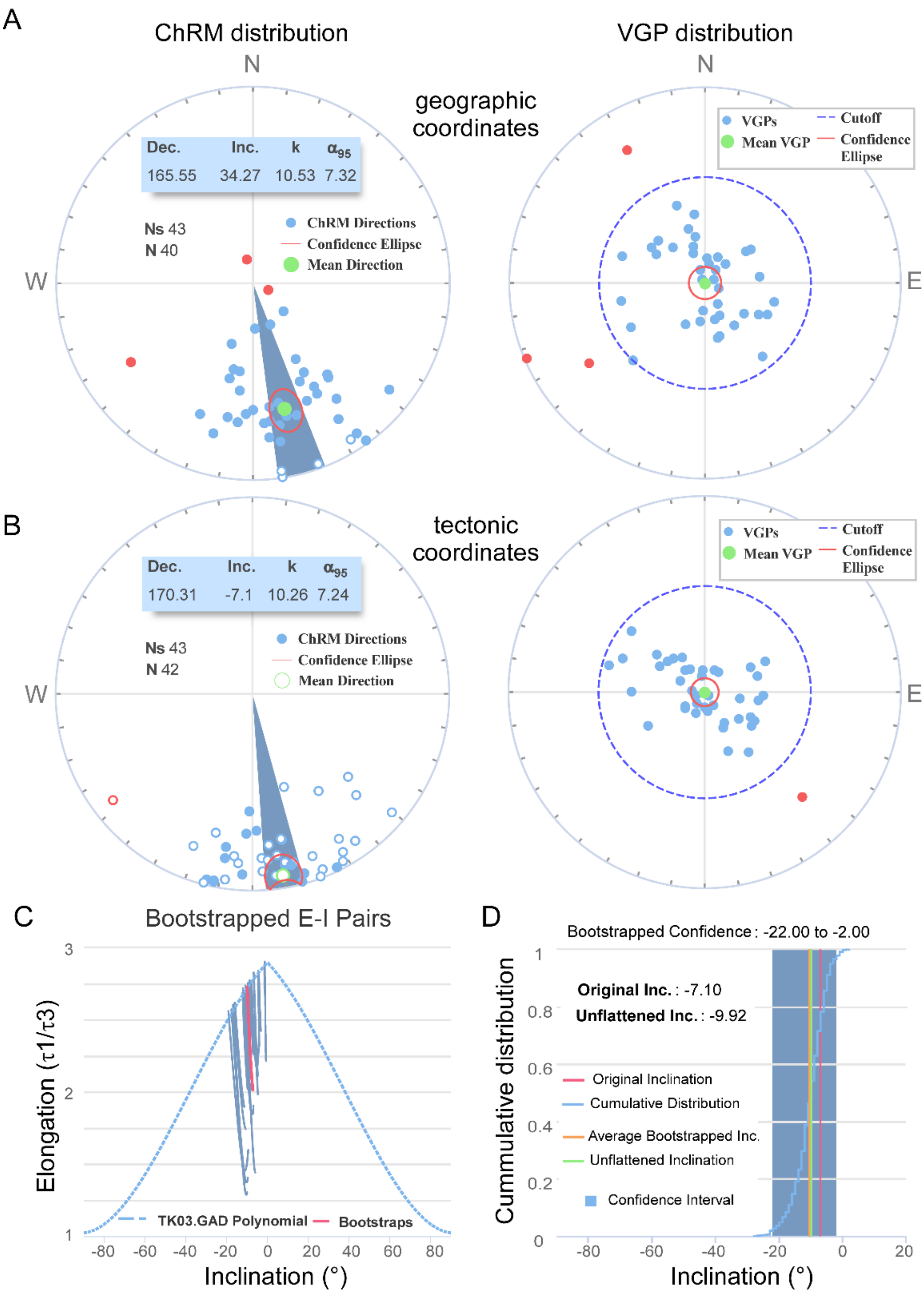
A
ChRM distribution
VGP distribution
geographic coordinates
Dec. Inc. k α95
165.55 34.27 10.53 7.32
Ns 43
N 40
ChRM Directions
Confidence Ellipse
Mean Direction
VGPs
Mean VGP
Cutoff
Confidence Ellipse
N
W
E
B
tectonic coordinates
Dec. Inc. k α95
170.31 -7.1 10.26 7.24
Ns 43
N 42
C
Bootstrapped E-I Pairs
Elongation (τ1/τ3)
TK03.GAD Polynomial
Bootstraps
Inclination (°)
D
Bootstrapped Confidence : -22.00 to -2.00
Original Inc. : -7.10
Unflattened Inc. : -9.92
Original Inclination
Cumulative Distribution
Average Bootstrapped Inc.
Unflattened Inclination
Confidence Interval
Cummulative distribution
Inclination (°)

Figure 6.

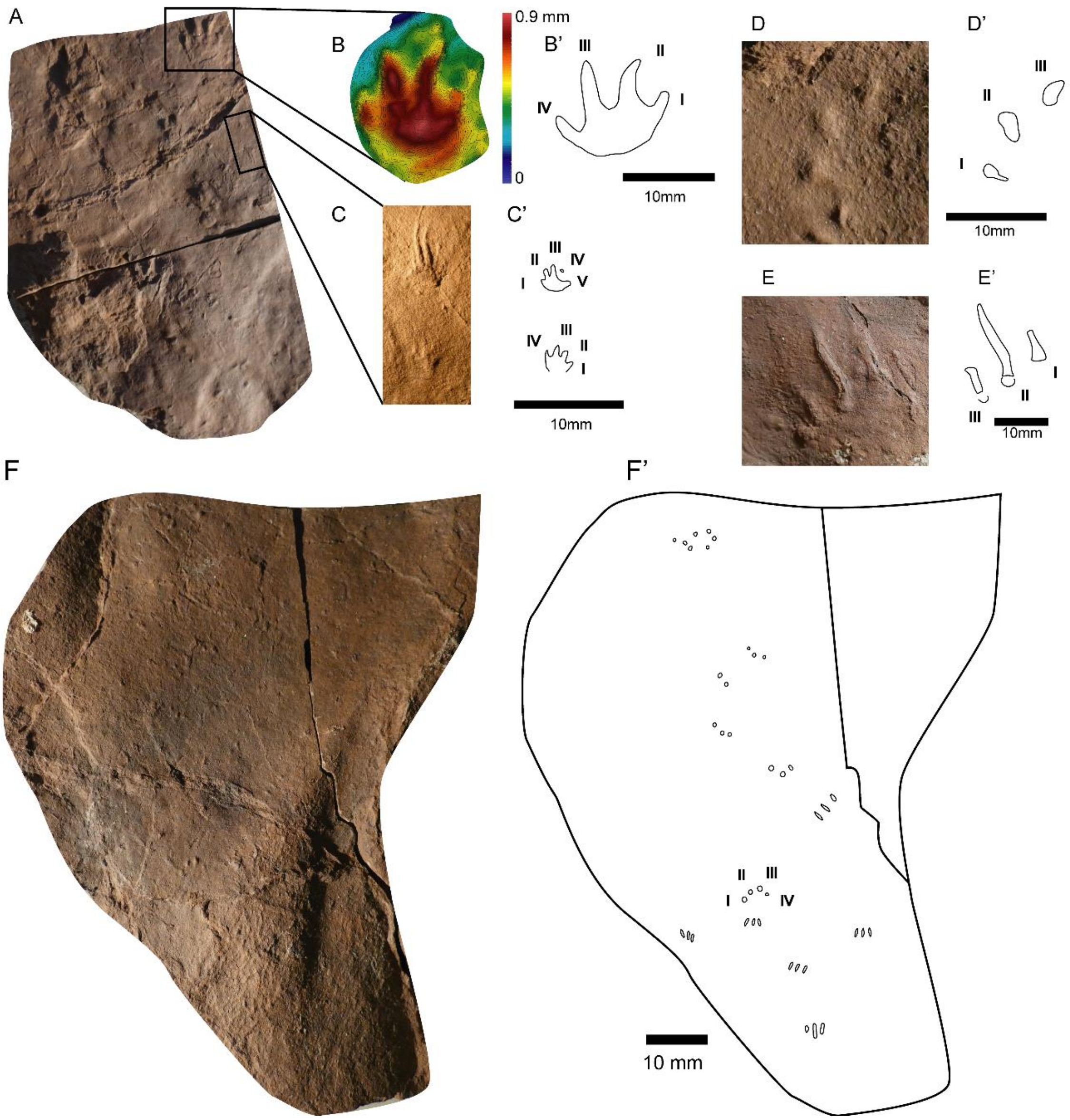
A
B
0.9 mm
0
B'
III
II
IV
I
10mm
C
C'
II
III
IV
I
V
IV
III
II
I
10mm
D
D'
III
II
I
10mm
E
E'
I
II
III
10mm
F
F'
II
III
I
IV
10 mm

Figure 7.

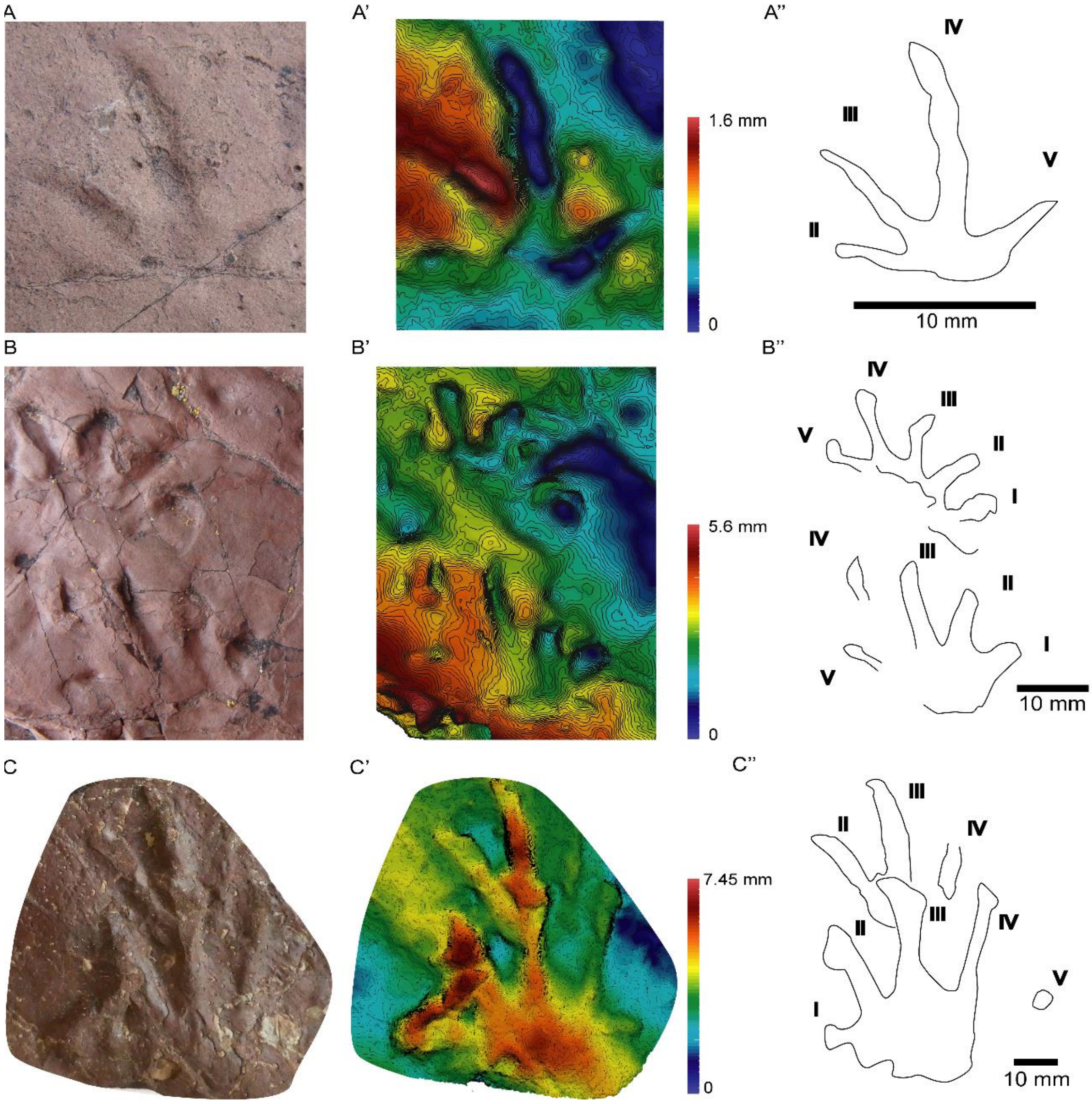

A
A'
A''
1.6 mm
0
IV
III
V
II
10 mm
B
B'
B''
5.6 mm
0
IV
III
V
II
I
IV
III
II
I
V
10 mm
C
C'
C''
7.45 mm
0
III
II
IV
II
III
IV
V
I
10 mm

Figure 8.

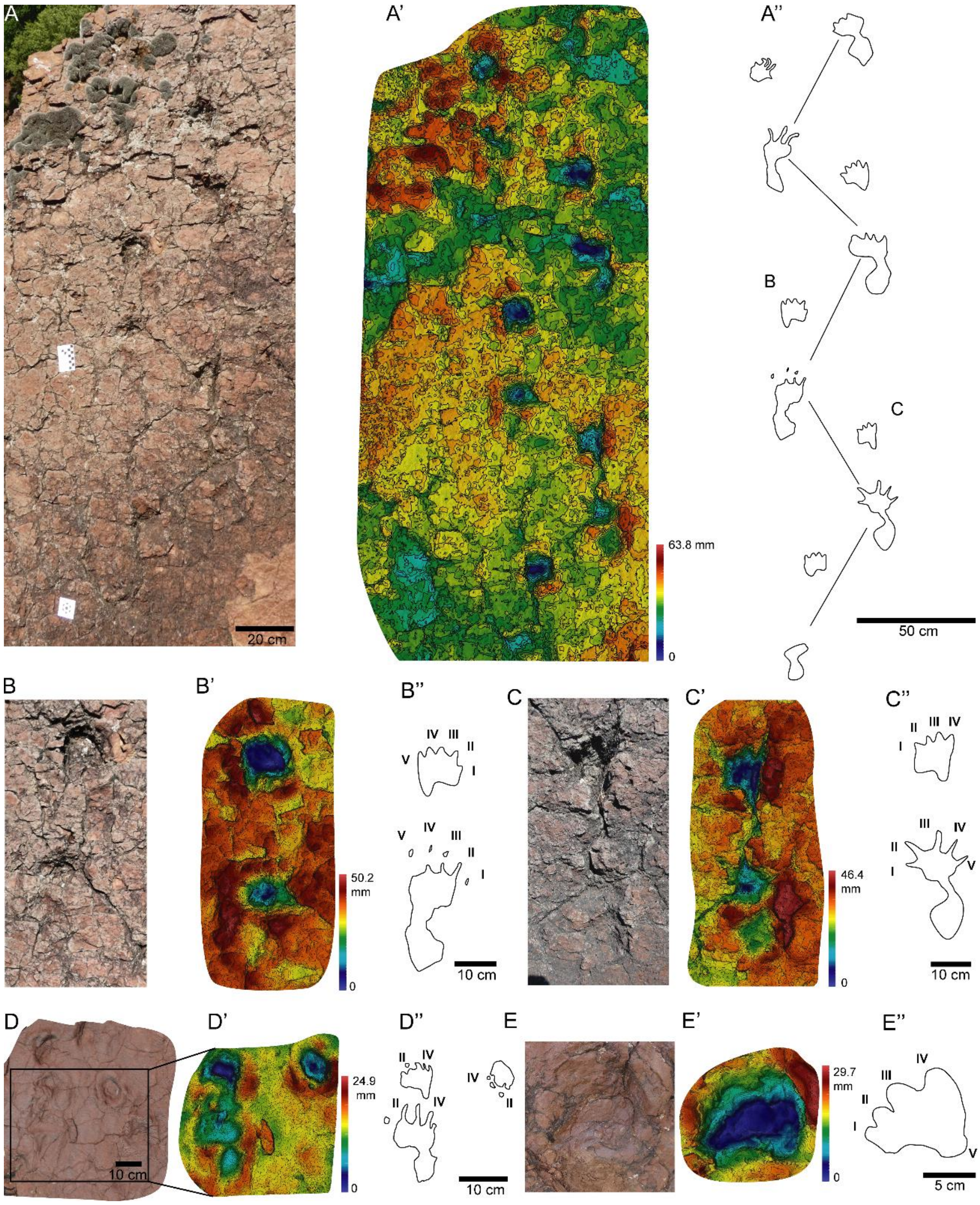
A
A'
A''
63.8 mm
0
20 cm
B
C
50 cm
B
B'
B''
IV III
V
II
I
V IV III
II
I
50.2
mm
0
10 cm
C
C'
C''
II III IV
I
III IV
II
I
V
46.4
mm
0
10 cm
D
D'
D''
II IV
II IV
E
IV
II
10 cm
24.9
mm
0
10 cm
E
E'
E''
29.7
mm
0
IV
III
II
I
V
5 cm

Figure 9.

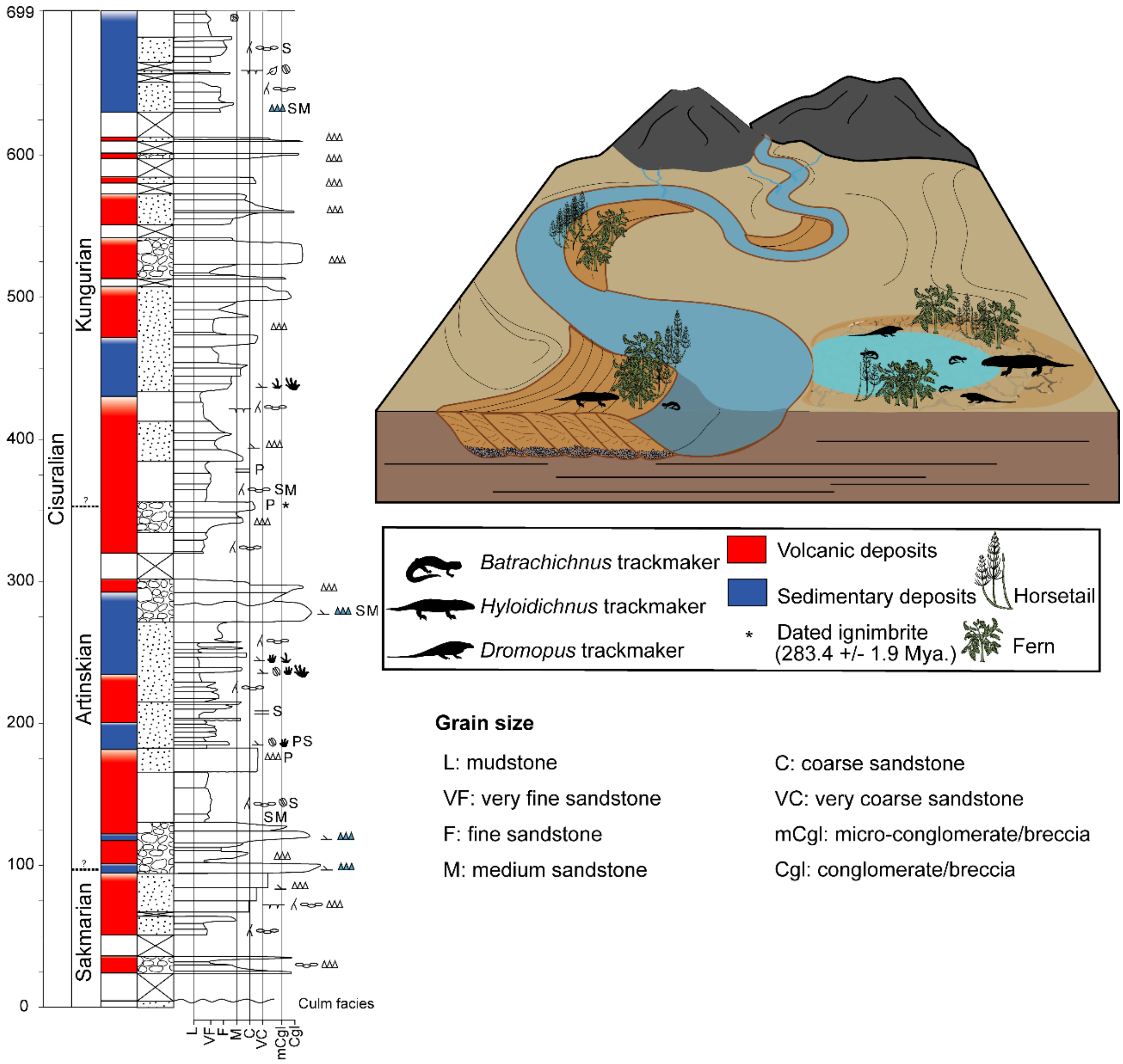
699
600
500
400
300
200
100
0
Cisuralian
Kungurian
Artinskian
Sakmarian
S
SM
P
P *
PS
Culm facies
L
VF
F
M
C
VC
mCgl
Cgl
Batrachichnus trackmaker
Hyloidichnus trackmaker
Dromopus trackmaker
Volcanic deposits
Sedimentary deposits
Dated ignimbrite (283.4 +/- 1.9 Mya.)
Horsetail
Fern
Grain size
L: mudstone
VF: very fine sandstone
F: fine sandstone
M: medium sandstone
C: coarse sandstone
VC: very coarse sandstone
mCgl: micro-conglomerate/breccia
Cgl: conglomerate/breccia

Figure 10.

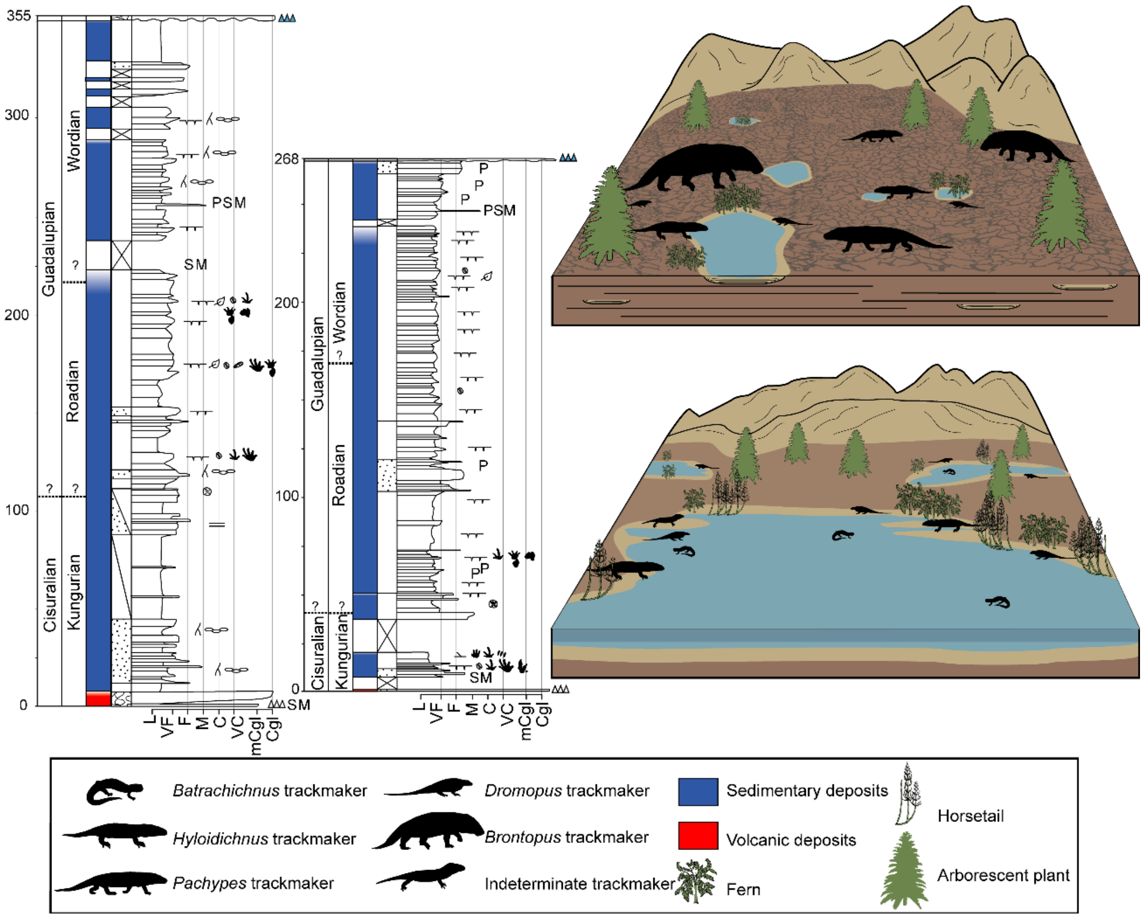

Guadalupian
Cisuralian
Wordian
Roadian
Kungurian
PSM
SM
P
L
VF
F
M
C
VC
mCgl
Cgl
Batrachichnus trackmaker
Dromopus trackmaker
Sedimentary deposits
Horsetail
Hyloidichnus trackmaker
Brontopus trackmaker
Volcanic deposits
Pachypes trackmaker
Indeterminate trackmaker
Fern
Arborescent plant

Figure 11.

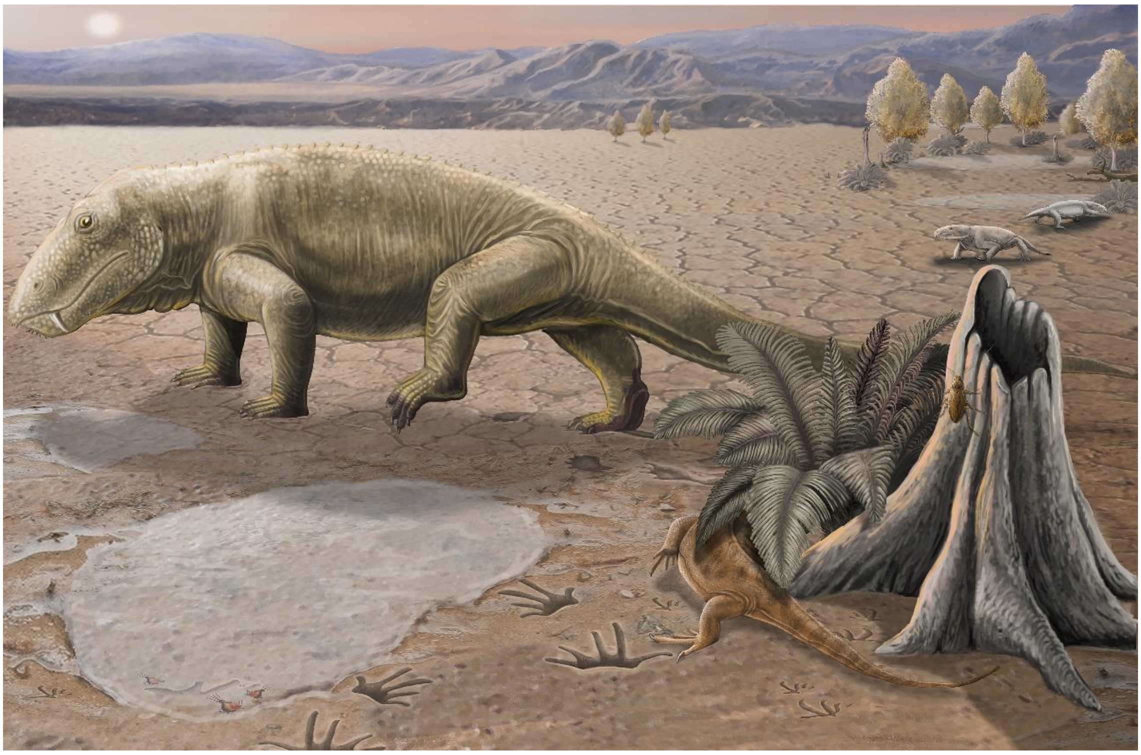

Figure 12.

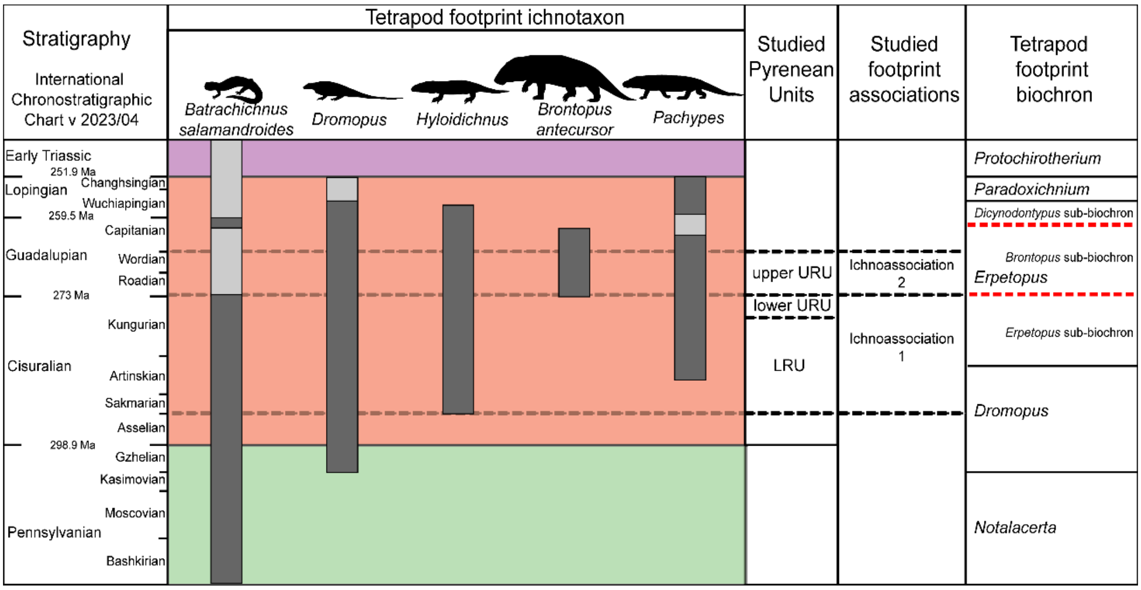

Stratigraphy
International Chronostratigraphic Chart v 2023/04
Tetrapod footprint ichnotaxon
Batrachichnus salamandroides
Dromopus
Hyloidichnus
Brontopus antecursor
Pachypes
Studied Pyrenean Units
Studied footprint associations
Tetrapod footprint biochron
Early Triassic
251.9 Ma
Lopingian
Changhsingian
Wuchiapingian
259.5 Ma
Capitanian
Guadalupian
Wordian
Roadian
273 Ma
Kungurian
Cisuralian
Artinskian
Sakmarian
Asselian
298.9 Ma
Gzhelian
Kasimovian
Moscovian
Pennsylvanian
Bashkirian
upper URU
lower URU
LRU
Ichnoassociation 2
Ichnoassociation 1
Protochirotherium
Paradoxichnium
Dicynodontypus sub-biochron
Brontopus sub-biochron
Erpetopus
Erpetopus sub-biochron
Dromopus
Notalacerta

Figure 13.